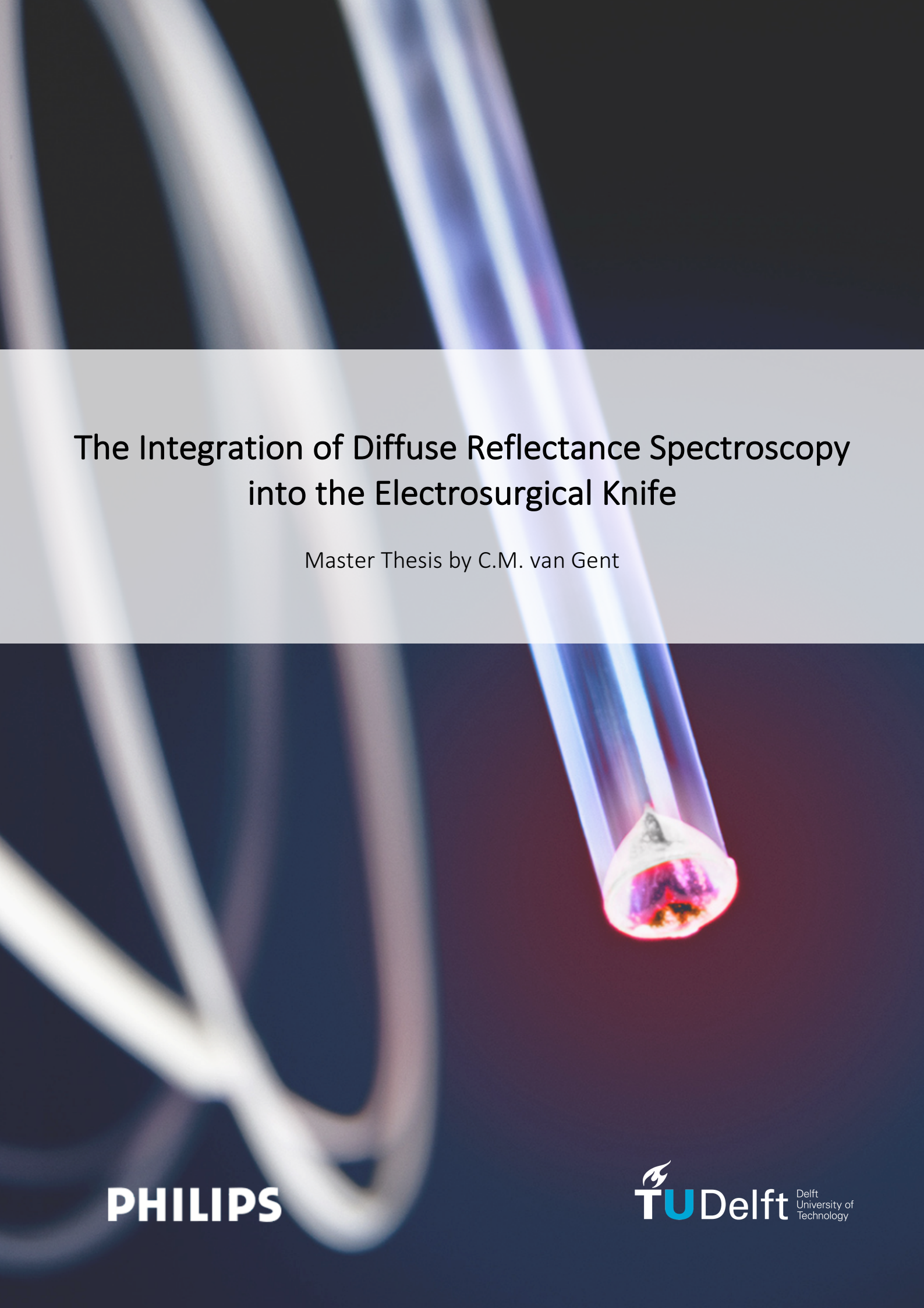

The Integration of Diffuse Reflectance Spectroscopy into the Electrosurgical Knife

Master Thesis by C.M. van Gent

PHILIPS

TU Delft Delft University of Technology

The Integration of Diffuse Reflectance Spectroscopy into the Electrosurgical Knife

Clarifying and Preventing Diffuse Reflectance Spectroscopy Signal Deterioration during Use of the Smart Electrosurgical Knife

By
C.M. van Gent

A thesis submitted in fulfilment
of the requirements for a degree in
Master of Science
in the department of
Biomedical Engineering

Delft University of Technology
To be defended on February 27th, 2019

Supervisors:
Prof. Dr. B.H.W. Hendriks
Prof. Dr. J. Dankelman

Author:
C.M. van Gent
MSc. Student Biomedical Engineering

Graduation Committee:
Dr. M. Nijemeisland
S. Azizian Amiri, MSc.

Preface

This report contains the culmination of my final master project: my master thesis. I performed this project in partial fulfillment of the requirements for the degree of Master of Science in Biomedical Engineering at the Delft University of Technology. It took me ten months of hard work to complete this project and deliver a report that extensively summarizes all my activities.

As soon as I found out about the possibilities for a graduation project within this particular research at the Delft University of Technology in collaboration with Philips Research, I got excited. I had already heard some very enthusiastic stories about experiences of previous students exploring smart electrosurgery and the subject of this research immediately appealed to me. The reason I decided to start a master Biomedical Engineering two years ago, was because I wanted to improve people's life quality and health through technique. In my opinion, this vision is perfectly reflected by this research. Unfortunately, breast cancer remains a very common disease, by which way too many man and women are diagnosed each year. We could say that everyone knows at least someone who has been diagnosed once, which makes this subject very sensitive and so much the more impactful. The idea of participating in a research contributing to the battle against breast cancer helped me to keep motivated, ambitious and enthusiastic through the course of this ten-month project.

In all honesty, I had never expected to learn as much as I just realized I have during this graduation research. I started my literature study with no knowledge at all about breast-conserving surgery, electrosurgery and photonic techniques; let alone that I had ever heard of tissue debris. However, during the course of the research I got more confident and slowly started to feel like a 'tissue debris expert' as my daily supervisor once called me. In addition, doing a project all by myself has taught me some helpful managing and project-based skills as well. I enjoyed working with inspiring people, all having different disciplines and expertise and I was amazed by their hospitality and willingness to help.

Finally, I would like to speak out my gratitude to the people without whose support I would not have been able to finish my master thesis in its current form. First of all, I would like to thank my daily supervisor prof. dr. B.H.W. Hendriks, who challenged me week after week to get the most out of myself in order to take this research to a higher level and who helped me to understand scientific research by comparing it with baking a cake. Secondly, I would like to thank prof. dr. Dankelman for her support from the Delft University of Technology and her clarifying, down-to-earth advice. Halfway through my project I received unexpected help from MSc. S. Azizian Amiri, who had started as a PhD researcher on smart electrosurgery. I would like to thank her for providing me with honest and thorough feedback, for accompanying me during most of the experiments and for introducing me to characterization methods and biomedical coatings. Lastly, I would like to speak out my appreciation to my friends and family for their informal support in any possible way.

Looking back at this project I feel both proud and confident, as I trust on the potential impact of this research and on the people taking responsibility for its continuation.

Abstract

Breast cancer is the most common cancer in women worldwide and the incidence is currently still increasing [1]. During breast-conserving surgery (BCS), the tumor is removed while the natural shape of the breast is maintained [2]. However, margin assessment during tumor surgery is a widespread problem in clinical practice and no standard method has been developed yet [3]. Together with the In-Body Systems department of Philips Research, the Delft University of Technology has been exploring the implementation of diffuse reflectance spectroscopy (DRS) into the traditional electrosurgical knife in order to accurately identify tumor and healthy breast tissues intraoperatively, based on optical parameters that are related to the fat-water ratio.

Previous research has shown that, during use of the smart electrosurgical knife, deterioration of DRS signal intensity occurs, obstructing proper functioning of the device. A layer covering the fiber tip has been observed and is generally thought to influence transmittance of the DRS signal. Therefore, this master thesis has focused on the influence of smart electrosurgery on both the morphology and composition of the outer surface layer of fiber tips. Optical microscopy and scanning electron microscopy (SEM) were used to examine the morphology, while energy-dispersive spectroscopy (EDS) and Raman spectroscopy were used to examine the composition. The results of these analyses showed that there are two factors leading to signal loss, both caused by extreme tissue heat: the fiber tip gets soiled by a layer of tissue debris covering the tip, and gets damaged due to degradation of the outer acrylate coating.

In order to eliminate these two main factors, two different surface modifications were tested: stripping off the acrylate coating to prevent melting damage, and applying a PTFE coating to prevent tissue debris adhesion. Unfortunately, both modifications were unable to completely prevent signal loss. However, eliminating the acrylate coating has shown to reduce signal loss from 45.8% to 36.4%, compared to the traditional optical fiber. Nevertheless, the results also show that this modification leads to an increased risk of fiber damage due to a lack of physical protection of the core and cladding. In contrast, the application of a PTFE coating has shown to slightly increase signal loss from 45.8% to 48.5%, compared to the traditional optical fiber. Research results indicate that this is due to additional tissue debris adhesion, caused by exceeding of the maximum operating temperature of the coating, leading to the opposite effect of non-sticking.

Based on the results of this research, it is suggested that the optimal solution for signal loss during use of the smart electrosurgical knife should respond to optical fiber damage and tissue debris adhesion, both caused by extreme tissue heat. Overall, it can be concluded that this extreme heat has been underestimated so far and should be one of the main points of focus in improving DRS signal deterioration. Therefore, this research credits most potential to the implementation of a heat-resistant optical fiber provided with an advanced heat-resistant, anti-adhesive coating.

Contents

THEORY

RESEARCH PHASE 1 - DESIGN DIRECTIONS

RESEARCH PHASE 2 - DESIGN CONCEPTS

List of abbreviations

AC	Alternating current
AvL	Antonie van Leeuwenhoek
BCS	Breast-conserving surgery
CDC	Center for Disease Control
CE	Conformité Européenne
DC	Direct current
DRS	Diffuse reflectance spectroscopy
EDS	Energy-dispersive spectroscopy
ECM	Extracellular matrix
ESGE	European Society of Gastrointestinal Endoscopy
ESU	Electrosurgical unit
Fg	Fibrinogen
FTIR	Fourier transform infrared
FUSE	Fundamental Use of Surgical Energy
IEP	Isoelectric point
L5	Liver – 5 seconds
L30	Liver – 30 seconds
NIOSCH	National institute of Occupational Safety and Health
NKI	Nederlands Kanker Instituut
OM	Optical microscopy
OR	Operating room
PB5	Pork belly – 5 seconds
PB30	Pork belly – 30 seconds
PEG	Polyethylene glycol
PTFE	Polytetrafluoroethylene (Teflon)
RGD	Tripeptide arginine-glycine-aspartic acid
SAGES	Society of American Gastrointestinal and Endoscopic Surgeons
SEM	Scanning electron microscopy
SLIPS	Slippery Liquid-Infused Porous Surfaces
SLNB	Sentinel lymph node biopsy
UV	Ultraviolet
vALUE	Advantages, Limitations and Unique Elements

1. Introduction

Breast cancer is the most common cancer in women worldwide, with nearly 1.7 million new cases diagnosed in 2012. The incidence of breast cancer is increasing, especially in developing countries [1]. The standard surgical treatment for early-stage breast cancer patients is called breast-conserving surgery (BCS). The goal of this treatment is to remove the tumor while maintaining the natural shape of the breast [2]. One of the most important aspects of BCS is margin assessment. Positive as well as negative margins during tumor surgery are a widespread problem in clinical practice, but no standard method has been developed yet [3]. Hence, over the last decades a lot of research has been done to all kinds of margin assessment techniques. Together with the In-Body Systems department of Philips Research, the Delft University of Technology has been participating in this research as well. The focus has been on adding a margin assessment technique to the traditional electrosurgical knife, generally used to remove breast tumors. Research studies of Fleischer, Adank and Mollerus have shown that diffuse reflectance spectroscopy (DRS) is the most appropriate technique for this specific application [4-8]. This photonic technique is used to accurately identify tumor and healthy breast tissues intraoperatively, based on optical parameters that are related to the fat-water ratio.

1.1 Problem statement

After the technical analysis and design phase, the research concerning the smart electrosurgical knife is now continued with the implementation phase. An important part of this phase, is that all issues encountered in the design phase need to be solved in order for the implementation to succeed. One of these issues concerns deterioration of the DRS signal intensity during use of the smart electrosurgical knife, which obviously obstructs proper functioning of the device. It is suspected that this problem is caused by a layer of tissue debris adhering to the tip of the optical fibers. Mollerus was the first to investigate this issue in more detail and as a result a prototype was developed in which the optical fibers can be pulled back during surgery [9]. Based on the pencil mechanism, the fibers of this design concept can be brought out whenever DRS measurements need to be performed.

However, knowledge about the actual cause of DRS signal deterioration, about formation of tissue debris and about the principles of tissue debris adhesion, still lacks. Also, research extensively exploring different kinds of solutions has not been done yet. Being aware of all available solutions is thought to be essential in finding the optimal solution for this particular problem. This graduation project will focus on the effect of smart electrosurgery on optical fibers, responsible for DRS signal deterioration. Subsequently, suggestions will be made that contribute to improvement of signal loss during smart electrosurgery. This focus leads to the following research question for this master thesis:

How can deterioration of the diffuse reflectance spectroscopy signal during use of the smart electrosurgical knife be prevented?

1.2 Research contribution

So far, three Biomedical Engineering students have graduated on smart electrosurgery during BCS. The different master theses and literature reports of these three students provide a strong basis on which this master thesis will built on. In order to contribute to the research that was already performed, this thesis will explore those topics that have not been touched upon yet. Appendix A shows a chapter that describes the extensive problem validation. In this chapter the findings, discussions and recommend-

dations of Mollerus are summarized in order to create a clear overview of which problems are solved, which problems remain and which new problems are raised. This information is used to provide guidance on the different design directions provided in chapter 7 and it helps to distinguish between main and side issues.

All findings of Mollerus belong to one of the following topics: influence of clinical use on tissue debris, influence of tissue debris on smart electrosurgery, and influence of electrosurgery on the tissue debris composition [9]. All three topics focus on tissue debris adhesion on the electrosurgical blade, while the actual problem of DRS signal loss occurs at the fibers of the smart electrosurgical knife. Unfortunately, thorough knowledge about the latter still lacks. Therefore, in order to contribute to the research concerning smart electrosurgery, this master thesis will focus on obtaining knowledge about the influence of smart electrosurgery on signal deterioration at the optical fibers. As will be clear by now, previous research has suggested that DRS signal loss is caused by a layer of tissue debris adhesion covering the tips of the optical fibers. This master thesis aims to reveal the actual role of tissue debris adhesion and other potential influencing factors. This knowledge is considered to be of great value in eventually finding the optimal solution for the problem of signal deterioration during use of the smart electrosurgical knife. Based on this intended research contribution the sub questions supporting the main research question are formulated as follows:

1. What is the influence of smart electrosurgery on optical fibers?
    a) What is the influence of smart electrosurgery on the morphology of the tissue debris layer covering the fiber tip?
    b) What is the influence of smart electrosurgery on the composition of the tissue debris layer covering the fiber tip?

2. What causes the DRS signal to deteriorate?
    a) What is the role of tissue debris adhesion on DRS signal deterioration?
    b) Are there any other factors influencing DRS signal deterioration?

3. How should an optical fiber be modified in order to decrease DRS signal deterioration during smart electrosurgery?
    a) What requirements should the optimal solution meet?
    b) Which design concept shows the most potential to solve signal deterioration?

1.3 Thesis outline

In order to answer the main and the sub research questions, this master thesis was structured according to Figure 1, provided on the next page. As shown in this figure, the report is divided into five different phases:

I. Theory
II. Research phase 1 – Design directions
III. Research phase 2 – Design concepts
IV. Research phase 3 – Concept testing
V. Evaluation

Each phase consists of several chapters describing the important information contributing to the specific goal of the phase. In addition, appendix B describes the structure of each research phase and how these phases relate to each other. This method is meant to systematically find the optimal solution.

Figure 1: Schematic overview of the outline of this master thesis.

I. THEORY

The goal of this phase, is to provide the complete context of this research. Except for chapter 4, all theory originates from the literature study that was performed prior to this master thesis. Only the essential and relevant parts of the literature study are enclosed. For additional information, the literature study may be consulted [11].

2. Smart electrosurgical knife

In this chapter, the concept of the electrosurgical knife is explained. The goal of this chapter is to gain sufficient knowledge about the electrosurgical knife, which will be used as input for design criteria for design concepts solving signal deterioration during smart electrosurgery.

2.1 Main principles of electrosurgery

Electrosurgery is a medical procedure used to efficiently cut or coagulate tissue while minimizing blood loss and reducing surgical time. This is done by using a high-frequency alternating electrical current (AC), which is converted to heat by resistance as it passes through living tissue. Over the years, a variety of devices and instruments that use electricity to heat tissue were created. Therefore, the clinical practice of electrosurgery has grown on a large scale. Currently, electrosurgical techniques are adopted by almost all surgical specialties and in 2010, electrosurgery was used in over 80% of all surgical procedures [10-14].

2.2 Clinical application of the electrosurgical knife

In this section, the clinical application of the electrosurgical knife is described. Later in this research the clinical application can be taken into account when design requirements for the smart electrosurgical knife are considered.

2.2.1 Breast-conserving surgery

Breast cancer is a type of cancer that forms in tissues of the breast. It occurs in both men and women, although male breast cancer is actually quite rare. A lot of different breast cancer types exist, but two of those are more common: *ductal carcinoma* and *lobular carcinoma*. The first one begins in the lining of the milk ducts, the second one begins in the lobules (milk glands) of the breast. A carcinoma represents a group of abnormal cells that initially remains in the place where it first formed. A carcinoma always begins in the skin or in tissues that cover internal organs [15]. Of all carcinomas, breast cancer is the most commonly diagnosed worldwide.

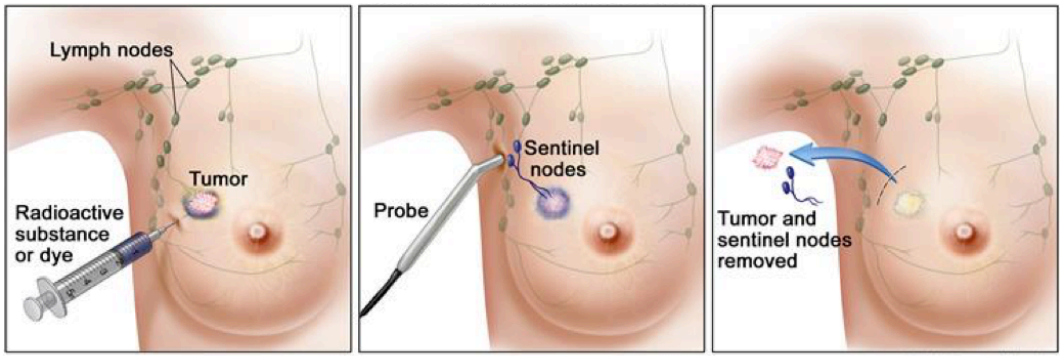

Figure 2: Sentinel lymph node biopsy during breast-conserving surgery [15].

With the current medical techniques, breast cancer can be diagnosed in relative early stages [16]. After diagnosis, surgery belongs to one of the most common treatment options. There are two types of surgery: *mastectomy* and *breast-conserving surgery (BCS)*. In mastectomy, the entire breast is removed, including all of the breast tissue. In breast-conserving surgery only the part of the breast containing the

cancer is removed. In this case the amount of tissue removed depends on the size and location of the tumor [8]. Today, BCS in combination with radiation therapy is seen as the standard treatment for early stage breast cancer. This therapy is preferred because it provides much better cosmetic effects, while it has the same level of survival as mastectomy [17]. Often an additional clinical procedure is performed during the BSC, in order to check for metastasis of malignant cells. During this procedure, called the *sentinel lymph node biopsy* (SLNB), the sentinel lymph node is identified, removed and examined for the presence of malignant tissue (see Figure 2). The sentinel lymph node is the first lymph reached by a cancerous cell migrating into a lymphatic path. The sentinel node being clean, is a highly reliable indicator for an absence of axillary node metastases [8, 18].

2.2.2 Surgical margins

In BCS the tumor should be removed surrounded by a rim of healthy tissue. This rim is called a clean margin and without the clean margin the initial surgery will presumably result in a re-excision procedure. In other words, the clean margin should make sure that all of the cancer has been removed. Re-excisions are undesirable because they can have negative consequences such as increased postoperative infections, negative cosmetic outcomes, increased costs and patient anxiety. Therefore, clean margins are an important topic in researches concerning breast-conserving surgery [19]. A clean surgical margin is often called a negative margin: no cancer cells are seen at the outer edge of the tissue that was removed and no additional surgery is needed. A margin is called positive when cancer cells are seen at the outer edge of the removed tissue and additional surgery is often needed. When a margin is close, cancer cells are found close to the edge of the tissue. In this case additional surgery might be needed [8, 20].

2.3 The smart electrosurgical knife

So far, the traditional electrosurgical knife was discussed. In this paragraph, the additional aspects of the smart electrosurgical knife will be explained.

2.3.1 Margin assessment

Margin assessment is one of the most challenging parts of the breast-conserving surgical procedure [7]. Positive margins require additional surgery, which is not preferable for both the patient and the medical staff. Negative margins are in 98,8% of the cases much larger than prescribed by the guidelines. Large negative margins increase the amount of dissected tissue, which often leads to a weak cosmetic outcome and an increased healing time [21]. Therefore, a lot of research has already been done to margin assessment techniques. Currently, there are no robust methods to help the surgeon identify tumor tissue at the surgical site during surgery.

In her literature study, F. Mollerus evaluated several existing techniques for margin assessment. This evaluation amplified the need for an intraoperative margin assessment technique during breast-conserving surgery. With her research, she showed the great potential of integrating new assessment techniques into traditional OR devices. She concludes that DRS has the most potential for being integrated into a surgical instrument, because it is relatively simple and does not require a contrast agent [8]. Moreover, it provides a relatively simple, flexible, accurate, real-time, and cost-effective way of obtaining tissue properties, without the need of an extra intervention or any additional discomfort for the patient [8, 22-24]. This statement is backed-up by the master thesis of M. Adank, who was the first to physically combine DRS with the commonly used electrosurgical knife, creating a *smart* electrosurgical knife [7].

2.3.2 Diffuse reflectance spectroscopy

Diffuse reflectance spectroscopy is a photonic technique that can be used during surgery to accurately distinguish between healthy and tumor tissue. Based on optical parameters that are related to the tissue

morphology and composition, tissue can be characterized instantly [25]. This is done by measuring the intrinsic light absorption and scattering properties at different wavelengths. A so to call optical fingerprint of the tissue is obtained by illuminating the tissue with a selected light spectrum. The optical fingerprint represents specific quantitative biochemical and morphological information [23]. In her master thesis, M. Adank has shown that the fat-water ratio is considered the most relevant property able to distinguish between healthy and tumor tissue [7, 8]. This result is amplified by a research of De Boer et al., who observed that the fat-water ratio provided excellent discrimination between tumor tissue and benign breast tissue. He even succeeded in detecting the border of a tumor in one test case [25]. Integration of DRS into the tip of an electrosurgical instrument, could provide the surgeon with essential information about the local margin assessment, while dissecting the tumor. This concept, called a smart electrosurgical knife, will highly contribute to the accuracy of tumor localization, leading to less negative margins and improved cosmetic outcomes.

2.3.3 Smart electrosurgical knife in practice

As mentioned before, M. Adank was the first to put the smart electrosurgical knife into practice. Although she did not pay any attention to the design of the prototype, she wrote down some recommendations about this aspect based on her experiences with the concept. In her design two fibers, that measure the fat-water ratio of the tissue by emitting and detecting light, are placed at the sides of the cutting blade of the electrosurgical knife (Figure 3). The fibers are encapsulated in metal to protect them from the current heat. However, the tips of the fibers are both exposed, because they need to emit and detect light [7]. During cutting or coagulation, carbonization of the tissue occurs, resulting in tissue sticking to the exposed fiber tips as can be seen in Figure 3. This leads to a soiled knife and both tissue sticking and cleaning the blade can lead to damaged fibers. A damaged fiber is unreliable, because it can provide a signal with relatively more noise [7]. Therefore, an improved design needs to contain a solution that prevents fiber damage due to tissue sticking during electrosurgical cutting.

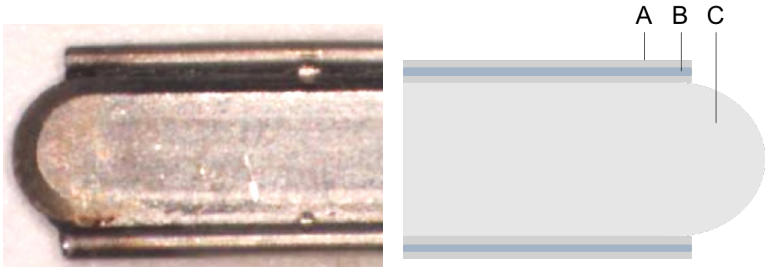

Figure 3: The tip of the electrosurgical cutting blade with both fibers attached to it. Left, a picture of the prototype [7]. Right, a schematic image of the electrosurgical blade (C) with the partly exposed fibers (B) covered in a metal sleeve (A).

2.4 Discussion and conclusion

The master theses of Fischer, Adank and Mollerus have shown that the concept of the smart electrosurgical knife works in theory as well as in practice. However, before bringing the knife into clinical practice, there are still some large complications that need to be solved. At this moment, the most crucial complication seems to be represented by the problem of tissue adhesion on optical fibers during use of the electrosurgical knife. This phenomenon leads to soiled and damaged fibers, making it very difficult for the smart electrosurgical knife to distinguish between healthy and tumor tissue. Therefore, an improved design is needed that prevents fiber damage due to tissue sticking to the surface of the fiber tip. In order to come up with an improved design, the actual cause of the problem needs to be investigated thoroughly. It is evident to know as much as possible about tissue adhesion on foreign surfaces and how to prevent this phenomenon. Therefore, the next few chapters dive deeper into this specific problem.

3. Tissue heating

A general problem of electrosurgery is tissue debris sticking to the cutting blade when using a high current during coagulation [26]. Within the first design of the smart electrosurgical knife, tissue debris does not only stick to the cutting blade, it also sticks to the exposed parts of the DRS fibers [7]. This chapter explains the influence of tissue heating on tissue debris formation.

3.1 AC effect on tissue

From the previous chapter, we know that electrosurgery is based on an electric current passing through human tissue, elevating cellular temperature in order to achieve certain tissue effects. In this paragraph, the mechanisms responsible for cellular temperature increase are discussed.

3.1.1 Electric current

Electric current can either be direct (DC) or alternating (AC). In DC there is only unidirectional travel of electrons possible [27]. In AC, the direction of the current is constantly changing. The speed at which the direction is changed per unit of time, is called frequency and is given in Hertz (Hz). The frequency that is coming from the power grid and is used to power homes and appliances is about 50-60 Hz. However, using this frequency in electrosurgery, would depolarize muscle and neural cells, leading to acute pain, muscle spasms and even cardiac arrests [12, 28]. In order to prevent depolarization of the susceptible tissues, the frequency used during electrosurgery should always be higher than 10 kHz [10]. Generally electrosurgical generators operate in the frequency range of 200 kHz to 5 MHz. Because this is the frequency range of amplitude modification (AM) radio broadcasts, the term radio frequency (RF) electrosurgery is often used [28].

3.1.2 Effect of Joule heating

The appearing electrosurgical tissue effects are a result of the change in temperature at and around the electrode. This temperature elevation is caused by at least two basic mechanisms, of which the first is called the Joule (or resistive) heating effect [27].

3.1.2.1 Basic level

Joule heating is the process by which the passage of an electric current through a conductor (tissue) produces heat, because the electric energy is converted into thermal energy. Joule's first law states that the power (P) of heat generated by an electrical conductor is proportional to the product of its resistance and the square of the current. In addition, the rise in temperature is calculated by multiplying the power by the time. The equations are as follows:

$P = I \cdot V = I^2 \cdot R$ [6, 28, 29] and $Q = I^2 \cdot R \cdot t$ [30, 31]. (3.1, 3.2)

Whereby *P* is the power in Watts (W), *I* is the current in Amperes (A), *V* is the voltage in Volt (V), *R* is the resistance in Ohm (Ω), *Q* is the heat generated in joules (J) and *t* is the time in seconds (s) (see Table 1). Joule's law indicates that in order to increase the heating power generated by the tissue, the current, the resistance or the time need to be increased. All happen during a typical electrosurgical procedure, although the former might be adjusted on purpose, while the resistance of tissue changes unintentionally [28].

Table 1: Definitions of variables that can impact the electrosurgical effect on cells and tissues [28].

Variable	Definition	Units
Current (*I*)	Flow of electrons past a point in the circuit/unit time	Amperes (coulombs/second)
Voltage (*V*)	Difference in electrical potential between the two points in the circuit; force required to push a charge along the circuit	Volt (joules/coulomb)
Resistance (*R*)	Degree to which the circuit or a portion of the circuit impedes the flow of electrons	Ohms
Power (*P*)	Work; amount of energy per unit time. Product of voltage and current	Watts (joules/second)
Energy	Capacity of a force to do work; cannot be created or destroyed	Joules (watts/second)

3.1.2.2 Atomic level

The Joule heating effect can also be explained at a deeper level, clarifying why more resistance leads to a temperature elevation. As stated before, an alternating electric current is a flow of electric charge carried by moving electrons in an electric circuit [32]. Under the influence of an electric field, free electrons move from one atom to another. The number of free electrons determines the conductivity of a material: the freer electrons the higher the conductivity. However, some electrons are held tightly within the atom and do not respond to an electric field. These are called captive electrons [27, 32, 33]. In the electrosurgical circuit, human tissue acts as a resistor containing free electrons, but also lots of captive electrons. The free electrons of the electric current bump into the captive electrons of the tissue. Each collision requires kinetic energy from the free electron, which is transferred to the captive electron. Because the captive electron is not able to move, the kinetic energy is converted to thermal energy. This results in a temperature increase [30]. The more collisions between free and captive electrons, the higher the rate of heating. So if a surgeon wants to increase the heating effect, he simply needs to make sure more collisions are achieved [27, 32]. This can be done by adjusting one or more of the following factors: current density, time, electrode size, tissue conductivity and the type of current waveform [11, 27]. These factors have been discussed in the previous chapter as well.

3.1.3 Effect of energy conversion

The second mechanism responsible for tissue heating is called energy conversion. Cells contain two types of particles: cations and anions. Cations are positively charged ions, such as sodium and calcium, that tend to migrate towards the negative electrode. Anions are negatively charged ions, such as chlorine and proteins, that tend to migrate towards the positive electrode. When a radiofrequency AC is applied on a biological tissue, it naturally crosses the tissue cells. Because of the continuously switching polarity of the AC, the anions and cations start to oscillate between the two electrodes. The rapid oscillation within the cellular cytoplasm leads to a conversion of electromagnetic energy into kinetic energy. Subsequently, frictional forces convert the kinetic energy into thermal energy, leading to an increase of the local tissue temperature [28, 34].

3.2 Effect of temperature

The previous section has shown which two mechanisms are responsible for an increased tissue temperature at the surgical site when using the electrosurgical knife. However, it is still unclear what kind of effect this heat has on human tissue and why heat application is necessary during electrosurgery. This is explained in this paragraph.

With higher tissue temperatures, specific surgical effects are obtained. These effects are dependent on the effect of temperature on cells. In order to understand the different surgical applications of RF

electrosurgery, a basic understanding of the effects of temperature on cells is required [35]. In general, the supraphysiological heating of cells leads to destabilization of lipid membranes, denaturation of proteins, obstruction of the cell cycle and induction of heat shock proteins. Table 2 shows an overview of the thermal effects on cells for different temperature ranges.

Table 2: Effect of temperature on cells and tissue. Composed from [28, 34, 36-38].

Temperature	Effect on cells
37°C	Normal body temperature
37-40°C	Hyperthermia: tissue heating
42-45°C	Retraction; devitalization
> 50°C	Reduction in enzymatic activity; cell death over minutes
45-60°C	Cellular desiccation; protein denaturation
60-90°C	Cellular desiccation; protein denaturation; instant cell death
90-100°C	Cellular desiccation; protein denaturation; tissue dehydration
> 100°C	Cellular vaporization; H20 ebullition; cell membrane destruction; glue effect
> 200°C	Carbonization
> 500°C	Vaporization

The normal human body temperature is 37°C. From time to time, temperature elevations that reach as high as 40°C may be experienced, caused by the time of the day, illness, environmental conditions, or exertion. However, the human body features a highly developed thermo-regulatory system to maintain the typical body temperature within a reasonable range. Temperatures up to 40°C do not yet cause any damage to the structural integrity of our cells and tissue. Body temperatures higher than 40°C can be life-threatening [28, 39].

However, local tissue temperatures exceeding 40°C are more common and do not lead to human death. They may occur accidentally during local thermal burns for example, or deliberately during some clinical procedures like electrosurgery. Cellular temperatures greater than 50°C can lead to necrosis in cells within only a few minutes and greater than 60°C can lead to instant cell death [28, 39].

Temperatures between 60 and 100°C cause protein denaturation and cellular desiccation. During protein denaturation, the hydrothermal bonds between protein molecules break due to the heat and then quickly reform as the local temperature cools. A homogenous coagulum arises during a process called coagulation. Cellular desiccation is actually dehydration of the tissue as the cells lose water through the thermally damaged cellular wall. The higher the temperature, the quicker this reaction occurs. The longer the duration of the heating, the more severe the reactions are. The process of protein denaturation is shown in Figure 4 [28, 37, 39].

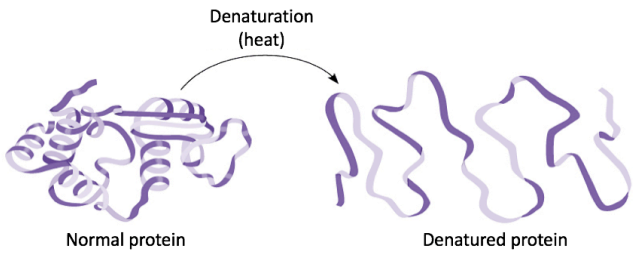

Figure 4: Schematic overview of protein denaturation due to temperature elevation [40].

At temperatures of more than 100°C, the intracellular water will start to boil and form steam. This leads to a massive intracellular expansion resulting in explosive vaporization of the cell. This reaction is

accompanied by a cloud of steam, ions and organic matter. Munro states that it is suspected that the acoustical vibrations caused by the explosive force contribute to the tissue cutting effect [28]. This will be further explained in the next paragraph.

At local temperatures of more than 200°C a process called carbonization occurs. During this process, the organic molecules are broken down, leaving only the carbon molecules that create a black and brown appearance. This accumulation of brown carbon molecules is referred to as black coagulation or carbonization [28] and it is suspected that this is part of the tissue that sticks to the DRS fibers of the smart electrosurgical knife. The carbonization process is further explained in the next paragraph as well.

3.3 Thermal tissue damage

Tissue is thermally damaged when cells lose their structural integrity. All forms of tissue heating lead to some kind of thermal tissue damage, as has been shown in paragraph 4.1. Below 45°C this thermal damage is reversible, but as soon as the tissue temperature reaches 45°C or more, tissue proteins become permanently denaturized [41, 42]. This paragraph describes the processes underlying thermal tissue damage on cellular scale.

3.3.1 Thermal tissue damage during ES

During electrosurgery some of the thermal damage is created on purpose in order to achieve the intended tissue effect, but other thermal damage occurs unintentionally. Unfortunately, this collateral thermal damage is inevitable because of thermal spread to adjacent cells, caused by the electrosurgical knife. Although surgeons are well aware of this kind of thermal injury, they seem to find it very hard to prevent. In some cases it is indeed impossible to prevent thermal damage, in other cases the amount of injury should be decreased significantly [28, 38].

The exact type of thermal damage is highly dependent on the tissue temperature and therefore indirectly on the electrosurgical settings. In general, it applies that the higher the temperature, the more severe the thermal damage. Thermal damage is unwanted because it does not only do harm to the outcome and well-being of the patient, it also obstructs the smart electrosurgical functioning. In general, thermal injury leads to an increased impedance, which prevents further transmission of energy to the deeper layers of tissue: a principle that forms the basis of the electrosurgical technique [28, 43-45]. Besides, cellular products of thermal damage can affect the DR spectra used for margin assessment during smart electrosurgery [7].

A lot of different terms are used in literature to describe thermal damage. In this paragraph, we will describe the thermal damages that happen both on purpose and unintentionally during electrosurgical procedures and that are suspected of obstructing the smart electrosurgical functioning in a certain way. The different thermal injuries are described in order from occurring at low to high temperatures.

3.3.1.1 Thermal coagulation

The first thermal damage that occurs when elevating the tissue temperature is coagulation. Coagulation is the result of heating tissue below the boiling point, causing tissue denaturation [46]. The hydrothermal bonds that exist between protein molecules are instantaneously broken due to the temperature elevation. However, the bonds quickly reform, as the local temperature in the adjacent tissue cools due to the alternating current. This leads to coagulation: the forming of a homogenous coagulum [28].

3.3.1.2 Thermal desiccation

When slowly increasing the tissue temperature a little bit more to about 100°C, desiccation occurs. During this process the cellular water content vaporizes, which causes quickly tissue dehydration [38,

46]. The desiccation process causes contraction of vessels and adjacent tissue, resulting in hemostasis. The dehydration leads to a dry tissue layer that acts to insulate the tissue electrically. This prevents electricity from reaching deeper tissue layers, increasing the tissue impedance and thereby obstructing the electrosurgical functioning. A third consequence of desiccation is the adhesive effect that results from desiccation of derivatives of collagen. According to Waye et al. this process is responsible for tissue sticking to high-frequency active electrodes [38].

3.3.1.3 Thermal caramelization

Caramelization occurs just before carbonization, when the tissue temperature is increased to temperatures just below 200°C. Thomsen defines this process as the melting, partial reduction and solidification of tissue sugars. In other words: proteins present in cells are reduced to sugars. According to Munro these sugars are the reason that caramelization facilitates adherence of tissue to the electrode. Because caramelization quickly passes into carbonization its further specific effects are frequently overshadowed [28, 35].

3.3.1.4 Thermal carbonization

Thermal carbonization is the heat mediated reduction of cellular organic molecules to elemental carbon, but is also defined as the partial oxidation of tissue hydrocarbon compounds due to elevated temperatures. The carbon molecules form a thin, visible black membrane that covers the wall of the targeted tissue surface. The remaining vacuolated tissues underneath the carbon layer are shrunken, desiccated and brittle. The carbonization reaction only occurs in an oxygen-containing atmosphere with a tissue temperature of at least 200°C. Only desiccated, dry tissue is able to reach temperatures above 100°C, which is achieved by the application of electric arcs. Carbonization is unwanted during smart electrosurgery, because it increases the impedance, leads to eschar build-up, causes toxic smoke which interferes with the surgeon's visibility and affects the DR spectra during margin assessment [7, 35, 38, 41, 47].

3.3.1.5 Thermal vaporization

According to Aye et al. thermal vaporization is defined as the combustion of desiccated or carbonized tissue at temperatures starting at 100°C and reaching 500°C. As the tissue temperature increases, water vapor is quickly generated and water is diffused out of the cell. When the water vapor generation occurs faster than the diffusion rate, steam vacuoles are formed within the cell. With the rising temperature, the pressure keeps increasing and the steam starts to expand rapidly. The brittle, carbonized cellular walls are stretched until they rupture. This process often leads to the so-called "popcorn effect": explosions throwing tissue fragments from the surface at the surgical site with a loud "pop" marking the rapid escape of steam into the atmosphere. With the steam escaping from the vacuoles, the temperature of the remaining tissue drops to approximately 100°C [28, 35, 38].

In Table 3 an overview is provided of all different forms of thermal tissue damage explained on the basis of the corresponding tissue effects, the occasion and the main function. The table shows that the processes of caramelization, carbonization and vaporization seem to be partly responsible for the two tissue effects that cause tissue sticking to the instrument: tissue adhesion and tissue throwing. Note that this overview is based on completely correct use of the electrosurgical instrument. When the instrument is used incorrectly, tissue effects as well as the occasion during which the damage happens could deviate.

In most literature coagulation and desiccation together are referred to as just coagulation, and caramelization and carbonization together are referred to as carbonization. Unfortunately, both coagulation and carbonization are more or less inevitable while using the electrosurgical knife. However, the level of both damages highly depends on the corresponding settings used during surgery. The main

factors affecting the depth and characteristics of the injury are the voltage, the waveform and the electrode speed [28, 38, 41].

Table 3: Overview of the different forms of thermal tissue damage.

Thermal damage	Tissue effect	Occasion	Function
Coagulation	· Protein denaturation · Coagulum formation	Desiccation Fulguration	Small hemostasis
Desiccation	· Tissue shrinkage · Tissue insulation	Desiccation Fulguration	Moderate hemostasis
Caramelization	· Protein reduction to sugars · Adhesive effect	Fulguration	Large hemostasis
Carbonization	· Molecule reduction to carbon · Tissue impedance increase · Smoke formation · Adhesive effect	Fulguration	Large hemostasis
Vaporization	· Intracellular steam formation · Cell explosion (popcorn effect) · Tissue throwing	Cutting	Incision formation

3.3.2 Eschar formation

Eschar formation has been mentioned before in previous sections. It is remarkable that this term is only used in literature to refer to tissue adhesion on the blades of an electrosurgical knife, while in fact eschar represents the cellular product of carbonization and caramelization. Eschar is composed of carbonized tissue and dried secretions, most often caused by a skin wound after burn injury [48]. In case of electrosurgery, the skin is burnt deliberately in order to stop de bleeding during dissection. Eschar forms when tissue cells die and bunch or stick together. Typically, eschar is crusty or leathery in appearance and is black or brown in color [49]. In general, eschar is part of the body's healing process and functions as a temporary coverage to protect the wound. After that, the eschar should be removed to further promote wound healing [50]. Normally, eschar is present for one month maximum, after which it dissolves itself [51, 52].

Eschar should not be confused with scabs, since eschar contains carbonized (necrotic) tissue, while scabs just consists of dried blood and exudate. The eschar tissue structure consist of many fibrous regions and fine fibrillary elements separated by areas of a more irregular nature [53]. Eschar builds up on the electrode tip of an electrosurgical knife, which increases the impedance causing arcing, sparking or flaming of the eschar. Interrupting the surgery in order to clean the instrument, delays the procedure and leads to even more eschar buildup [54]. However, very little is known about the further composition and adhesion effect of eschar and Thomas et al. emphasizes the importance of discovering more about this composition to enable treatments for example [50]. Lack of this knowledge unfortunately also inhibits clear statements about eschar adhesion.

3.4 Discussion and conclusion

Chapter 3 has shown the different tissue effects caused by local electrosurgical heating due to AC application. When the processes behind these effects are approached on cellular scale, it turns out that electrosurgery is actually purely based on doing thermal tissue damage. Part of this thermal damage is applied on purpose in order to achieve a cutting, fulguration or desiccation effect to facilitate proper surgery. However, the remaining part of the thermal tissue damage happens unintentionally. Preventing thermal tissue damage is not only of great importance for the outcome and well-being of the patient, it also influences the functioning of the smart electrosurgical instrument. However, decreasing the amount of collateral thermal damage could, in this context, only be achieved by educating surgeons

how to properly use the smart electrosurgical device. Unfortunately, this medical aspect is out of our scope and therefore, other opportunities to prevent tissue adhesion during smart electrosurgery need to be explored.

4. Tissue debris

This chapter provides theoretical information about the composition and morphology of tissue debris at a molecular and elemental level. This knowledge could help to better understand tissue debris adhesion and may serve as input for selecting suitable solutions for the signal deterioration problem.

4.1 Tissue debris composition

The composition of fresh tissue and tissue debris is not the same. In the previous chapters it became clear that tissue heating causes severe damage, such as protein denaturation, cellular vaporization, carbonization and tissue dehydration [55]. The irreversible thermal tissue damage due to electrosurgery therefore changes the composition of tissue. For example, tissue dehydration and cellular vaporization both lead to a reduction or complete absence of water.

As soon as all water molecules are vaporized, carbon atoms are released during tissue carbonization [56]. Carbonization is defined as partial oxidation of tissue hydrocarbon compounds, which removes hydrogen and oxygen from the tissue so that the residue matter is primarily composed of carbon [57]. This reaction leads to blackened tissue and smoke rising from the operational site. The blackened tissue is often referred to as *char* or *carbon*, which has a honeycomb-type structure [58]. The process of thermal decomposition looks as follows:

$$C_{tissue} \rightarrow C_{char} + \text{liquids} + \text{gases}. \quad (4.1)$$

Furthermore, Zheng et al. recently investigated the tissue composition of tissue debris and compared it with both fresh tissue and completely carbonized tissue. His research showed that fresh porcine liver mainly contains the elements C, H, O, P and K, and a small amount of other elements [59]. While porcine liver tissue debris is mainly composed of the elements C, O, P and K, and small amounts of Na, Mg and Ca. The composition has obviously changed. When comparing Fourier-transform infrared (FTIR) spectra of tissue debris and completely carbonized tissue, it becomes clear that the tissue debris spectrum is different from the carbonized one. This means that tissue debris cannot be the result of carbonization only. Furthermore, no sugar was found in tissue debris, which excludes sugar from the potential adhesion mechanisms described in chapter 5.

4.2 Tissue debris morphology

Zheng et al. also investigated the effect of a high-frequency electric field on tissue debris due to electrosurgery [59]. Both an electrosurgical cutting test and a heat-adherence test were performed *ex vivo* on fresh porcine liver. The heat-adherence test without electric field was used as a control group. Zheng emphasizes that both debris tissues obtained from these tests are partially carbonized, but that their microstructure and bonding with the knife are different. This implicates that tissue debris adhesion due to electrosurgery is not just a result of tissue heating, but also of using a high-frequency electric field.

Zheng explains the formation of tissue debris and its adhesion on the electrosurgical knife as follows. Human cellular cytoplasm contains charged ions: cations are positively charged ions, while anions are negatively charged ions. As soon as the active electrode of an electrosurgical knife approaches tissue, a high-frequency current is led through the tissue causing heavy oscillation of the charged intracellular particles [59]. As mentioned before, due to friction the oscillation leads to heat generation which in turn

leads to an electrosurgical cutting effect by destroying the cell structures. However, an additional effect seems to appear, which has been overlooked so far. The oscillation does not only cause heat generation, a high shear rate that disintegrates the intracellular substances is produced as well. This shear rate leads to fragmentation of the substances into nanoparticles with uniform size, while the intracellular fluid is vaporized because of tissue heating. When cells eventually burst, the nanoparticles escape in the form of smoke. Subsequently, the electric field accelerates the charged smoke particles causing them to hit the hot active electrode. The particles are quickly packed and carbonized on the knife blade and form sticky tissue debris with a compact microstructure. Additionally, the high-speed impact of the particles leads to a rough electrode surface which makes bonding between the surface and tissue debris very easy. Figure 5 shows a schematic diagram of the process described above.

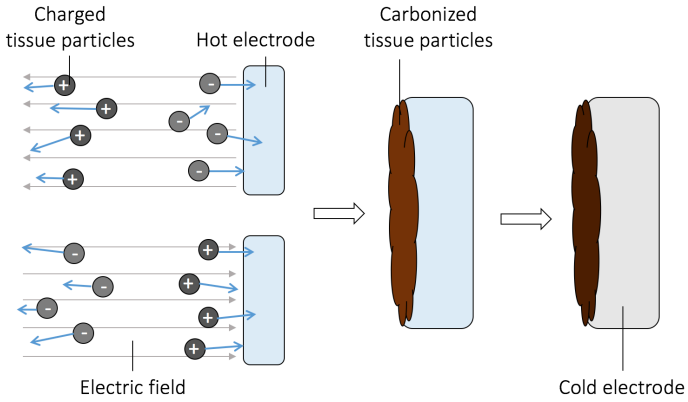

Figure 5: Schematic representation of the formation of sticky tissue debris on the active electrode [59].

4.3 Discussion and conclusion

In contrast to fresh tissue, very little is known about the composition and morphology of tissue debris. Due to carbonization both the morphology and the composition of tissue debris changes significantly compared to fresh tissue. However, according to research performed by Zheng et al., carbonization cannot be the only factor responsible for the composition of tissue debris, because the composition of purely carbonized tissue shows slight differences.

The results of Zheng et al. also implicate that tissue debris, found on an electrosurgical blade, has a compact microstructure, which is the result of a high shear rate caused by the electric field used for electrosurgery. He states that without an electric field, tissue debris has a loose and porous microstructure composed of particles of unequal size, leading to a relatively weak binding with the surface of the electrode. Therefore, one might say that removal of the electric field during electrosurgery could take the smart electrosurgical knife one step closer to being free of tissue debris adhesion. However, the electric field is an element of electrosurgery that cannot be removed, because it would simply take away the cutting function of the knife, making it completely useless. Another solution for tissue debris adhesion during smart electrosurgery in particular, could be to remove the DRS fibers from the electric field to make sure that the charged particles do not accelerate towards its surfaces. However, it is important to perform DRS measurements as close to the tip of the blade as possible. This enables real-time tissue characterization of the tissue that is being cut by the knife, which is an essential function of the smart electrosurgical instrument. Besides, the information provided in this chapter is completely based on tissue debris adhering to the electrosurgical blade, while the focus of this research is on optical fibers. Experimental results should reveal whether the mechanisms described in this chapter apply to tissue debris contamination of DRS fibers as well. Furthermore, the mechanisms responsible for tissue debris adhesion and other existing methods to prevent this need to be explored. This is the focus of the following two chapters.

5. Tissue debris adhesion

In the previous chapter, some detailed information is provided about the morphology and composition of tissue debris sticking to the blade of an electrosurgical knife. However, it is still unclear what mechanisms are behind the adhesive effect of tissue debris. In order to be able to prevent this adhesion, it is very important to be aware of these mechanisms.

5.1 Cell adhesion

When focusing on tissue adhesion, it can be stated that the process of cell adhesion is the origin of this phenomenon. There are two types of cell adhesion: cell-cell adhesion and cell-matrix adhesion. In cell-cell adhesion, physical bonds are formed between adjacent cells, while in cell-matrix adhesion, physical bonds are formed between cells and adhesive proteins in extracellular matrices or foreign surfaces [60, 61]. The latter one is involved in binding of a cell to any kind of surface using cell adhesion molecules, which transmit information from the extracellular matrix to the cell. This paragraph focusses on the fundamentals of cell adhesion in the context of smart electrosurgery.

5.1.1 Fundamentals of cell adhesion

In the context of smart electrosurgery, cell adhesion could also be explained as the interaction between a living cell and a solid, foreign surface *in vitro*. Predicting and controlling the outcome of this molecular interaction resulting in cell adhesion, has been of great interest in the past decades [62, 63]. This phenomenon affects the performance of many processes and materials in areas such as medicine and biochemical engineering [64]. When tissue, consisting of cells and blood plasma, first contacts a foreign surface, a sequence of events is initiated. Vitte et al. considers three sequential steps in this cell-surface interaction: 1) protein adsorption, 2) adhesive bonds formation and 3) specific cell program triggering [62]. Especially the first step, protein adsorption, is mentioned and described extensively in literature.

5.1.1.1 Protein adsorption

All studies focusing on the initial events occurring during cell-surface interaction conclude that protein adsorption is the first step in this process [60, 62-66]. Protein adsorption eventually leads to cell adhesion. In some processes this effect is highly valued, in other processes it can be fatal [62]. Protein adsorption can trigger adhesion of particles, cells or bacteria, possibly leading to inflammation cascades or fouling processes. The latter is the case for the smart electrosurgical instrument and other comparable techniques in the field of analytical science. Protein adsorption on protein chips or sensor surfaces is a serious problem inhibiting the analytical performance of such devices [64, 67]. For decades, the protein adsorption process has been referred to in literature as ‘complicated’ and a unified predictive theory on this process still seems to lack [62, 64, 66, 67]. However, a general approximation of the protein adsorption process is shown in Table 4.

Step 1: First the entire surface exposed to the tissue is covered by a layer of water molecules. This event happens within nanoseconds and is highly dependent on the surface properties of the material, which determines the structural arrangement of the molecules. The layer of water molecules prepares the surface for a reaction with proteins [68].

Step 2: Second, in order for the proteins to adsorb, they need to encounter the solid surface. Especially the diffusion constants and concentrations of different species determine the order of encounters [62, 69].

Step 3: The third step is the most comprehensive one. As soon as living cells get in direct contact with a foreign surface, rapid deposition of a strongly adherent proteinaceous film occurs within seconds or less [62, 65]. This protein layer is the result of instantaneous binding of proteins to the surface. Protein binding is based on the idea that adsorption occurs when more energy is released than gained. This idea is reflected in Gibbs law of free energy and is provided by the following equation at constant temperature and pressure:

$$\Delta G = \Delta H - T\Delta S \text{ [70].} \quad (4.1)$$

With G is the Gibbs free energy, H is the enthalpy in joule, T is the temperature in kelvin and S is the entropy in joule per kelvin. When the Gibbs free energy is negative, the protein adsorption will occur spontaneously.

Step 4: During the protein adsorption, all proteins are constantly competing for binding site on a surface. According to the Vroman effect, small, rapid proteins will be the first to coat a surface. However, over time, the small proteins will be replaced by larger ones with a higher adhesive affinity for that particular surface [62].

Step 5: Eventually, the adsorbed proteins will undergo conformation changes that often make the adhesion stronger. Proteins initially approach a surface in their native state. However, structural reorganizations take place, driven by an entropy gain and interactions between protein and surface that are more favorable.

Table 4: The five different steps of the protein adsorption process. Composed from: [61, 62, 67-69].

Step	Protein adsorption process
1	Solid surface is covered with water molecules
2	Proteins encounter the solid surface
3	Binding of proteins to surface
4	Progressive modification of adsorbed layer composition: Vroman effect
5	Adsorbed proteins undergo conformation changes

5.1.1.2 Adhesive bonds formation

According to Vitte et al. three theoretical frameworks have been suggested in literature to explain the actual formation of adhesive bonds between cells and surfaces: the DLVO theory, physical chemistry of surfaces and identification of specific molecular interactions [62]. The DLVO theory uses the total potential energy to explain that the ionic atmospheres of two particles approaching each other, begin to overlap and a repulsion force is developed. Only two forces are considered to impact the particle stability, namely the Van der Waal forces and Coulombic forces. The total potential energy is subsequently described as the sum of the attraction and the repulsion potential, resulting in irreversible adhesion at very small distances [71].

Figure 6 shows the DLVO potential energy dependent on the distance between the particles. At large distances, the exponential repulsion vanishes more rapidly than the Van der Waals attraction, which results in an overall attraction. At small distances a repulsive potential barrier must be overcome to reach irreversible adhesion [62]. However, despite the explanatory aspects of the DLVO theory, Vitte et al. concludes that the framework cannot be used to provide an accurate description of cell-surface adhesion, because of incorrect assumptions and a lack of experimental proof [62].

By using physical chemistry of surfaces researchers have tried to explain cell adhesion based on thermodynamic equations, interfacial energies and contact angles between cells and surfaces.

However, Vitte et al. concludes again that this framework is not able to describe the entire cell-adhesion mechanism. Prediction of cell adhesion with a function of physical chemical properties of interacting surfaces was never demonstrated [62].

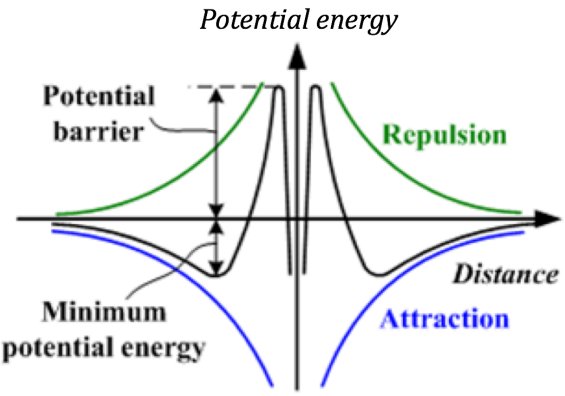

Figure 6: DLVO theory: potential energy dependent on the distance between two approaching particles leading to irreversible adhesion [72].

5.1.2 Factors influencing cell adhesion

In the previous section the different processes involved in cell adhesion are described generally. The next step is to discover which factors are responsible for controlling these processes. This is important knowledge, which eventually may help to get closer to a method preventing cell adhesion. Most parameters that influence cell adhesion are part of the protein adsorption process. These parameters can be divided into three different types: external factors, protein properties and surface properties. All the main factors are described below.

5.1.2.1 Influence of protein properties in protein adsorption

Proteins are composed of all different kinds of amino acids. Unique combinations of amino acids cause an extreme wide variety of existing proteins with different functions. This results in a huge structural and functional complexity, making forecasts of protein behavior and adsorption extremely hard. However, all the different proteins could be classified with respect to their interfacial behavior, considering size, structural stability and composition. Another method is to decompose the complex structures into individual domains of specific properties like hydrophilicity, polarity and electric charge [73]. In protein mixtures the adsorption behavior often is a mixture as well, resulting from an overlap of transport, repulsion processes and adsorption [67]. One of the most cited classifications is the one from Norde. He divided proteins into “hard” and “soft”, based on their adsorption behavior. Hard proteins adsorb on hydrophilic surfaces only under electrostatic attraction. Soft proteins are more easily altered and adsorb on hydrophilic surfaces, not only under electrostatic attraction, but also under electrostatic repulsion due to structural reorientation [74]. However, the tissue composition and the corresponding protein properties cannot be changed during smart electrosurgery. This should just be considered as a fixed parameter and therefore this study will not further elaborate on the influence of protein properties.

5.1.2.2 Influence of external factors on protein adsorption

The external conditions under which the cell adhesion takes place have a decisive influence on the adsorption behavior. The factors with the most influence are temperature, pH, concentration of dissolved ions and concentration of salt. The different effects of varying these factors are summarized in
Table 5.

Temperature Elevated temperatures lead to a release of surface adsorbed water molecules and salt ions and to structural rearrangements inside the proteins. Both result in an increased entropy gain, which is the driving force of protein adsorption. The entropy gain causes accelerated diffusivity of proteins towards the surface, leading to an increased amount of surface adsorbed proteins. Therefore, more proteins are adsorbed at higher environmental temperatures [67, 75, 76].

pH value The environmental pH determines the charge of proteins. Each protein has its own isoelectric point (IEP) at which the protein is neutrally charged. When the pH is lower than the IEP, proteins are positively charged and when the pH is higher than the IEP, proteins are negatively charged. At the IEP repulsions between proteins are minimized, leading to higher packing densities on the surface. Therefore, maximum protein adsorption generally occurs at or near the IEP. Since opposite charges are attracted, it depends on the surface charge whether a protein is better adsorbed at low (positive) or high (negative) pH [67, 77].

Ionic strength The ionic strength refers to the environmental concentration of dissolved ions. As the ionic strength is increased, the lateral diffusivity decreases and resulting in an increasing occupied area per adsorbed molecule. In other words, an increasing ionic strength causes the surface potential to become smaller, leading to less capacity for proteins to be adsorbed. So, the higher the ionic strength, the lower the protein adsorption [67, 78, 79].

Salt concentration Although it was recognized by Hofmeister that salt ions can either promote or decelerate protein precipitation, it has recently turned out to be more difficult than expected to predict the exact effect of salt ions on protein adsorption. Before, it was thought that salt ions were able to (de-)stabilize the native conformation of proteins, influencing their adsorption tendency. Gao et al. found that an increase of salt concentration leads to shielding of the electrostatic interaction, which decreases the adsorption capacity. However, other studies concerning this external factor show contradicting results, so a lot of uncertainties exist. In general, literature tends towards the theory that increasing the salt concentration would lead to a lower protein adsorption [64, 67, 80].

Contact time Xu et al. conclude that protein adhesion forces increase with contact time in seconds to minutes. This is due to surface-induced conformational changes in the proteins. These changes strengthen the binding between proteins and surface [81].

Table 5: Influence of external factors on protein adsorption.

External factor	High/strong protein adsorption	Low/weak protein adsorption	Source
Temperature	High temperatures	Low temperatures	[67, 75, 76]
pH	At IEP and above/below IEP	Above/below IEP	[67, 77]
Ionic strength	Low ionic strength	High ionic strength	[67, 78, 79]
Salt concentration	Low concentration	High concentration	[64, 67, 80]
Contact time	Long contact time	Short contact time	[81]

5.1.2.3 Influence of surface properties on protein adsorption

Surface charge Surface charge is needed to form bindings between proteins and surface particles. A study of Gessner et al. showed a dependence of protein adsorption on the particle surface charge density. The higher the surface charge, the more proteins are adsorbed. However, this change is only of quantitative and not of qualitative nature [67, 82-85].

Polarity Chemical polarity is a physical property causing a molecule to have an electric dipole or multipole moment resulting from an uneven partial charge distribution between various atoms. Polarity is related to other physical properties such as surface tension solubility and melting and boiling points. In polar molecules opposing charges from polar bonds are arranged asymmetrically, which results in a net dipole. Nonpolar molecules have no overall dipole, because they either have an equal sharing of electrons or because there is a symmetrical arrangement of polar bonds. According to Belfort et al. non-polar surfaces destabilize proteins leading to conformational reorientations. This results in rather strong protein-surface interactions and therefore proteins tend to adhere more strongly to nonpolar than to polar surfaces [67, 86].

Wettability Surface wettability is one of the most important factors influencing protein adsorption. A protein can either be hydrophilic or hydrophobic. Hydrophilic molecules are able to dissolve in water, while hydrophobic molecules are water-insoluble. This property is based on the polarity of a molecule. Since water molecules are polar, all polar molecules are soluble in water and are therefore hydrophilic. Nonpolar molecules on the other hand, are hydrophobic. Lee at al. observed that cells adhere more on the hydrophilic (nonpolar) sites of the membrane surface than on the hydrophobic (polar) sites, which may sound obvious considering the close relation between polarity and hydrophilicity [67, 81, 87, 88]. Hydrophobicity of a solid material is often expressed in terms of a contact angle, which is a quantitative measure of the wetting of a solid by a liquid. The contact angle θ is represented by the angle between the solid surface and outer boundary of the liquid (measured through the liquid), as shown in Figure 7. In the case of $\theta > 90°$, the solid surface is hydrophobic, which leads to poor wettability and strong protein adsorption. When $\theta < 90°$ the solid surface is hydrophilic, which leads to a good wettability and weak protein adsorption [89, 90].

Morphology Several studies have indicated that the structure and in particular the nanoscale morphology of the foreign surface can be of influence on cell adhesion, spread, growth and differentiation. Adhesion of connective tissue cells increases at a surface with a rough structure, compared to smooth surfaces. This is because of the small pores of a rough surface that generate conditions for protein nucleation inside the pores. If the surface roughness is increased, both the number of nucleation sites and the volume available for nucleation increase as well. This causes a significant elevation of the amount of adsorbed proteins [91, 92].

Besides the protein properties and the external factors, the surface properties have a large influence on protein adsorption as well and moreover, this process is highly surface dependent. The factors that need to be considered are surface energy, polarity, charge and morphology.

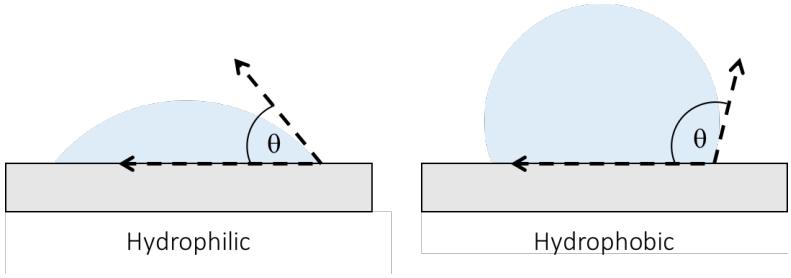

Figure 7: Contact angle between the solid surface and the outer boundary of the liquid. > 90 matches a hydrophobic surface with poor wettability leading to strong protein adsorption, while < 90 matches a hydrophilic surface with good wettability leading to weak protein adsorption [89].

Table 6: Influence of surface properties on protein adsorption.

Surface property	High/strong protein adsorption	Low/weak protein adsorption	Source
Surface charge	High charge	Low or no charge	[67, 82-85]
Polarity	Non-polar	Polar	[67, 86]
Wettability	Hydrophobic	Hydrophilic	[67, 87, 88]
Morphology	High surface roughness	Low surface roughness	[91, 92]

5.2 Blood clotting

In the previous section, we have only considered tissue sticking to the smart electrosurgical knife. However, despite the electrosurgical coagulation effect, there is also blood involved in tissue adhesion. Cutting tissue does not exist without blood loss, triggering a process leading to blood clotting: hemostasis.

5.2.1 Hemostasis

Hemostasis is the first step of wound healing and it represents a dynamic process, which is initiated to stop the bleeding after a blood vessel is damaged. During hemostasis, a blood clot is formed, used to seal the vessel hole until the tissue is repaired. This process is divided into three different steps: 1) vasoconstriction, 2) platelet plug formation and 3) blood clotting [93].

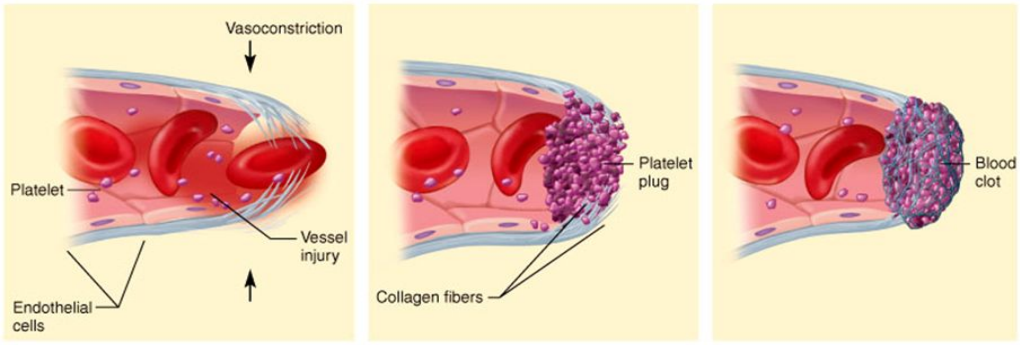

Figure 8: Hemostasis divided into three main steps: vasoconstriction (left), platelet plug formation (middle) and blood clotting (right) [133].

5.2.1.1. Vasoconstriction

Vasoconstriction (Figure 8, left), or vascular spams, is the body's first response to vessel injury. Initiated by local sympathetic pain receptors, the damaged vessels will constrict heavily, reducing the amount of

blood flowing through the vessel which consequently limits blood loss. Vasoconstriction is proportional to the vessel damage and can last minutes or even hours, until a sufficient platelet plug has formed [93].

5.2.1.2 Platelet plug formation

The second step is platelet plug formation (Figure 8, middle), which is activated by adhesive proteins, such as collagen exposed at the damaged site of the vessel. Other major agonists for activation of platelets are ADP, thromboxane A2, thrombin, epinephrine and platelet activating factor [93]. Platelets are small and very simple cell fragments in the blood [94]. The primary function of platelets is to form a hemostatic clot that prevents blood loss and maintains vascular integrity [95]. Therefore, the platelets need to aggregate to each other and to the vessel wall. Normally platelets do not adhere at all, but once they are activated, their shape changes and they become sticky by the secretion of active factors and expression of receptors. These receptors at the surface of the platelet interact with other platelets and with the vessel wall in order to produce aggregation and adhesion. Subsequently, activated platelets also release important chemicals from their storage granules, leading to more platelets to aggregate. In this way, the process is continued in a positive feedback loop. Thanks to inhibiting factors released by the adjacent normal endothelium, the platelet plug is limited to the vessel defect and does not spread to the nearby undamaged vascular tissue [93, 95, 96].

5.2.1.3 Clot formation

The last phase of hemostasis is clot formation (Figure 8, right): the conversion of liquid blood into a solid blood gel. This process results from a triggered chain reaction involving plasma clotting factors. The clotting factors are activated and eventually lead to fibrin formation. The fibrin forms an additional layer on top of the platelet plug to hold it in place. At the same time, red and white blood cells are trapped in the fibrin mesh, causing the plug to be stronger and harder and becoming a blood clot or thrombus. The thrombus stops the bleeding until the tissue at the site of the vascular damage has healed [93, 97]. The outer surface of the blood clot dehydrates and forms a rusty brown crust, called a scab. This scab covers the underlying healing tissue, protecting it from dehydration and infections. As soon as the tissue underneath the scab has been repaired, the scab falls off naturally [98].

5.2.2 Platelet adhesion on foreign surfaces

During a medical procedure involving foreign materials, blood is generally the first body fluid that comes into contact with the material. This is also the case for electrosurgery. Therefore, blood compatibility, which is highly affected by the interactions between blood and a foreign material, is a very important aspect during these procedures [99]. As soon as blood is in contact with a foreign surface, rapid absorption of the blood plasma proteins occurs, leading to platelet adhesion and subsequently to thrombus formation [99-101]. This event typically plays an important role in material associated clotting and represents a significant source of a wide range of clinical complications that are caused by blood-foreign material interaction [99, 102, 103]. Therefore, understanding of the interaction between proteins and material surfaces is essential [99, 101]. A research of O'Brien studies platelet adhesion to glass. He states that the rapid adhesion of platelets to glass is independent of clotting, but dependent on calcium and that salicylates and procaine inhibit the adhesion of platelets to glass [104].

Many conditions affect the interaction between platelets and foreign surfaces. For example, the type of surface, the conditions of the blood flow and the absorbed proteins. However, platelets never adhere directly to a foreign surface. First plasma proteins are adsorbed almost immediately [96]. Surfaces absorbing proteins that activate platelets, is the main problem in platelet adhesion. Although blood contains all kinds of proteins that can be absorbed by material surfaces, one in particular has been identified as one of the most important proteins to induce a platelet adhesion response: fibrinogen (Fg). It is widely stated in literature that both the amount and the conformational state of fibrinogen affect the platelet adhesion response [105, 106]. This last statement implies that adsorption of Fg leads to a conformational change that exposes hidden sites of Fg that are recognized by platelet receptors [103].

5.3 Discussion and conclusion

So far, it is assumed that tissue debris consists of necrotic tissue cells, living tissue cells and blood cells. Each of these components has its own way of sticking to the electrosurgical knife. Three mechanisms are suspected to be responsible for tissue adhesion during electrosurgery: char formation for necrotic cell adhesion, general cell adhesion for living cell adhesion and hemostasis for blood adhesion. Each mechanism is composed of several processes of which some are essential for tissue adhesion. It is therefore suggested that preventing carbonization during char formation, protein adsorption during general cell adhesion and platelet adhesion during hemostasis will lead to the prevention of tissue debris adhesion.

6. Preventing debris adhesion

In the previous chapters, three different kinds of tissue were identified that are assumed to adhere on the optical fibers of a smart electrosurgical knife: necrotic tissue, living tissue and blood. The aim of this chapter is to explore different kinds of existing methods to prevent either tissue adhesion in general, or one or more of the responsible processes. A lot of different forms of material adhesion and methods to prevent this specific adhesion are discussed in literature. For this study, it was chosen to distinguish between methods in medical care, nature and society.

6.1 Examples from medical care

This first paragraph is about the available methods to prevent tissue adhesion in medical care. However, the last section of this paragraph is different. This section introduces an additional tissue adhesion problem that has not been solved yet, but could be in the future by the same method that will solve tissue debris adhesion.

6.1.1 Endoscope visibility

Currently, the most optimal method to prevent tissue adhesion during endoscopic procedures seems to be surface modification by the application of an antifouling coating on the camera lens. Sunny et al. demonstrate the application of a liquid-infused surface coating onto the endoscopic lens during bronchoscopy (endoscopy performed in the lungs) performed in vivo on a porcine model. The coating strongly repels sticky biological secretions and improves the operative field visibility. Lens cleaning times are either unnecessary or at least 10-15 times shorter compared to an untreated endoscope [107].

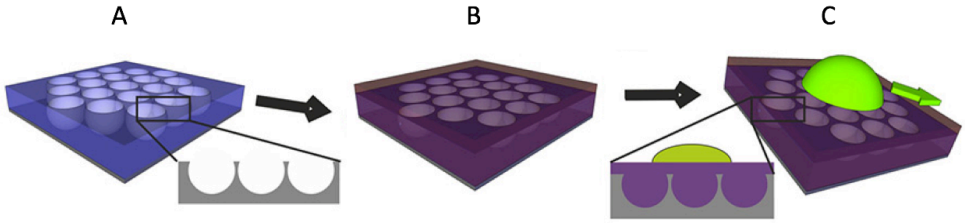

Figure 9: Schematic overview of the liquid-infused surface coating. A) Silica nanoparticles are deposited in order to create a glass honeycomb-like structure with craters. B) Subsequently, the surface is infused with a medical-grade silicone oil binding to the honeycomb cells and forming a stable liquid film. C) The liquid film repels droplets of both water and oily liquids [108].

The coating developed by Sunny et al. is based on the Slippery Liquid-Infused Porous Surfaces (SLIPS) technique, which prevents a wide variety of materials from sticking to surfaces. Although the application of SLIPS onto a surface makes it self-cleaning, this technology does not have the ability to survive the in-body environment and the physical stress of the endoscope surface. Therefore, SLIPS had to be modified in order to qualify for improving the optical field of view of camera-guided endoscopes. First, silica nanoparticles are deposited onto the glass camera lens. The silica layers create a rough, porous surface filled with caverns. Subsequently, the surface is infused with a medical-grade silicone oil, which fills the surface cavities. As a result, a stable lubricant layer is formed on the surface and creates a dynamic slippery barrier. This barrier protects the surface against direct contact with the body fluids, which inhibits adsorption of various contaminants like bacteria and proteins [107, 108].

The liquid-infused surface coating satisfies the general requirements for coatings of medical devices saying that the coating must be conformal, mechanically robust, biocompatible and antimicrobial. Besides, the coating meets the more specific requirements as well: it is highly transparent, extremely resistant to body fluid adhesion and it has antifogging properties. Additional beneficial characteristics are enhanced damage tolerance and self-healing capabilities. Sunny et al. emphasize that this specific technology is not only applicable in medical procedure, but in other industries as well. A wide variety of scenarios could benefit from the improved visibility, reduction cleaning times and lower overall costs [108].

6.1.2 Medical implants

One of the most common solutions of this moment for tissue adhesion on medical implants, is the development of novel antifouling materials to resist protein adsorption and cell adhesion. During this procedure, an antifouling polymer is grafted onto the surface of the implant. The most extensively studied antifouling polymer is polyethylene glycol (PEG). This specific polymer is water soluble, has low toxicity and has been widely used in medicine before. When grafted onto a surface, PEG reduces adsorption of proteins, cells and bacteria. Numerous studies demonstrated that, among other parameters, the grafting density, the hydrophilicity, the chain formation and the chain length play important roles in resisting protein adhesion [109].

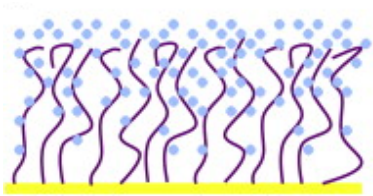

Figure 10: Schematic illustration of chain hydration and chain flexibility of PEG-based polymers [154].

The antifouling ability of PEG-based coatings is correlated with a hydration layer near the surface: a strongly bound water layer forms both a physical and energetic barrier that prevent proteins from absorbing on the surface. Aside from the water layer, polymer chain flexibility also plays an important role. When a protein approaches the PEG-coated surface, compression of the chains causes steric repulsion due to unfavorable decrease in entropy. This results in protein adsorption resistance. If surface hydration and steric repulsion work together, the best antifouling ability is achieved [110].

6.1.3 Laser surgery

In order to prevent the adhesion problem during laser surgery, active cooling of the laser fiber is employed. Cooled catheters make use of a double-lumen design to circulate room-temperature water around the fiber during use. This system prevents carbonization on and around the laser fiber.

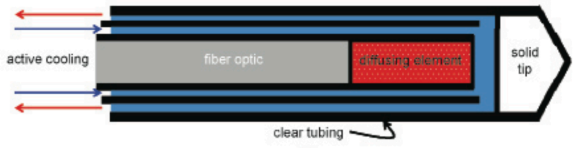

Figure 11: LITT laser fibers utilize actively cooled catheters to prevent tissue carbonization. Room-temperature water is running around the optic fiber in a clear tubing to actively cool the solid tip [163].

6.1.4 Introduction to Spectranetics

As announced in the introduction of paragraph 6.2, this section is a bit different from the previous ones. Instead of an example of an adhesion problem in medical care, this section describes an additional problem similar to the problem of tissue debris adhesion during smart electrosurgery. In this case, tissue

adhesion occurs during use of Spectranetics laser devices. Solving tissue debris adhesion during electrosurgery could possibly solve the Spectranetics problem as well. Both the smart electrosurgical knife and the Spectranetics laser devices are under development at the Philips in-body department. From now on, Spectranetics will therefore also be considered every now and then in the search for a method to prevent tissue debris adhesion.

Spectranetics is a cardiovascular health company focusing on the ongoing management and maintenance of pacemakers, implantable cardiac defibrillators and leads that connect them to the heart. In August 2017, Philips completed the acquisition of the Spectranetics Corporation and took over this growing company. According to F. van Houten, CEO of Royal Philips, the ultimate goal of the take-over is to deliver enhanced care for patients by enabling clinicians to decide, guide, treat and confirm the appropriate cardiac and peripheral vascular treatment [111]. The products of Spectranetics are used to treat arterial blockages in both the heart and the legs and in the removal of pacemaker and defibrillator leads. Therefore, Spectranetics offers lead management, coronary and peripheral intervention.

6.1.4.1 Lead management

The lead management product line of Spectranetics includes mechanical sheaths, laser sheaths, dilator sheaths and accessories for the removal of pacemaker and defibrillator cardiac leads. Leads may need to be removed for several reasons including lead or device infection, manufacturer advisory or lead damage. The products of Spectranetics ensure that this removal is performed in a safe and precise manner [111]. Due to the body's natural healing process, often strong attachments are created between the lead and the wall of a vessel or heart chamber. So, when a lead is removed, it first must be detached. This procedure requires skill and experience and it relatively risky because of the vulnerability of vital body structures involved. The laser sheath of Spectranetics consists of a flexible tube that passes over the lead and surrounding it. A ring of tiny lasers at the tip of the sheath, gently vaporizes the scar tissue attachments, freeing the lead from the body so that it can be removed safely [112].

6.1.4.2 Vascular intervention

The vascular intervention product line includes a variety of excimer laser catheters for ablation of blockages in arteries, support catheters to facilitate crossing of peripheral and coronary arterial blockages and guidewire retrieval devices used in peripheral arterial blockages treatment. Arterial blockages are most often caused by atherosclerosis, a disease in which the inside of an artery narrows due to the buildup of plaque. The general treatment of atherosclerosis consists of two procedures: first the plaque needs to be removed and then a stent is placed to prevent new plaque buildup. The excimer laser catheters of Spectranetics are used to clear the vessel by modifying plaque and to provide easier stent delivery [111]. Excimer lasers use a mixture of a rare gas and halogen as an active medium to generate pulses of short wavelength: high energy ultraviolet (UV) light. This light elevates the local tissue temperature, which causes cell rupture disrupting the obstructive intra-vascular material. During this process tissue fragments, smaller than a red blood cell, are released and are subsequently absorbed by the reticula-endothelial system. In this way microvascular obstruction is avoided [113].

While using the different laser devices of Spectranetics, the tips of the small lasers are constantly in contact with tissue. Due to elevated temperatures, the tissue is heated and sticks to the laser tips inhibiting the proper functioning of the device. So far, no method has been found to prevent tissue adhesion during use of the laser devices of Spectranetics.

As mentioned before, Spectranetics has recently been taken over by Philips and only by then the tissue adhesion issue was identified. Notice that this problem is very similar to the tissue debris adhesion problem. Since both the smart electrosurgical knife and the Spectranetics laser devices are under

development at the Philips in-body department, it might be possible that there is one solution solving both issues.

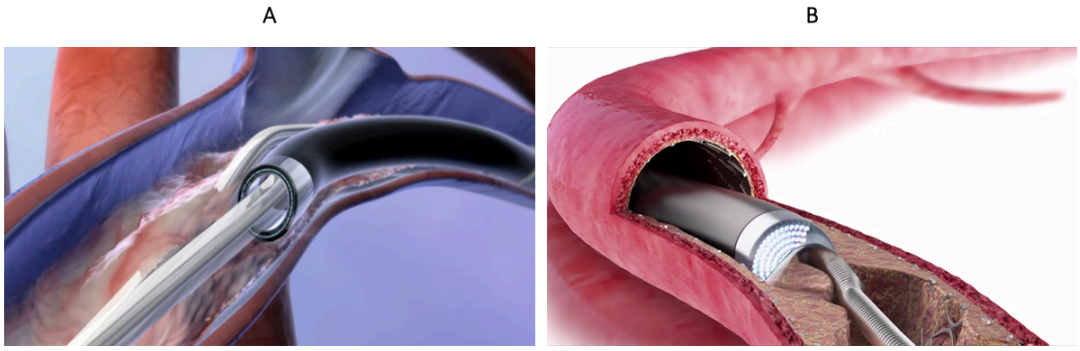

Figure 12: A) Using a Spectranetics Laser Sheath to free the lead from scar tissue. B) Using a Laser Atherectomy Catheter to clear a vessel from plaque buildup [162].

6.2 Examples from nature

This paragraph is about the available adhesion prevention methods in nature. Over the last decades, researchers have greatly studied natural phenomena, wishing to understand and exploit the different attributes as inspiration for the imagination and creativity of scientist.

6.2.1 Gecko detachment

In this particular example, the adhesion of the gecko tissue on the surface of the wall or ceiling is not really a problem, but it is more of a skill. However, as mentioned before, in order to be able to walk across the surface, quick detachment is required. So, when we approach this example in that way, strong adhesion is an issue anyway and a solution is needed that enables the gecko to not only stick to walls and ceilings but walk really fast as well. In order to detach its foot from the substrate, the gecko simply rolls his toes out again. The setae return to their initial free state with the shaft angle being 30° and the spatulae will come off in sequence from right to left (Figure 13-C) [114]. For different motions, geckos can control their feet and toes at different positions, angles and stresses to acquire the desired friction and adhesion forces

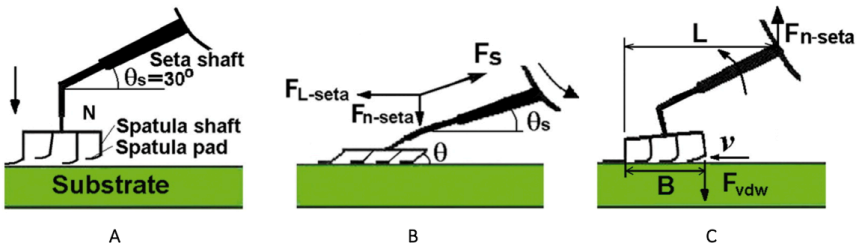

Figure 13: The role of gripping geometry in the adhesion/detachment mechanism of a gecko. A) First the seta is loaded vertically. B) Proximal dragging (rolling toes in) decreases the shaft angle and increases the adhesion. C) Rolling toes out increases the shaft angle and detached the spatulae [114].

6.2.2 Shark skin

Another example from nature described in literature is the antifouling property of shark skin. Researchers believe that the antifouling property of a shark's skin is due to the complicated micro rib-structure, the flexion of scales and due to a mucous layer [115]. According to Peng et al. the skin structure is made up of placoid scales, that consist of rectangular bases with tiny spines poking up from the surface [116]. This structure results in micron grooves in the epidermis of the shark skin, that

effectively prevent marine lives from adhering. The skin scales are called dermal denticles and they are covered with riblets oriented parallel to the swimming direction. By lifting the riblets during swimming, the total shear stress is reduced and low drag is achieved. Lower drag allows the water directly next to the shark skin, to move faster. This reduces settlement time, making it very difficult for marine lives to adhere. Furthermore, the mucous found on the shark skin has a lubricating effect stimulating the antifouling benefits even more [116-118].

6.2.3 Lotus leaves

According to Ensikat et al. the lotus effect is caused by a combination of two different optimized features: the micro- and nanostructure of the surface and the chemical composition of the wax coating covering the leaves. This makes that each lotus leaf is superhydrophobic, which is the basis for its self-cleaning ability [119]. On a superhydrophobic surface, water drops sit up high in order to minimize their contact area with the material. This results in a contact angle between the surface and the water drop of more than 150° [120]. The greater the contact angle, the more hydrophobic the surface. Neinhuis et al. measured an average contact angle of 162° on the lotus leaves.

The hierarchical, rough surface structure of the upper epidermis of the leaves is complex. There are two levels: mound-like structures on micro-scale and hair-like structures on nano-scale. Together they form some kind of bumps, called papillae, that cause water to form spherical droplets with very little surface contact, rolling across the surface very easily. It is believed that the two-level roughness facilitates the rolling behavior of the drops by amplifying the apparent contact angle [119, 121, 122]. Both the lower and the upper side of the lotus leaf are covered with wax tubules, but the composition is different. Since the upper side seems to have a higher self-cleaning ability, the focus will be on that side. The wax tubules are very short and thin, but the density is very high. This means that the spacing between the tubules is quite small, which leads to a higher-pressure necessary for the intrusion of a water droplet between the tubules. The chemical composition of the wax gives an explanation for the different properties. For example, a high content of nonacosanediols provides extraordinary characteristics like a relatively high melting point of 90 to 95°C. For predicting the exact behavior of water repellent surfaces, precise knowledge of the complete chemical composition and the molecular structure of the wax is essential [119].

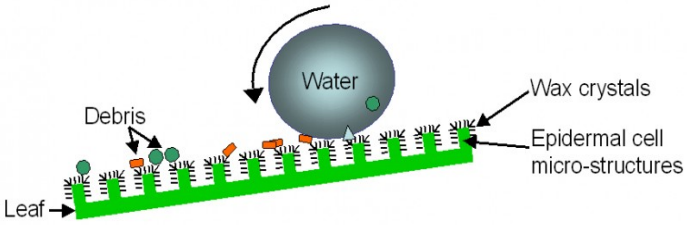

Figure 14: Schematic representation of the lotus effect - the self-cleaning behavior of the lotus leaf [172].

6.3 Examples from society

This paragraph is about the available methods in society. In order to narrow down the large number of examples for this sector, only the most relevant methods are selected.

6.3.1 Food adhesion on cookware

The most common method to prevent food adhesion during cooking is the use of a non-stick coating, in particular polytetrafluoroethylene (PTFE), known by the DuPont Company trademark Teflon. Teflon is a plastic polymer consisting of long chains of carbon and fluorine atoms. Between carbon and fluorine, extremely strong cohesive forces exist which causes the chains to firmly stick together. However, there are practically no adhesive van der Waals forces between the Teflon chains and other materials. This leads to frictional forces close to zero, which prevents any material from sticking to the Teflon coating.

Besides, Teflon has superior chemical and thermal properties and is used in a wide variety of other applications such as aerospace, computers and clothing [123-125].

6.3.2 Marine biofouling

Over the years a wide variety of antifouling coatings has been developed to control marine biofouling. However, recent environmental toxicity issues related to the use of toxic antifouling coatings have shifted the focus of research to environmentally friendly alternatives, such as foul-release technology [126]. In general, foul-release coatings are based on silicone elastomers that are completely different from other products typically used in the marine industry [127]. Moreover, this type of coating does not use copper (originally used in antifouling) or any other metal toxicant. Instead, the unique surface composition of foul-release coatings creates a surface to which fouling adhesion is very difficult. Foul-release coatings employ a physical rather than a chemical way of fouling reduction [128]. The low surface tension, low roughness and high flexibility of silicone elastomers ensure a weak attachment of fouling organisms. Organisms that do succeed in adhering, are easily removed by moving water [127]. Due to the application of small modifications in the composition of the foul-release coating, a wide variety of antifouling coatings exist. Dependent on the purpose of the coating, a specific composition with corresponding properties must be chosen.

6.3.3 Fouling heat exchangers

Innovative coating technologies have been proven to effectively prevent fouling and improve the efficiency of heat exchangers by up to 50% [129]. Researchers at the Leibniz Institute for New Materials recently introduced a new nanocoating that reduces the effort required for cleaning. In these coatings, antiadhesive and antimicrobial qualities are combined. The antimicrobial qualities are achieved by using colloidal copper in the coating. Oxygen or water present in the milk or juice lead to the creation of copper ions from the copper as soon as the liquid comes in contact with the coating. These ions have an antimicrobial effect that prevent microbes from adhering to the surfaces of the heat exchanger. The antiadhesive properties are achieved by using hydrophobic compounds that are similar to Teflon (discussed in paragraph 6.4.1). These compounds prevent the formation of biofilm and allow residues to be transported out more easily. The coating can be used on stainless steel, alloys, titanium or aluminum and by adapting individual constituents, responding to the particular requirements of interested users is possible [130].

6.4 Discussion and conclusion

This chapter has shown that adhesion is not only a problem in medical care, but in a wide variety of other sectors as well. Over the years, lots of research has been done to come up with tailor-made solutions for all the different, specific adhesion situations. The most relevant examples were described and compared in the prior literature study. The evaluation of the different methods is also to be found in appendix C.

Two different types of evaluations were performed in order to properly compare the nine prevention methods. Both evaluations were based on four main criteria being: 1) the method should prevent tissue adhesion, 2) the method should ensure constant optical measurements after calibration, 3) the method should be biocompatible and 4) the method should be functional at temperatures reaching 500°C. Both evaluations resulted in the same four methods showing the most potential: 1) liquid-infused coating used for endoscope visibility, 2) PEG-based coating used for medical implants, 3) Teflon coating used for cookware and 4) nano-coating used for heat exchangers. These four methods may be subject to further research. It should be noted however, that the Harris Profile evaluation is quite subjective since the scores are based on the opinion one person only.

II. RESEARCH PHASE 1

DESIGN DIRECTIONS

The goal of phase is to describe the different design directions and select the most promising one. Some of these directions have been described before, others have had no attention within this research so far. In chapter 7 the different design directions are compared, so that a well-founded selection can be made. Chapter 8 elaborates on the selected design direction.

7. Design directions

Based on conclusions found in literature and recommendations read in previous master theses, it is assumed that tissue debris contamination is the main factor causing DRS signal deterioration. Therefore, this chapter describes three design directions for solving tissue debris contamination on optical fibers during smart electrosurgery. The principles, unique elements and the benefits and limitations of each direction are described. At the end of the chapter, the most promising direction is selected to continue this research with.

7.1 Design direction 1: Preventing tissue debris contact

7.1.1 Principles

The main principle of the first design direction is that contact between the optical fibers and tissue debris formed during use of the electrosurgical knife is prevented completely. By preventing all contact, tissue debris does not get the chance to adhere to the surfaces of the optical fibers. Initially, this might seem like an easy solution. However, in practice the implementation of this idea is much more complicated and very broad. A wide variety of actual solutions exists within this design direction. However, all solutions are based on creating a physical distance between the fibers and the tissue debris, which basically means that the actions 'cutting' and 'margin assessment' need to be separated and cannot be executed simultaneously.

In her master thesis, Mollerus came up with three different concepts preventing contact between optical fibers and tissue debris. All three concepts consist of an electrosurgical knife with an integrated mechanism to hide and present the optical fibers at the surgeon's request. The principles of the mechanisms are different for each concept. The concept that was selected as the most promising one is called 'sliding' and contains a presenting mechanism based on the sliding principle of a Stanley knife or a 6-color pen. Sliding a button forward presents the optical fibers and enables DRS margin measuring, while sliding the button backwards hides the optical fibers. As soon as the fibers are hided, the electrosurgical knife may be used for cutting again. Notice that this concept inhibits to cut and measure margins at the same time.

7.1.2 Unique elements, benefits and limitations

Unique elements: Contact between tissue debris and the fiber surface during electrosurgical cutting is prevented completely, which leads to complete elimination of the influence of the amount of tissue debris formation on the DRS signal.

Benefits: The risk of tissue debris contamination on the surfaces of the optical fibers is considerably low, since contact during cutting between the two materials is prevented completely. Furthermore, the amount of tissue debris formation does not have any influence on DRS margin measurements.

Limitations: The actions 'cutting' and 'margin assessment' cannot be executed simultaneously, which is at the expense of the current workflow. The same applies to the fact that an additional action is required within the electrosurgical procedure in order to assess margins.

7.2 Design direction 2: Removing tissue debris contamination

7.2.1 Principles

The second design direction is about tissue debris removal after contamination. The principle of this design direction is actually based on simply cleaning the surfaces of the optical fibers of the smart electrosurgical instrument during and after the procedure. In contrast to the other two design directions, the principle of this direction solves the adhesion problem afterwards. Removing tissue debris from the fibers might be done in each possible way, just as long as the signal intensity of the fiber is (partly) restored.

The method currently applied to remove tissue debris from the blade of the electrosurgical knife, relies on principles similar to this design direction. Instead of preventing tissue debris formation or adhesion, the debris is simply removed from the blade during surgery. It has become one of the standard procedures within the electrosurgical workflow. More information on the current cleaning process of the electrosurgical knife can be found in the literature study prior to this master thesis and the master thesis of Mollerus [9, 55].

7.2.2 Unique elements, benefits and limitations

Unique elements: The current electrosurgical workflow is hardly affected by solutions within this design direction. Another unique element, is that the tissue debris contamination problem is solved after adhesion. Furthermore, in contrast to solutions within design direction 1, margin assessments can be performed continuously and may be combined with cutting simultaneously, until tissue debris contamination disturbs the signal.

Benefits: The current clinical workflow is hardly affected by a solution from this design direction. Furthermore, 'margin assessment' and 'cutting' may be performed simultaneously.

Limitations: Cleaning a surface often leads to some kind of damage (scratches) to the surface. Especially in the case of a lens, this damage might very likely be crucial for its functioning and is therefore highly undesired. Damage to the tip of the optical fiber could lead to a disturbed DRS signal. Furthermore, the research of Mollerus has shown that the electrosurgical knife needs cleaning every two minutes. Assuming that the optical fibers need a similar amount of cleaning, the solutions within this design direction would generally take quite some effort and moreover, would be very time consuming. Also, cleaning methods that are currently used for removing tissue debris from the blade of the knife do not guarantee a complete recovery of the capacity of the instrument. The research of Mollerus showed that the intensity of the DRS signals was restored to a maximum of only 43% of the initial intensity after thorough cleaning. This observation indicates that removing tissue debris contamination from the surface of the optical fiber tip is not a sufficient solution on the long term.

7.3 Design direction 3: Preventing tissue debris adhesion

7.3.1 Principles

The third design direction prevents tissue debris contamination on optical fibers while maintaining contact between the two materials. This would imply continuous margin assessment during electrosurgical cutting, without disturbed DRS signals as a result. An often-suggested example of such a solution is the use of a coating. Applying an anti-adhesive coating to the surface of an optical fiber, inhibits bond formation between tissue debris and fiber material. Once tissue debris is unable to stick, it will slip off of the surface, resulting in a clean lens and a clear sight at all times.

7.3.2 Unique elements, benefits and limitations

Unique elements: The current electrosurgical workflow is affected minimally: no additional actions are required to keep the tip of the optical fiber clean. Furthermore, the optical fibers are allowed to interact with tissue at all times, which means that margin assessment can be performed continuously.

Benefits: Solutions within this design direction eliminate the influence of the amount of tissue debris on DRS measurements. Furthermore, the current workflow is affected minimally. No additional actions are required besides the normal procedures involved in electrosurgery. Also, margin assessment may be performed continuously and during use of the electrosurgical knife.

Limitations: Solutions within this design direction need to meet a lot of different requirements, because they are in direct and constant contact with tissue debris that is elevated to high temperatures. It will be a challenge to achieve such a broad solution.

7.4 Discussion and conclusion

In the previous paragraphs three different design directions and their benefits and limitations were described. The goal of this paragraph is to compare the three design directions and eventually select the direction with the most potential to continue this research with. In order to evaluate the different directions in a quick and systematic way, the vALUe (Advantages, Limitations and Unique elements) method is used [131]. According to the Delft Design Guide using this method gives more insight into valuable directions for solution finding and provides a better understanding of interesting and promising ideas. By writing down the design directions in terms of advantages, limitations and unique elements, further selection is made easier.

Table 7 summarizes all unique elements, benefits and limitations of the three different design directions. Listing these characteristics, enables comparison of the three directions, leading to insight in the relative amounts of benefits and limitations. These amounts quickly reveal the most attractive design direction. The number of unique elements on the other hand, indicates the level of originality of the design direction. Whether a high or low level of originality is preferred for a design direction, completely depends on the content of unique elements.

Based on the amounts of benefits and limitations provided in Table 7, it may be concluded that design direction 2 is the least attractive one with only one benefit and four limitations. Design direction 3 on the other hand, has the most benefits, the least limitations and the most interesting unique elements. Therefore, design direction 3: *preventing tissue debris adhesion* is selected as the most promising direction to continue this research with. Note that this does not necessarily mean that the other two design directions have no potential at all. If the final solution is not to be found within design direction 3, design direction 1 and 2 might be explored further to search for more interesting solutions. The current research, however, will focus on solutions to prevent tissue debris adhesion during smart electrosurgery.

Table 7: The unique elements, benefits and limitations of all three design directions. The more benefits and the fewer limitations, the more attractive the design direction.

#	DESIGN DIRECTION 1 *No contact*	DESIGN DIRECTION 2 *Removing debris*	DESIGN DIRECTION 3 *Preventing adhesion*
		UNIQUE ELEMENTS	
1	Interaction between tissue and fiber eliminated	Limited interaction between tissue and fiber	Unlimited interaction between tissue and fiber
2	No simultaneous cutting and margin assessment possible	Limited continuous margin assessment	Unlimited continuous margin assessment
3	Contamination evaded	Relatively low impact on current workflow	No additional procedures required
4	-	Contamination solved after adhesion	Contamination prevented
		BENEFITS	
1	Low risk of tissue debris contamination	Relatively low impact on current workflow	Simultaneous cutting and margin assessment
2	Influence of tissue debris amount eliminated	-	Unlimited continuous margin assessment
3	-	-	Relatively low impact on current workflow
4	-	-	Influence of amount of tissue debris eliminated
5	-	-	No additional procedures required
		LIMITATIONS	
1	No simultaneous cutting and margin assessment	High risk of fiber damage	Large design development challenges
2	Additional procedures required	Permanent loss of signal intensity	-
3	Relatively high impact on current workflow	Additional procedures required	-
4	-	Use is relatively time consuming	-

8. Surface engineering

In the previous chapter, design direction 3: *preventing tissue debris adhesion* was chosen as the most promising direction to continue this research with. Literature shows that the most common way to influence the interaction between a foreign surface, such as the optical fiber tip, and tissue is to apply a technique called surface engineering.

Material surface engineering enables modification of solid materials and biological responses through changes in surface properties [132]. Surface engineering has especially become popular in the field of biomaterials in order to improve the functionality of a medical device, without the necessity to develop new expensive materials, which is very time-consuming [68]. Because tissue debris only comes into contact with the outermost atomic layers of the DRS fibers, surface modifications should be enough to influence the interaction between the two materials. Approaches to modify surface properties include the application of coatings, molecule binding, chemical reactions and etching [68, 132]. Coatings have the benefit of being able to provide a surface with properties completely different from those of the unmodified material. Surface engineering techniques are generally classified according to the surface properties that are being altered: physical and chemical. Specific functionalization can be established by combining different techniques [68]. Since the goal of this research is to prevent tissue debris adhesion, this chapter will only focus on those surface engineering techniques that may contribute to this particular function.

In general, one can choose between two strategies to reduce protein adsorption at surfaces: designing a surface that is completely non-fouling, or allowing the adsorption of some specific proteins to the material surface [133]. Designing a surface that prevents adhesion of all proteins is preferred in this research. However, so far it has been difficult to achieve this due to the large number of proteins that exist *in vivo* and their structural and chemical diversity. However, some promising methods have been developed in the past few decades. This chapter describes some examples of both physical and physiochemical surface modifications. This information might be used as input for the design concepts.

8.1 Physical surface characteristics

Physical surface structure is among the factors directly influencing the interaction between a surface material and cells [68, 132]. Over the last decades, research has been done to the effect of all kinds of surface morphology on the adhesion of cells to foreign surfaces. This paragraph describes examples of physical surface modifications used to decrease tissue adhesion.

8.1.1 Surface micro- and nanopatterning

Nanotechnology has entered the biomedical field as it became clear that surface features in the nanoscale can influence cellular events such as adhesion [68]. Several methods have been developed to produce materials with nanoscale-controlled surface properties in terms of chemistry, topography and micromechanics. Texturing a material surface with micro- or nanoscale architecture is a complementary approach explored to control protein adsorption [133]. It has been proven that protein adsorption might be tuned by designing a material with appropriate surface roughness or curvature. Roach et al. showed that the surface curvature can influence both protein binding and its subsequent conformation [134]. A limitation to surface micro- and nanopatterning is that all different architectures tested so far only prevented binding of a small subset of proteins [133]. Currently, it remains unclear whether a generic surface roughness will be able to prevent all proteins from binding.

8.1.1.1 Surface attachment points

Literature shows that irregularities in polymeric surfaces promote adhesion and biofilm formation, while ultra-smooth surfaces on the other hand inhibit adhesion and biofilm formation [135]. This effect is explained by the fact that rough surfaces provide a greater surface area with more favorable sites for cellular colonization. One theory about attachment points between liquid and solid explains the effect of surface topography on cellular adhesion [136]. Theoretically, a cell has the highest amount of attachment points when it perfectly fits in the notches of the microstructure. However, when the cell is slightly larger than the microstructure wavelength, it could have only two attachment points (see Figure 15). This means that in general, surfaces with fewer attachment points are better resistant to cell adhesion.

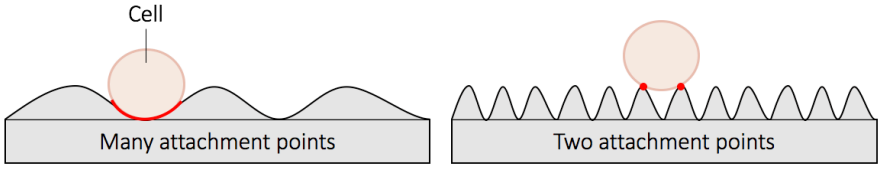

Figure 15: Schematic representation of correlation between cell size and wavelength of the microstructure. Based on [136].

8.1.1.2 Surface superhydrophobicity and superhydrophilicity

As described before, cellular adhesion starts with an initial adsorption of proteins on a foreign surface. Strategies to prevent this protein adsorption often include superhydrophobic surfaces [137]. These surfaces are inspired by the lotus leaf (described in chapter 6.2.3 Lotus leaves) and are characterized by a water contact angle $\theta > 150°$ and a low sliding angle [138]. Superhydrophobic surfaces are created by the application of nano-roughness, causing a relatively small contact area between a liquid and a solid surface. When a superhydrophobic surface is in contact with water, air is maintained at the liquid-solid interface, enclosed by water and the nano-roughened surface (Figure 16) [133].

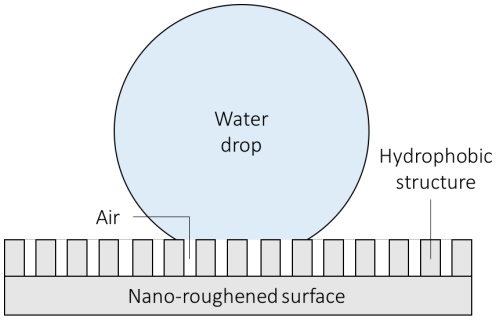

Figure 16: Schematic representation of a water drop on contact with a superhydrophobic surface. Based on [133].

This layer of air limits the available water-solid surface area, causing a decrease of the total area available for protein binding. This leads to less protein bonds between the water and the solid surface, which in turn leads to a relatively weak adhesion. However, superhydrophobic surfaces still suffer from a weak durability due to its micro- and nanostructures and fast degradation of surface chemistry [135]. This means that after a while the surfactant properties of proteins lead to loss of the air layer, which causes the amount of protein binding to increase again [133]. It is therefore very important to consider the required duration for the superhydrophobic surface to be effective. Furthermore, note that, in contrast to superhydrophobicity, mild hydrophobicity ($90° < \theta < 150°$) does not always reduce cellular adhesion. Besides the reduction of protein binding, superhydrophobic surfaces are also being explored for their potential use in preventing material-blood interactions [133]. Several studies have reported successful prevention of platelet adhesion and activation using superhydrophobic surfaces *in vitro* [139-144]. The decrease in platelet activation would be due to a decrease in protein adsorption and the

presence of entrapped air, just like the mechanism described in Figure 16. However, blood compatibility of superhydrophobic surfaces is only observed for relatively short periods of time of less than two hours, after which materials start to adsorb proteins and cells after all [133]. In the case of tissue debris adhesion, this would not be a problem, because the DRS fiber and the tissue are in contact for several minutes only.

In contrast to superhydrophobicity, superhydrophilic surfaces are also known for their self-cleaning abilities [145]. Superhydrophilicity is the opposite extreme of superhydrophobicity in term of wettability and it is generally defined as a surface exhibiting a water contact angle of <10 °. On such surfaces, water droplets spread very quickly and the water runs off the surface with considerable velocity, creating no streaks. During spreading, the water droplets go beneath the contaminants adhering to the surface, moving them out and washing them away (see Figure 17). However, although a thin film of water created on the surface evaporates rapidly, the surface may remain wet for a longer period compared to a superhydrophobic surface, which is undesirable in some cases.

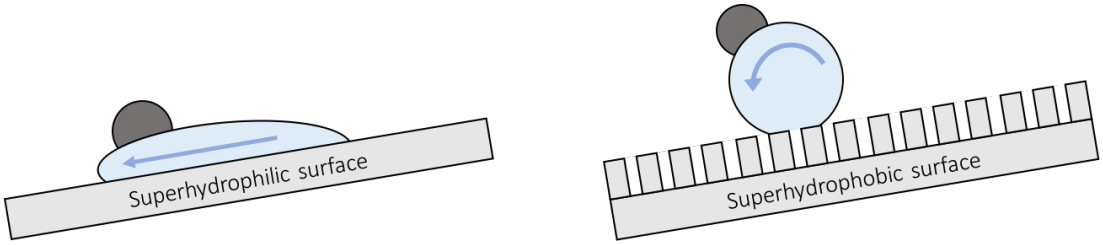

Figure 17: Self-cleaning property of superhydrophilic (left) and superhydrophobic (right) surface.

8.2 Physicochemical surface characteristics

Examples of physicochemical characteristics that can be altered are surface energy, surface charge and surface composition [132]. The aim of these kind of modifications is to change both the material and the biological responses. This paragraph describes the physiochemical surface modifications that influence tissue debris adhesion on foreign solids.

8.2.1 Surface energy

Surface energy results from non-symmetric bonding of solid surface atoms in contact with a vapor [146]. The dimension of surface energy is energy per unit area, which is an important indicator of surface contamination. Surfaces with a high surface energy will try to lower the energy by adsorbing low energy materials, such as hydrocarbons. In general, surface energy is measured by the contact angle method, which was explained before. High surface energy leads to a large contact angle, indicating low wettability (hydrophobic surface). Low surface energy leads to a small contact angle, indicating high wettability (hydrophilic surface).

8.2.2 Surface charge

Surface charge typically is the result of atom substitution in a crystal structure, defects, broken bonds or the ionization of certain surface groups. This property affects the distribution of ions in the surrounding interfacial region, which results in an increased concentration of counter ions close to the surface [135]. Surface charge has been discovered to influence adhesion of cells to solids [147]. In general, it was discovered that negative charged surfaces increase cell adhesion, while positively charged surfaces inhibit cell adhesion. This means that opposite charges cause opposite effects. However, the actual dependence of cell adhesion on the surface charge of a material, is not yet accepted because of a lack of sound evidence.

8.2.3 Surface composition

The molecular composition of a surface dictates the biological system response in terms of protein adsorption, cell adhesion and subsequent events [68]. Furthermore, it has been found that the presence of nonpolar groups in the chemical composition of a material, may inhibit cellular attachment, cell growth and function. One way to change the chemical composition of a surface, is ion implantation [132]. This method has been used to modify both material and biological responses. During ion implantation, high-energy ions impact the surface and initiate a collision cascade. This interaction between ions and the surface causes chemical changes and structural changes are induced by the energetic species. For example, implementation of silver ions has shown to provide surface antimicrobial activity for catheters. Another way to change the chemical composition of a surface, is macromolecule grafting onto the material [132].This method leads to more dramatic changes in surface chemistry. For example, grafting of polyethylene oxide onto a material, has shown to reduce protein adsorption and, subsequently, cell adhesion. Methods that use immobilization of surface molecules to resist protein adsorption, such as PEG and zwitterion, have demonstrated great anti-adhesive abilities and are generally regarded as the standard approach for anti-adhesion coatings [148].

8.2.3.1 PEG-based surfaces

The most widely used method for preventing bioadhesion is characterized by the use of polyethylene glycol (PEG) polymers [149]. Grafting a large number of flexible hydrophilic PEG chains off of a material surface, creates a brush structure at the surface. Due to their hydrophilicity, the PEG polymer chains trap water at the material interface. As soon as a protein binds to this interface, the brush-water structure compresses leading to expulsion of water molecules. The resulting energy barriers exceed the enthalpy term associated with protein adsorption, therefore preventing both protein adsorption and the consequential tissue adhesion. Recent studies have shown that the ability of PEG-based surfaces to resist nonspecific protein adsorption depends on the density of the surface packing [150].

8.2.3.2 Zwitterion-based surfaces

A zwitterion is a molecule with two or more functional groups, of which at least one group has a positive electrical charge and one group has a negative charge. The charges of the different groups balance each other out, which makes the molecule as a whole electrically neutral [151]. Multiple studies demonstrated that zwitterionic polymer surfaces are viable alternatives to the more traditional non-fouling PEG-based surfaces that were described in the previous section [150]. Just like PEG, zwitterionic polymer brushes cause a hydration layer surrounding the ionic surface, which prevents non-specific protein adsorption [137]. An increase of the surface packing density of non-fouling groups leads to an improved resistance to this non-specific protein adsorption [150].

8.2.3.3 Silanization

Untreated glass contains silicate and silanol groups that can act as nucleophilic centers and ion-exchange [152]. In order to prevent these kind of processes, glass can be silanized. Silanization helps to prevent adsorption of solute material to the surface or to increase the hydrophobicity of the glass surface. Various reactive silanes are used to mask the silicate and silanol groups and to coat the glass surface. In the same way, silanization may also be used to introduce functional groups or large molecules onto the surface of the glass, leading to a light coating of oil onto the glassware.

8.3 Contact angle analysis

During a contact angle analysis the angle (θ_c) of contact between a liquid and a surface is measured (Figure 18) [132]. This contact angle provides information about the way a surface interacts with some kind of gas, liquid or biomolecule. The contact angle actually represents the inverse measure of the ability of a certain liquid to wet the surface. When a liquid drop is brought into contact with a certain surface, the drop will spread to reach a force equilibrium consisting of three different tensions: solid-

gas surface tension (γ_{sg}), liquid-solid surface tension (γ_{ls}) and liquid-gas surface tension (γ_{lg}). The sum of these tensions in the plane of the surface is zero.

$$\gamma_{sg} - \gamma_{ls} - (\gamma_{lg} \cdot \cos\theta_c) = 0 \quad (8.3)$$

A contact angle smaller than 150° indicates a hydrophilic surface (high wettability), while a contact angle larger than 150° indicates a hydrophobic surface (low wettability). In the case of tissue debris adhesion, the surface should be as hydrophobic as possible to prevent adhesion. A large contact angle between tissue debris and the DRS fiber surface (coating) is therefore preferred. Determining the current contact angle indicates whether wettability is a property that needs optimization.

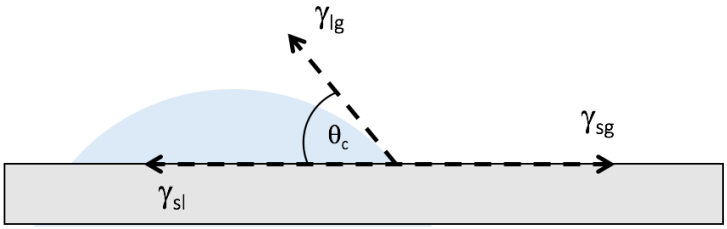

Figure 18: Contact angle analysis measures the ability of a liquid to spread on a certain surface. Based on [132].

8.3.1 Materials and methods

8.3.1.1 Equipment

In order to measure the contact angle of the surface of the tip of the DRS fiber, a contact angle measurement device (CAM 200, KSV instruments, Finland) was used. This device is fully computer controlled and is based on video capture of images and automatic image analysis for measuring static or dynamic contact angles. The CAM 200 consisted of a linear stage, a dispenser filled with water and a microscope. Furthermore, the device was connected to a windows computer and a piece of clay was used to keep the DRS fiber in place.

8.4.1.2 Setup and methods

A schematic representation of the contact angle analysis is provided in Figure 19. The experiment took place at the faculty of Aerospace Engineering at the TU Delft, where the device was located.

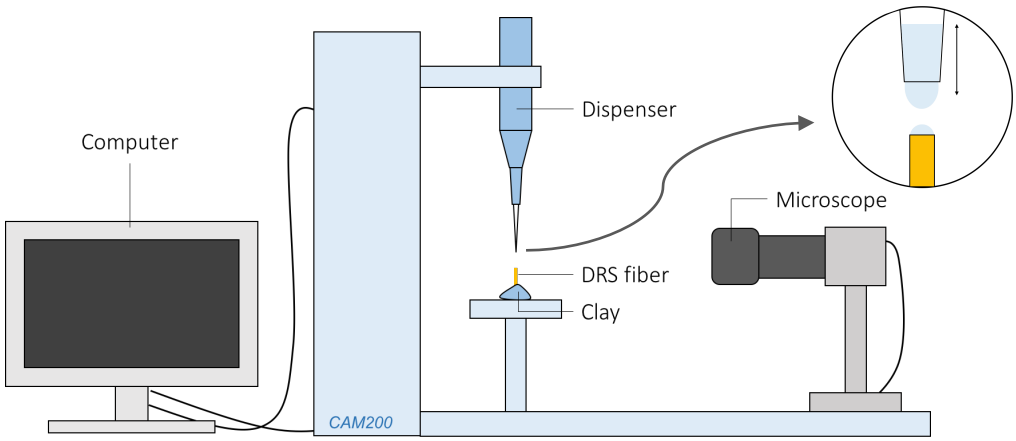

Figure 19: Experimental setup of the DRS fiber contact angle analysis including the CAM 200 with a dispenser and a microscope, a computer, a DRS fiber and a piece of clay to keep the fiber in place. The approach and pull back of the pipette with regards to the DRS fiber is shown enlarged.

Because the surface of the fiber tip was relatively small (only 200 µm in diameter), the standard settings of the CAM 200 needed to be adjusted. The smallest drop size possible was used which contained 0,1 µl. A drop rate of 0,7 µl/s was used and the dispense rate was set on 4,0 µl/s. With the help of a piece of clay, the DRS fiber was placed exactly underneath the dispenser. Subsequently, the microscope was calibrated until a sharp image was obtained on the computer screen. Using the CAM 200 software, the dispenser was dropped down, stopped (as soon as the water drop touched the fiber surface) and pulled up again. Directly after pulling up the dispenser, an image was taken and the contact angle was measured. This procedure was repeated three times.

8.3.2 Results

The images shown in Figure 20 represent the results of the three different contact angle measurements performed for one DRS fiber surface. These results provide an average left contact angle of 71,07°, an average right contact angle of 64,68° and an average general contact angle of 67,89°.

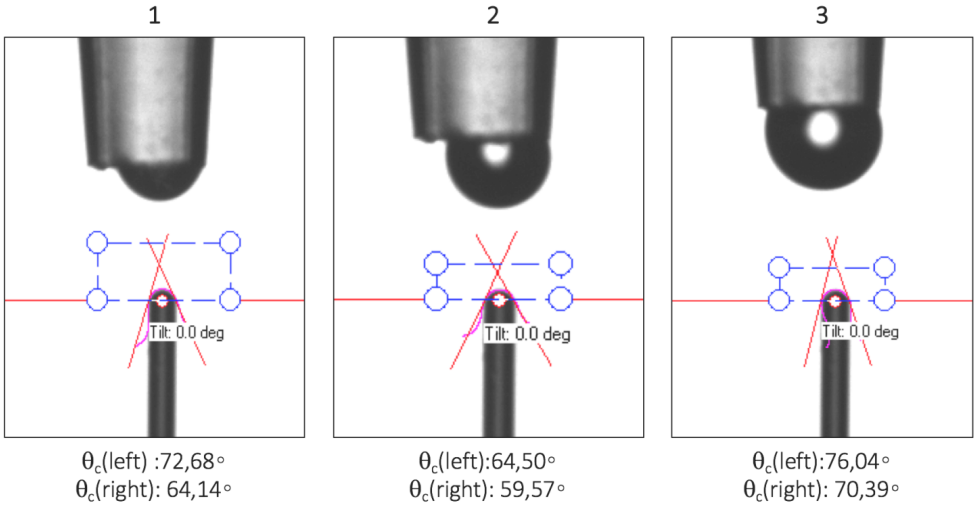

Figure 20: Contact angle measurements of images taken directly after pulling up the dispenser.

8.3.3 Discussion and conclusion

The contact angle analysis performed here deviates from the standard procedure, because of the extreme small size of the DRS fiber. Normally, the water drop is much smaller than the surface it will approach. However, the CAM 200 was not able to produce drops of the required size. Therefore, only a small part of the total drop adhered on the fiber surface. Since this caused the attached drop to be of the exact same size as the fiber surface, it remains unclear whether the shape of the drop is the result of surface morphology or if it is caused by the surface tension of water. This uncertainty should be taken into account. However, when this experiment is repeated in exactly the same way, the results might be compared after all.

However, since all contact angles provided in the previous section are smaller than 150°, it can be concluded that the surface of the DRS fiber tip is hydrophilic and has a high wettability, which leads to strong adhesion of liquids. In order to achieve prevention of tissue debris adhesion, the contact angle of the fiber surface needs to be increased.

8.4 Discussion and conclusion

In this chapter, several methods were described that can be used to modify a glass surface in such a way that tissue debris adhesion is obstructed. Based on the information and examples found in literature, it may be concluded that creating superhydrophobicity or super-hydrophilicity is the most

reliable and often used method in biomedical engineering to prevent both tissue and platelet adhesion. However, the contact angle analysis performed in paragraph 8.3 has shown that the surface of the optical fiber, currently used during smart electrosurgery, is just hydrophilic. Obviously, surface modification is required here to achieve either super-hydrophobicity or superhydrophilicity. This effect can be accomplished in different ways. The particular optical fiber used in this research is fabricated externally and so surface engineering of the surface of the fiber tip becomes a post-processing, which must therefore be relatively easy to carry out. In this situation, the application of a coating therefore seems like the most suitable method to achieve superhydrophobicity or superhydrophilicity.

Combining superhydrophobicity or superhydrophilicity with other anti-adhesion methods will probably lead to even better results. However, due to a lack of expertise, it was chosen to focus in this research on existing non-stick coatings instead of developing a new tailor-made coating. This means that the exact composition of coating properties cannot be hand-picked, but is dependent on what is available. In order to search literature for promising non-stick coatings, a complete list of requirements is needed that, besides anti-adhesiveness, describes the minimum set of properties a coating must possess in order to be considered. The list of requirements will help to select only those coatings with potential to solve the problem of DRS signal loss. However, to be able to compose an extensive list of requirements, more detailed information is needed about the exact situation at the tip of the optical fiber during smart electrosurgery. This is the focus of chapter 9. In chapter 10, the list of requirements will be touched upon again.

III. RESEARCH PHASE 2

DESIGN CONCEPTS

The goal of this research phase is to come up with several design concepts within the design direction selected in the previous phase. Chapter 9 describes a thorough DRS fiber tip analysis. Based on this analysis, chapter 10 provides an extensive list of requirements for the proposed concepts and subsequently three different design concepts are described.

9. Optical fiber tip analysis

In order to find the optimal solution for the tissue debris contamination problem, more detailed information about the optical fiber tip and tissue debris adhering to this fiber tip is essential. While exploring the potential of anti-adhesive biomedical coatings, it is very useful to know what it is exactly that this coating needs to deter. Moreover, although it is assumed that tissue debris contamination is the main factor influencing DRS signal deterioration, it remains to be determined whether other factors contribute to this deterioration as well.

The literature study prior to this master thesis explains which components are suspected to be found on the fiber tip of the smart electrosurgical knife and how these components adhere [55]. On cellular level, it is assumed that tissue sticking to the fibers of the electrosurgical instrument is composed of necrotic cells, living cells and blood. An extensive, practical tissue debris analysis should show whether this is indeed the case. Surface analytical techniques provide information about the outer layers of a material on an atomic level [132]. This information characterizes the surface properties that are needed to relate important surface characteristics to biological responses. For example, chemical, mechanical, electrical and topographic properties may all affect how proteins and cells interact with a certain material. Within this research it is therefore very important to analyze the DRS fiber tip as extensive and thorough as possible. This requires the use of multiple analytical methods, since there is not one technique capable of providing all the information needed [132].

In her master thesis Mollerus already performed a basic tissue debris analysis [9]. She used DRS and Fourier Transform-Infrared (FTIR) measurements to determine the composition of tissue debris sticking to the blade. The DRS measurements showed the presence of water and lipid molecules. The FTIR measurements on the other hand, indicated proteins (matching with hemoglobin and hydrolyzed protein) and fatty acid esters. The rather different results of these tissue characterization techniques make that the reliability of this experiment is questionable. Besides, only six samples were used and scattering during the DRS measurements obstructed the ability to draw further conclusions on the weak indications of other constituents. Furthermore, the analysis of Mollerus focused on the tissue debris composition only, while other properties are of equal importance for a complete material characterization. Moreover, the analysis of Mollerus focused on tissue debris sticking to the electrosurgical blade, while this research is all about tissue debris sticking to the tip of the DRS fiber. Therefore, a new analysis is started in this master thesis so that that more, and more reliable conclusions can be drawn about the exact characteristics of the tip of the DRS fiber after smart electrosurgical use.

9.1 Sample preparation

The goal of this first experiment is to create used DRS fiber samples that represent the worst-case scenario of signal deterioration within the clinical practice of smart electrosurgery. It is assumed that any solution able to prevent the worst level of signal loss, will be able to prevent all other levels as well.

9.1.1 Materials and methods

9.1.1.1 Specimen

For the creation of tissue debris samples, two different types of tissue were used: pork belly, which is a combination of muscle and fat tissue, and porcine liver tissue. The use of pork belly should show the influence of both muscle and fat tissue on tissue debris characterizations, while the use of porcine liver

should mainly show the influence of blood on tissue debris characterizations. Therefore, 0.5 kg fresh pork belly and 0.5 kg fresh porcine liver, obtained at Slagerij Vet in Amsterdam, were used for this experiment.

9.1.1.2 Equipment

For this experiment a hand-controlled, disposable ESK was used provided with a blade tip active electrode (both: Hangzhou Valued MedTech Co., China). Only one ESK was used, whereas 12 different blades were needed.

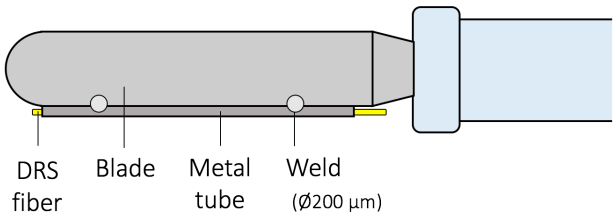

Figure 21: Schematic representation of the smart electrosurgical blade (70 mm) provided with inactive DRS fibers.

In order to create *smart* electrosurgical blades, a small metal tube (outer diameter of 0.5 mm and 19 mm long) was attached to one side of each blade using laser welding. Per side 2 welds were created with a diameter of approximately 200 µm. DRS fibers were inserted into the tubes, so that the ends were exposed (Figure 21). It is important to note that in this particular case the DRS fibers do not need to function, because this experiment focusses on tissue debris adhesion, unrelated to DRS measurements. The smart ESK was connected to an electrosurgical unit called the Force FX generator (Valleylab, Boulder, United States) and the electrical circuit was completed by a dispersive pad attached to two metal plates.

9.1.1.3 Setup and methods

A schematic representation of the setup of the used DRS fiber sample creation experiment is shown in Figure 22. This experiment took place at the In-Body Systems department of Philips Research in Eindhoven.

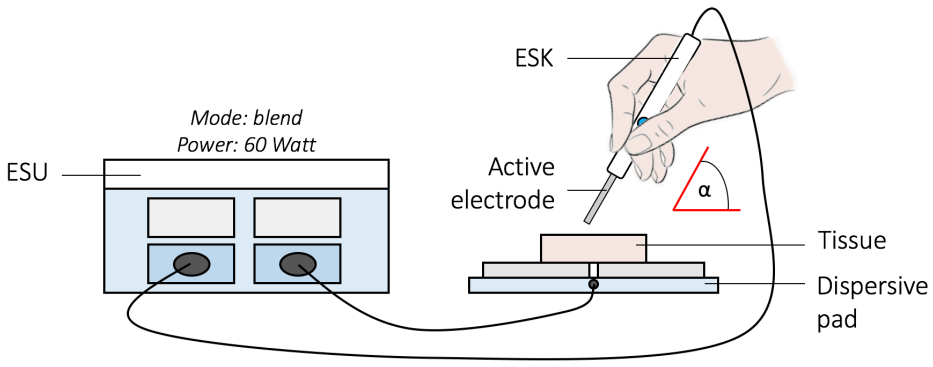

Figure 22: Experimental setup of the tissue debris sample creation including an electrosurgical unit, a dispersive pad attached to two metal plates, porcine muscle/adipose tissue, an electrosurgical knife and an active electrode with inactive DRS fibers. Angle α represent the angle between the ESK and the tissue and is 60°.

The ESK was used in the *blend* mode, as this mode is mostly used in clinical practice [9]. The *blend* mode was combined with a power of 60W to create a worst-case scenario within the framework of practice. In order to validate the worst-case scenario, different settings were tested of which the results are provided in appendix D. As mentioned before, it is assumed that any solution capable of preventing tissue debris adhesion in the worst-case scenario, will be able to prevent tissue debris adhesion of less

severe levels as well. Furthermore, the ESK is used in a constant angle α (see Figure 22) of approximately 60°, which is the estimated average working angle in clinical practice [9]. In order to simulate the clinical practice as well as possible, there was no fixed distance between the ESK and the tissue. For the cutting duration, two different time frames were used: 5 and 30 seconds. These durations are based on the exponential correlation between time and the intensity of the DRS signal, as obtained by Mollerus in her master thesis [9]. She showed that the signal intensity hardly changes after 30 seconds, which makes the first 30 seconds the most interesting to investigate. Comparing two different time frames should show the influence of cutting duration on tissue debris characteristics.

As shown in the condition matrix (Table 8) each unique set of settings was repeated three times leading to a quantity of: 2(duration) x 2(tissue) x 3(repeats) = 12 tissue debris samples.

Table 8: Condition matrix with 4 different experimental conditions. For each condition 3 repeats are performed, resulting in 12 samples in total. The independent variables are tissue type and cutting duration, whereas the dependent variables are represented by the tissue debris characterizations.

n = 3		Tissue type	
		Pork belly	Porcine liver
Cutting duration	5 seconds	EC11	EC12
	30 seconds	EC21	EC22

9.1.3 Results

The experiment described in the previous section resulted in 12 tissue debris samples of which pictures are provided in Figure 23. Number 1 and 2 represent the blades used on pork belly (muscle and fat) for 5 and 30 seconds respectively. Number 3 and 4 represent the blades used on porcine liver, for 5 seconds and 30 seconds respectively.

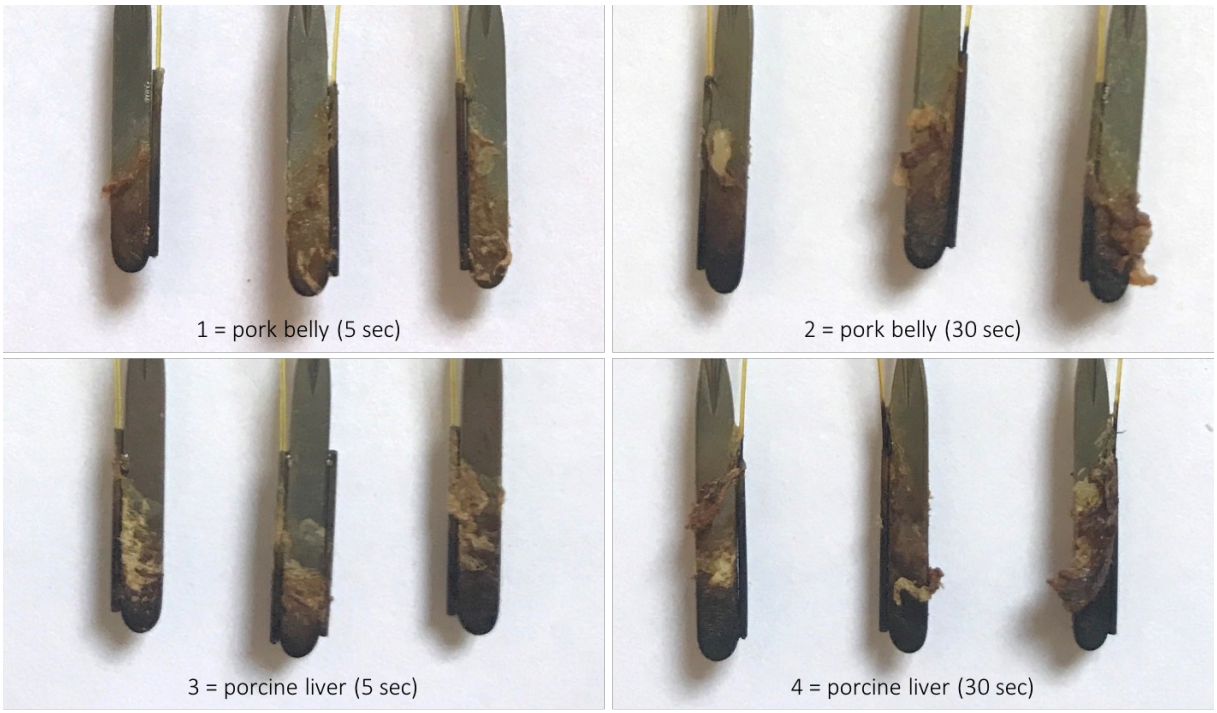

Figure 23: Tissue debris samples as created at the In-Body Systems department of Philips Research in Eindhoven.

After 30 seconds of cutting, the blades contain large pieces of tissue debris sticking to the surface, while after 5 seconds only small pieces are observed. For both tissue types, it can be seen that tissue debris contamination reaches further (starting at the blade/fiber tip) after 30 seconds. Furthermore, the tissue

debris on the pork belly blades has a brown color and consists of a fatty substance, while the tissue debris on the liver blades has a black color and consists of a dry substance. This observation is amplified by the fact that excessive sticking pieces of liver tissue tend to break off, while excessive pieces of pork belly tissue keep sticking on the blade surface. Furthermore, when focusing on the DRS fibers, it can be seen that after 30 seconds the samples of both tissues show pollution of the exposed fibers coming out at the back of the tube. It is unclear whether these fiber parts are contaminated by tissue debris or whether they are simply burnt.

9.1.4 Discussion and conclusion

Studying the smart electrosurgical blades clearly shows that the amount of tissue debris increases over time, both for pork belly and porcine liver. Also, the substance of pork belly tissue debris clearly differs from the substance of the liver tissue debris. It is suspected that the black color is caused by carbonization, which seems to be more severe for tissues containing more blood (liver). Furthermore, after 30 seconds all exposed parts of the fiber close to the blade might become polluted. However, all of the above conclusions are based on simple observations with the naked eye. The in-depth analyses described in the next few paragraphs should lead to more reliable and in-depth conclusions.

9.2 Morphology analysis

This paragraph describes the analysis investigating the morphology of the samples created in the previous paragraph. The focus of this analysis is on tissue debris adhering to the surface of the DRS fiber tip, but also the morphology of the blade will briefly be discussed.

9.2.1 Optical microscopy

In order to understand what exactly is happening at the surface of the DRS fiber tip, digital optical microscopy is used. An optical microscope uses visible light and a system of lenses to magnify images of small subjects. Digital images obtained from this optical microscope should provide a first indication of the morphology of DRS fiber tips that have been used during smart electrosurgery. Digital optical microscopy was preferred over standard microscopy, because the contains functions that help to provide much more detail. For example, it enables part observation in complete focus even if there is significant height variation, which is the case for used fiber tips. This kind of features result in improved observation of the fiber samples.

9.2.1.1 Materials and methods

Equipment

The samples that were subject to this analysis were created beforehand as described in paragraph 9.1. For this specific analysis, the DRS fibers were disconnected from the blades to make sure they could be placed under the lens of the microscope. To perform this analysis a digital microscope (Keyence VHX-5000, Keyence corporation, Japan) was used. The Keyence VHX-5000 is a versatile optical microscope designed for high depth of field measurements specialized for industrial applications. A special quality of this microscope is that it can recognize the focus information automatically when the field of view is moved and subsequently it can quickly create depth composition images. This quality is essential for studying the DRS fiber tips, because of the large height differences in the fiber tip surface morphology. High resolution images are obtained with single-wavelength light and a special function that captures multiple images to produce a fine detail image. These two functions enable high resolution and high contrast observation. The Keyence microscope was used with the medium magnification lens (VH-Z250T 250x-2500x) which enables magnification between 250x and 2500x. Furthermore, a small metal plate and a piece of clay were used to keep the samples in place.

Setup and methods

A schematic representation of the optical microscopy analysis is shown in Figure 24. The experiment took place at the faculty of Mechanical Engineering at the TU Delft, where the device was located.

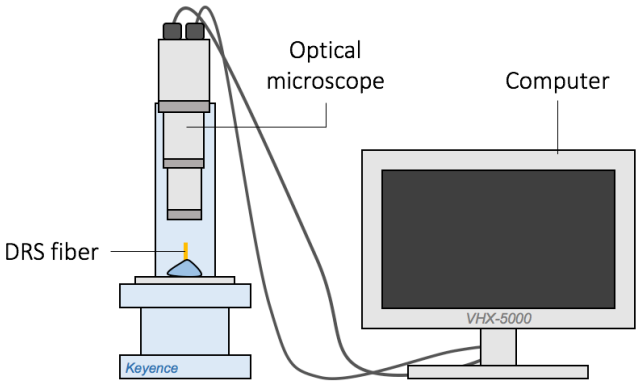

Figure 24: Experimental setup of the optical microscopy analysis, including the Keyence digital microscope, a computer and the DRS fiber samples.

One by one, each sample was placed under the lens of the optical microscope. A metal plate and a piece of clay were used to keep the sample in place. Several magnifications were used to obtain high resolution images of the specific parts of interest. First, all blades were studied and pictures were taken (in side view) from both the blade tip and the tube + exposed fiber tip. Afterwards, the fibers were disconnected from the blades and were studied. Pictures were taken (in top view) from the fiber tip only. Finally, an unused, polished fiber sample was studied with the microscope and pictures were taken (both side and top view) from the tip. All images were saved and compared. The software ImageJ (Image Processing and Analysis in Java) was used to measure certain distances within the images obtained with optical microscopy.

9.2.1.2 Results

This experiment resulted in a certain number of magnified images of different parts of the smart electrosurgical blades. Some examples are shown in Figure 25, the rest of the images is to be found in appendix E. Overall, 12 blade tips were studied, 10 tube/fiber tips were studied in side view, 3 fiber tips were studied in side view and 11 fiber tips were studied both in top and 3D view.

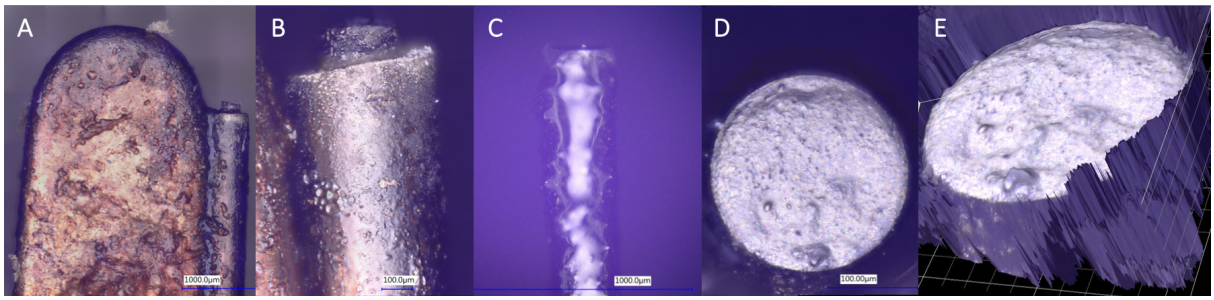

Figure 25: Examples of images of the smart electrosurgical blade obtained via digital optical microscopy. A) blade tip (side view), B) tube/fiber tip (side view), C) fiber tip (side view), D) fiber tip (top view), and E) fiber tip (3D). Note that these pictures do not belong to one and the same blade.

Blade tip

Comparing the six blades used on pork belly to the six blades used on porcine liver clearly shows some differences. Tissue debris on the blades used on pork belly looks greasy and has a smooth structure, while tissue debris on the liver blades looks dry and has a refined grain structure (Figure 26). In general,

the color of liver tissue debris is black compared to the color of pork belly tissue debris. Furthermore, it is clear that pork belly tissue debris contains larger loose pieces of tissue than porcine liver tissue debris.

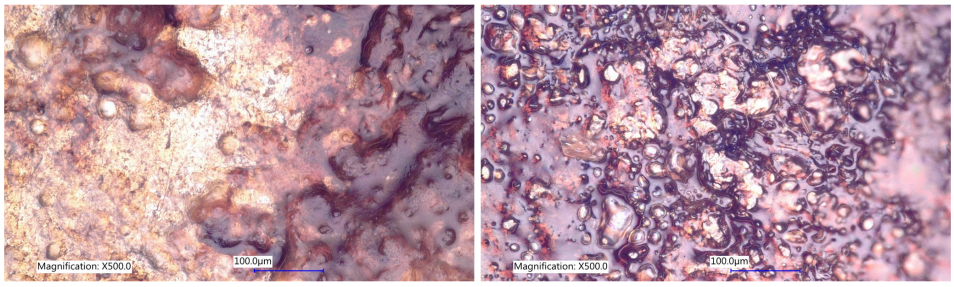

Figure 26: Magnification (500x) of the structure of tissue debris on two blade tips. Left: pork belly, 5 seconds. Right: porcine liver, 5 seconds. Differences can be seen in substance, structure and color.

Comparing the pork belly 5 seconds (PB5) blades to the pork belly 30 seconds (PB30) blades shows a big difference in color and structure. The PB30 blades are blacker and the structure of debris directly adhering to these blades looks more refined. Furthermore, larger pieces of loose tissue are to be found on the PB30 blades. Comparing the porcine liver 5 seconds (L5) blades to the porcine liver 30 seconds (L30) blades also shows differences, again both in color and structure. The color of the L30 blades is blacker and the structure looks more refined. In contrast to the pork belly blades, the L30 blades contain less pieces of loose tissue.

Tube/fiber tip

For the tube/fiber tips the same observations apply as for the blade tips. In general, pork belly tissue debris has a fat substance and a smooth structure, while liver tissue debris has a dry substance and a refined grain structure. Large pieces of loose tissue can be seen on the pork belly tube tips, while the liver tube tips seem to be relatively free of loose tissue.

Fiber tip – side view

Two different layers can clearly be distinguished in the image of the unused, polished fiber tip (Figure 27-2). Comparing this image to the schematic representation of the fiber, provided by the manufacturer (Figure 27-1), explains the origin of the different layers: the outer yellow layer represents the acrylate coating and the cladding, while the dark layer with white in the middle represents the silica core. Comparing the image of the unused fiber with both images of the used fibers (Figure 27-3&4), shows that the shape of the fiber layers has changed over time. The layers are obviously affected by the use of smart electrosurgery: although the layers can still be distinguished, they overlap and the boundaries are not as sharp and clear as before. This observation could indicate layer melting, caused by the high electrosurgical temperatures. In Figure 27, a red circle points out a location where the core of the optical fiber seems to be broken. The upper and lower part of the fiber seem the have lost contact, which inhibits light transmittance and thus proper functioning of the optical fiber.

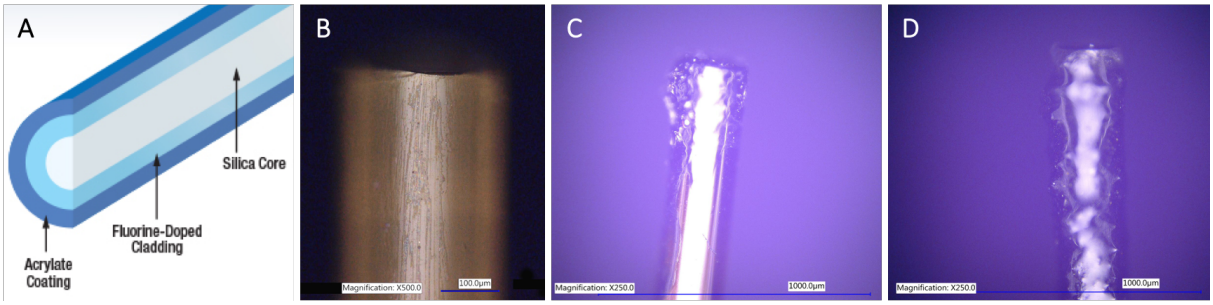

Figure 27: Side view from different fiber tips. A) Schematic representation of fiber layers [153], B) unused, polished fiber tip, C) L5 fiber tip (250x), and D) PB30 fiber tip (250x).

Fiber tip – top view

When looking at the used tips only, large differences are observed (Figure 28). First, it can be seen that the pork belly fiber tips are white/grey, while all liver tips are black. Also, the substance and the structure are different. In contrast to the blades, the substance of the pork belly fiber tips looks dry and has a refined grain structure, while the substance of the liver tips looks fatty and the structure is smooth and rough. When comparing the PB5 tips to the PB30 tips, it appears that the color stays the same, but that the structure becomes rougher. This observation is confirmed by the scaled 3D images of the fiber tips (to be found in appendix E).

The unused, polished fiber tip has a very smooth, equally white surface and a clear distinction can be made between the outer layer (acrylate coating) and the inner two layers (fluorine-doped cladding and silica core). It is obvious that all used fiber tips look quite different. None of the tips is smooth and none of the tips is equally white either. Also, a clear distinction between the different layers is either hard or impossible to make for the used fiber tips.

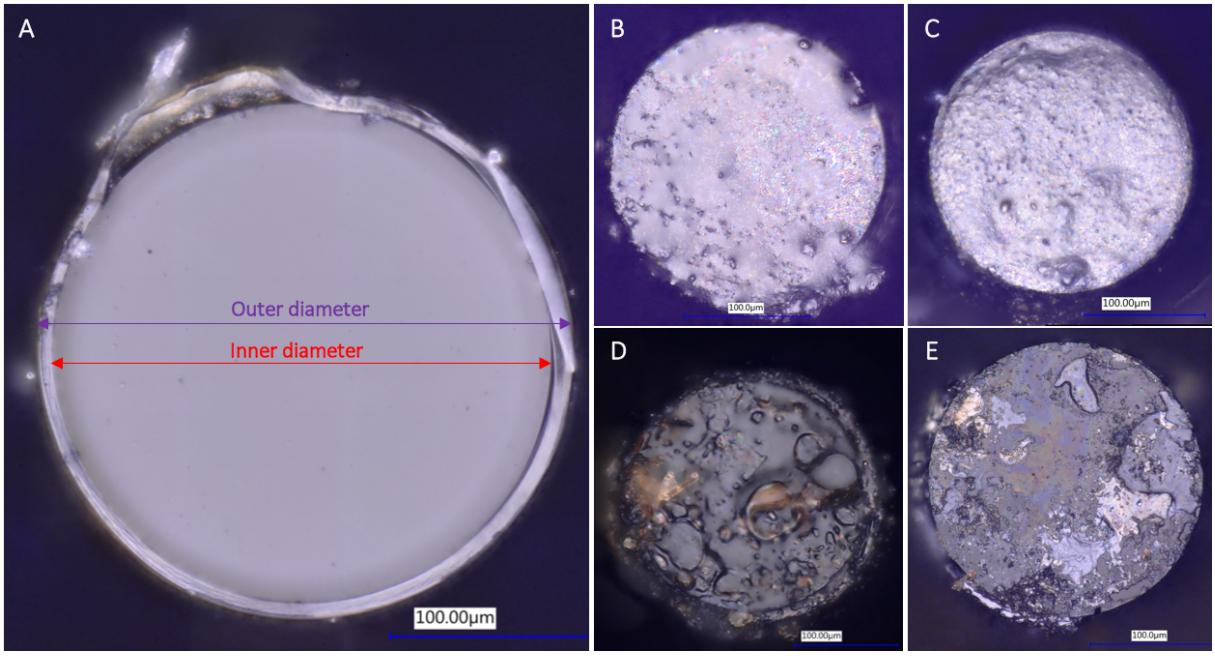

Figure 28: Top view of different fiber tips. A) Unused, polished fiber tip, B) PB5 fiber tip, C) PB30 fiber tip, D) L5 fiber tip and E) L30 fiber tip. Differences can be observed in substance, structure and color.

Analyzing the images with the help of the software ImageJ, provides information about the exact measurements of the different layers of the DRS fiber. The outer diameter of the unused fiber (Figure 28-A) is 237.4 µm, the diameter of the inner two layers is 220.2 µm, which means that the thickness of the coating is about 8.6 µm.

Table 9: Average measurements of the different layers of DRS fiber tips per category. In cases where no clear distinction was possible between layers, the inner diameter was held 'none existent'.

Fiber tip	Outer diameter	Inner diameter
Unused	237.4 µm	220.2 µm
PB5	216.7 µm	None existent
PB30	220.5 µm	None existent
L5	252.9 µm	222.3 µm
L30	217.3 µm	None existent

Table 9 shows the average measurements of the outer and inner diameter of the fibers. For some fiber tips, it was impossible to make a clear distinction between different layers. In those cases, only the outer diameter is provided and the inner diameter is held none existent. The average thickness of the coating is only provided when a piece of the coating could clearly be detected in the image. It is clear that the diameters of all fiber tips have changed with respect to the unused fiber tip.

9.2.1.3 Discussion and conclusion

The goal of this analysis was to determine the influence of tissue type and cutting duration on the morphology of tissue debris sticking to the DRS fiber tip. In addition, pictures were taken from the tips of the electrosurgical blades and the tips of the tubes protecting the fibers. With the help of all these images, conclusions can be drawn about the influence of tissue type and cutting duration on optical fibers and tissue debris adhering to the blade. But first, it should be taken into account that inaccuracies might have taken place during this analysis. In some cases, the pictures being compared had different magnifications, which might have influenced the observations described. Furthermore, during use of the ImageJ software, the scale had to be set manually for each picture separately and the distances to be measured were determined manually as well, which might have led to small inaccuracies in the final measurements. Furthermore, the fiber tips should have been aligned with the tips of the tubes in order to avoid as much damage to the tip as possible. However, in practice the alignment was properly performed which might have influenced the results.

When focusing on the electrosurgical blades, some obvious conclusions can be drawn. The difference in substance and structure of pork belly debris and liver debris on the blades can be explained by the different composition of the two tissue types. Pork belly consists for a large part of adipose tissue, which obviously leads to a fat, smooth morphology, while liver tissue mainly consists of water and blood, which (due to high temperatures) leads to a dry and brittle morphology. The color differences are caused by carbonization. A higher amount of black carbonized tissue is observed on the liver blades, which is probably due to a higher presence of blood in liver tissue. Also, from the observations it may be concluded that the amount of carbonization gets worse over time.

However, for this research it is much more important to know what exactly happens at the fiber tips, because for a large part these findings will eventually determine which solution is suitable for solving the signal deterioration problem. Figure 29 shows two images of the same fiber. In 29-A, the yellow arrow indicates the silica core of the optical fiber and the red arrow indicates a small remaining part of the acrylate coating, clearly indicating that the rest of the coating has disappeared.

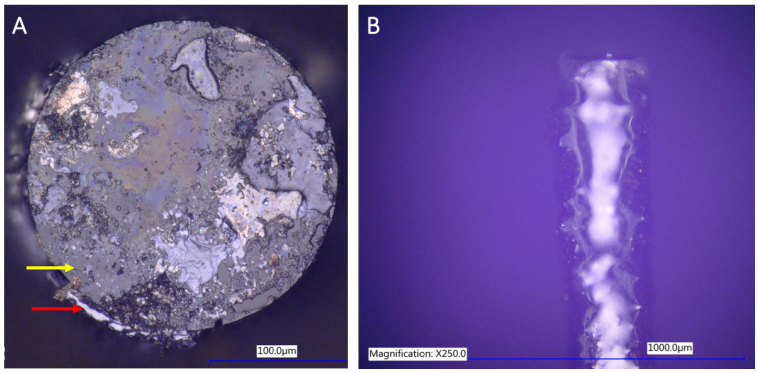

Figure 29: A shows that the outer acrylate coating has disappeared. B shows that the fiber looks damaged.

The coating prevents mechanical and chemical damage which otherwise could weaken the fiber and compromise its performance [153]. The images clearly show that a large part of the coating has completely disappeared after electrosurgical use. This observation is confirmed by the measurements

of the used fibers compared to those of the unused fiber (Table 9). For three of the four categories (PB5, PB30 and L30) the outer diameter is more or less the same as the inner diameter of the unused fiber. In other words, the outer layer has vanished. According to the manufacturer of the optical fiber that was used for this experiment, the general operating temperature of the fiber is -45°C to 85°C [153]. This specific range indicates that the fiber has probably been affected by the high electrosurgical temperatures within the tissue, reaching 350°C [59]. Typically, acrylate coatings have a maximum operating temperature of 80°C [154]. The electrosurgical temperatures obviously exceed the operating temperature, which makes it is very likely that the acrylate coating degrades and melts away during use of the smart electrosurgical knife. As soon as the coating has disappeared, both the fluorine-doped cladding and the silica core are exposed and become very vulnerable to external influences, risking mechanical and chemical damage. The function of a cladding is to provide a lower refractive index at the core interface in order to cause reflection within the core, so that light waves are transmitted all the way through the fiber [155]. However, as soon as damage occurs, the core and its cladding get deteriorated. Figure 30 shows how damage to a fiber core and cladding results in a change of the refractive index of the medium, leading to light scattering and significant signal loss [156].

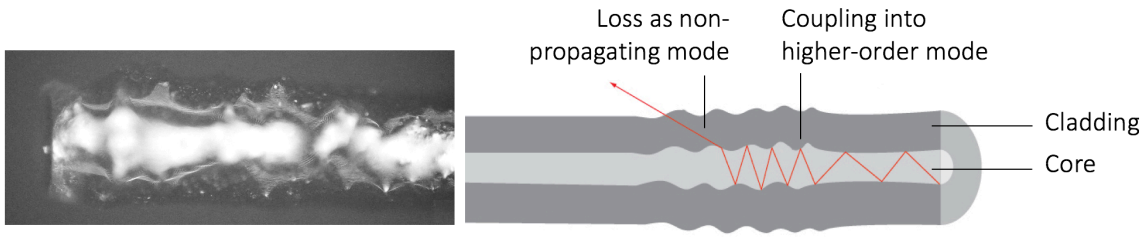

Figure 30: Clear similarities between a microscopic image of a used fiber tip and a schematic representation of a damaged fiber core and cladding. The latter shows how signal is lost after the optical fiber core and cladding have been damaged [156].

The microscopic images in Figure 27 show that the melting of the coating starts at the tip and works its way down along the fiber. This indicates that the fiber damage gets worse over time. This conclusion is confirmed by Toosi et al. who showed that temperature has a significant influence on the optical behavior of fibers [157]. He states that the signal of an optical fiber degrades with time, above a certain threshold temperature. On the other hand, the exact influence of the tissue type on fiber melting remains unclear. However, it is observed that fibers used on liver tissue react differently on high temperatures. After 5 seconds of electrosurgical cutting, the coating is still detectable and even seems to have grown in thickness, while after 30 seconds of cutting the coating has completely disappeared. This could be due to different temperature rates of the two tissue types. However, temperatures have not been measured during this experiment, so unfortunately this statement cannot be confirmed.

It may now be concluded that melting of the outer acrylate coating seems to play an important role in the deterioration of the optical fiber. However, it remains unclear what happens at the top surface of the fiber tip. For the porcine liver fiber tips, it is observed that both the morphology and the color change with respect to the unused fiber tip. In both timeframes, it seems as if an additional layer has formed on top of the surface. This observation indicates that there might indeed be some tissue debris present, blocking the fiber tip. However, this analysis is not sufficient enough to confirm this statement. When cutting in pork belly, the morphology obviously changes with respect to the unused fiber, but the color stays more or less the same. This observation raises the question whether in this case there is any tissue debris contamination at all? Or could it be that thermal fiber damage alone is responsible for the morphology change and signal deterioration and that tissue debris has no role in this issue?

In order to find out to what extent these two phenomena cause DRS signal deterioration during smart electrosurgery, additional research is required. To confirm that thermal damage plays an important role in signal deterioration of the optical fiber, this experiment should be repeated with either heat-resistant

optical fibers or fibers without coating at all. Comparing the results of these fibers (after use) to the original ones, should demonstrate whether the choice of fiber makes a difference. On the other hand, to confirm that not only thermal fiber damage plays a role in this problem, a chemical composition analysis should be performed. This analysis will reveal whether any tissue debris components are present at the fiber tip surfaces. Subsequently, additional tests should indicate the influence of tissue debris contamination on DRS signal deterioration. However, to confirm the observations in this paragraph and to make sure no essential information was missed, another morphological analysis is performed first.

9.2.2 Scanning electron microscopy

In order to collect even more information about the morphology of the fiber tips, scanning electron microscopy (SEM) was used. SEM is a technique that uses a focused electron beam to scan the surface of a sample and create high-resolution, high-magnification images [158]. These images provide information about the surface morphology based on signals produced by the interaction between the electrons and the atoms in the sample. It depends on the characteristics of the sample what kind of signals are emitted due to illumination with the electron beam, but the SEM normally detects secondary electrons to form an image for observation [159]. Because the wavelength of an electron beam is shorter than that of light, SEM enables observations of a nanostructure, which is not possible with an optical microscope. Furthermore, SEM provides images with deeper focal depth which enables focused observation of the full sample instead of only a small part. Because of these features, it was decided to perform an SEM analysis additional to the observations done with the optical microscope.

9.2.2.1 Materials and methods

Equipment

For this experiment, five different fiber samples were used: 1) Fiber used on pork belly - 5 seconds, 2) fiber used on pork belly – 30 seconds, 3) fiber used on liver – 5 seconds, 4) fiber used on liver – 30 seconds and 5) unused fiber. The samples were created beforehand as described in paragraph 9.2. For this specific analysis, the DRS fibers were again disconnected from the blades to make sure they could be placed under the lens of the microscope. A sputter coater (Q300T-D, Quorum Technologies Ltd., United Kingdom) was used to prepare the samples. An SEM (JSM-7500F, JEOL Ltd., Japan) was connected to a computer and both were used to make high-resolution images. Furthermore, a small metal holder and conductive adhesive were used to keep the samples in place.

Setup and methods

Figure 31 shows a schematic representation of the setup of the SEM experiment. The experiment took place at the faculty of Aerospace Engineering at the TU Delft.

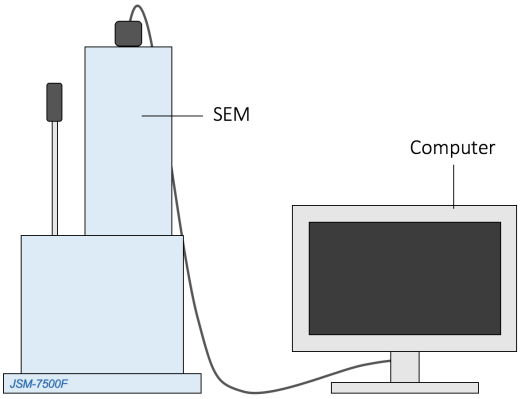

Figure 31: Experimental setup of the SEM analysis, including the SEM and a computer. The samples are placed inside the SEM under high vacuum.

First, with the help of a double-sided sticker, all five sample were attached to a small metal holder to keep the samples in the right position. Subsequently, the samples needed to be prepared for the SEM analysis. Nonconductive specimens collect charge when scanned by the electron beam which causes image artifacts. For conventional imaging with SEM, samples therefore need to be electrically conductive. Because DRS fibers are nonconductive, they were sputtered with a very thin layer of gold using a sputter coater. After this preparation, the samples were placed inside the SEM under high vacuum. With the help of an internal camera, the microscope was steered into the right direction. One by one, the fiber tips were placed under the microscope. Different magnifications were used to have a good look at the specific parts of interest on the tip of the fibers.

9.2.2.2 Results

Unused, polished

Figure 32 shows the SEM images of the unused, polished fiber tip. Apart from some small pieces of pollution, both the coating and the silica core look smooth. The middle and the right image show a clear distinction between the three fiber layers: core, cladding and coating.

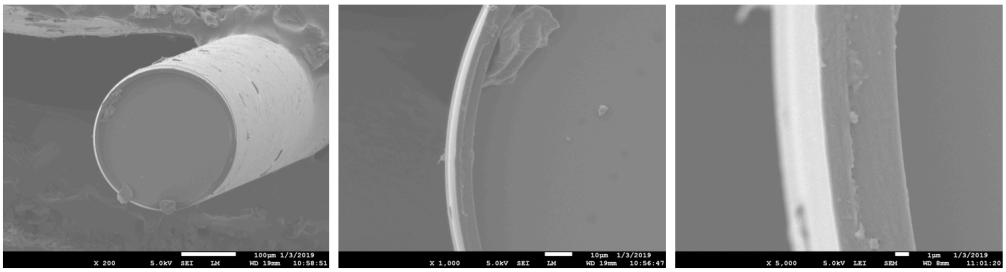

Figure 32: SEM images of an unused, polished fiber.

Pork belly – 5 seconds

The SEM images of the fiber tip used on pork belly for 5 seconds are shown in Figure 33. Unfortunately, the images are not that clear because they seem overexposed. This makes it hard to see more detail than provided in the optical microscope images. However, in the right image in Figure 33, a damaged or melted coating may be distinguished. Also, some kind of non-transparent layer is detected on the fiber tip, covering the silica core.

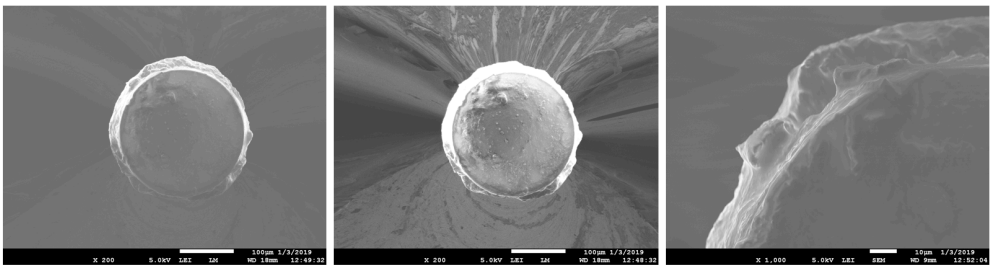

Figure 33: SEM images of a fiber used on pork belly for 5 seconds.

Pork belly – 30 seconds

The SEM images of the fiber tip used on pork belly for 30 seconds are shown in Figure 34. Just as the images of the previous sample, these images are overexposed, which makes it hard to see any additional details. But again, the left image shows some kind of nontransparent layer covering the silica core and the right image clearly shows an affected coating.

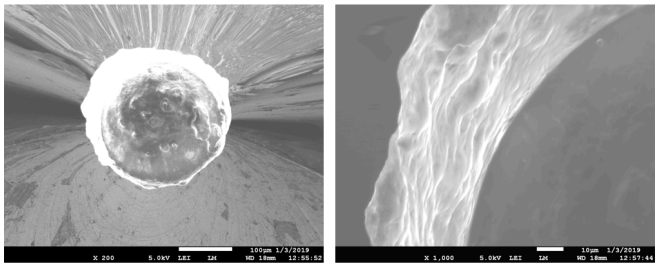

Figure 34: SEM images of a fiber used on pork belly for 30 seconds.

Porcine liver – 5 seconds

The SEM images of the fiber tip used on porcine liver for 5 seconds are shown in Figure 35. The quality of these images is clearly better than the quality of the pork belly images. The left image shows the complete fiber tip adhering to the stickers that hold the fiber in place. It is obvious that the upper part of the coating is damaged and that part of the coating has even disappeared. The middle image shows a part of the silica core and a part of the coating. Again, the coating looks heavily damaged. Furthermore, the tip of the silica core seems to be covered by a hard layer. This is observation is amplified by the right image, showing different layers of contamination with some cracks in it.

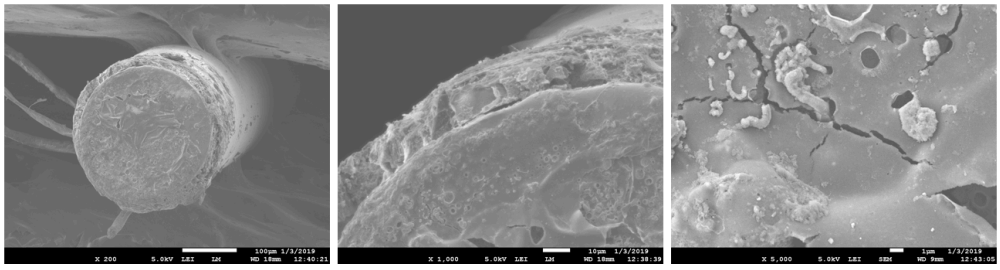

Figure 35: SEM images of a fiber used on porcine liver for 5 seconds.

Porcine liver – 30 seconds

The SEM images of the fiber tips used on porcine liver for 30 seconds are shown in Figure 36. The left image shows the complete fiber tip. The silica core tip looks smooth and appears to be mostly clean. However, some contamination is detected and the coating looks damaged again. This is confirmed by both the middle and the right image showing the affected coating up close.

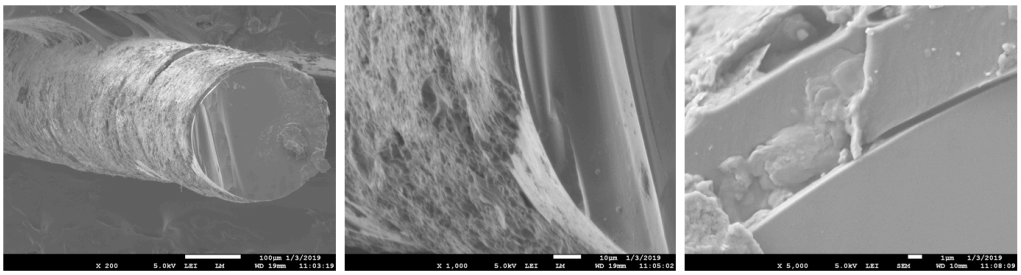

Figure 36: SEM images of a fiber used on porcine liver for 30 seconds.

9.2.2.3 Conclusion and discussion

Based on the results received from the SEM analysis, it may be concluded again that the acrylate coating of the optical fiber is affected by use of the smart electrosurgical knife. Damage of this coating may lead to damage to the silica core, which in turn may lead to deterioration of the DRS signal intensity. Using either a heat-resistant or a stripped fiber (without coating) may help to overcome this problem.

Furthermore, the SEM images clearly show that the tip of the silica core is covered by a layer of contamination. This layer inhibits light transport through the fiber, which probably also leads to deterioration of the DRS signal intensity. A composition analysis should indicate the exact cause of this additional layer covering the silica core.

The SEM images of both the pork belly samples are overexposed. This indicates that these samples were not conductive enough, which was probably the result of a failure in the application of the thin gold layer on the sample. This failure could have been caused by a weak binding between gold and the surface of the pork belly sample. Due to the overexposure, these images are less usable and less reliable. Furthermore, it is assumed that the damage to the fibers is caused by heat. Although this seems like the most obvious cause, there could be other causes as well. For example, the fibers could have been damaged during their removal from the tubes. This is something that must be precluded in further research. Lastly, it remains unclear what exactly causes the contamination layer covering the tip of the silica core. In order to find out, more information is needed about the composition of the layer. This information should indicate whether this material originates from the tissue or from other components, like the acrylate coating. This analysis is described in the next paragraph.

9.3 Composition analysis

In the previous paragraph, morphological analyses have shown that a layer is formed on the tip of the DRS fiber, blocking the DRS signal. Paragraph 9.3 describes the different analyses that were performed in order to investigate the composition of this layer covering the tip of the silica core. Information about the composition should indicate one of the causes of DRS signal deterioration, which should help to come up with a suitable solution. First, energy-dispersive spectroscopy (EDS) is used to gain knowledge about the elemental composition and subsequently, Raman spectroscopy is used to gain knowledge about the molecular composition.

9.3.1 Energy-dispersive spectroscopy

Energy-dispersive spectroscopy is a technique that uses the interaction of electron excitation and a sample to analyze the elemental composition of the sample [160]. A high-energy beam of charged electrons is focused into the sample to excite ground state electrons at an inner shell, creating electron holes. Subsequently, these holes are filled by electrons from outer, higher-energy shells. The difference in energy between these two shells may be released in the form of an X-ray. An EDS device measures the number and the energy of the emitted X-rays, resulting in a unique set of peaks in the electromagnetic emission spectrum. This unique set of peaks represents the atomic structure of the elements present in the sample. In this way EDS enables measurement of the elemental composition of a specimen. EDS is non-destructive, quick, versatile and does not require any sample preparation. This makes EDS a very suitable technique for the investigation of the DRS fiber tips. Furthermore, EDS will provide a perfect first indication of what kind of elements are present on the fiber tips after use of the *smart* electrosurgical knife. This knowledge may help to decide on which solution has the most potential to solve the signal deterioration problem.

9.3.1.1 Materials and methods

Equipment

Again, five different sample were used: 1) Fiber used on pork belly - 5 seconds, 2) fiber used on pork belly – 30 seconds, 3) fiber used on liver – 5 seconds, 4) fiber used on liver – 30 seconds, and 5) unused fiber. These samples were also created beforehand as described in paragraph 9.2. For this specific analysis, the DRS fibers were again disconnected from the blades to make sure they could be placed under the lens of the microscope. The SEM device used for the SEM analysis (JSM-7500F, JEOL Ltd., Japan) was configured with an energy-dispersive spectrometer (Noran system SIX, Thermo Scientific,

United States). These two techniques were combined into one device, which was connected to two computers: one for SEM measurements and one for EDS measurements. Furthermore, a small metal holder and conductive adhesive were used to keep the samples in place.

Setup and methods

Figure 37 shows a schematic representation of the setup of the EDS experiment, which looks exactly the same as the SEM setup, because the two techniques were combined into one device. The experiment took place at the faculty of Aerospace Engineering at the TU Delft, where the device was located.

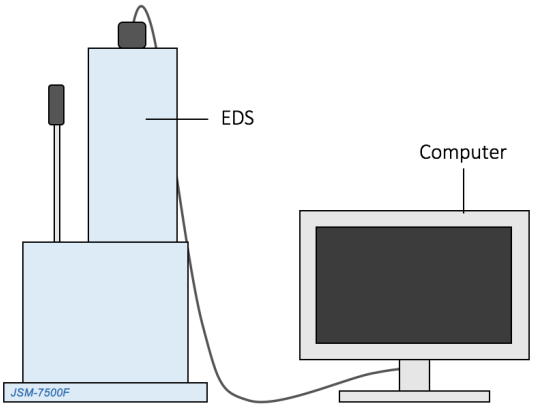

Figure 37: Experimental setup of the EDS analysis, including the EDS and a computer. The samples are placed inside the EDS under high vacuum.

First, the samples were attached to the metal holder as described in paragraph 9.4.1.1. The samples were placed inside the EDS under high vacuum. One by one, the fiber tips were positioned under the microscope to have a good look at the specific parts of interest. These parts were captured by taking pictures, which were subsequently analyzed with EDS.

9.3.1.2 Results

The EDS analysis has provided interesting results containing information about the composition of the layer covering the tip of the optical fiber. Five different samples were analyzed on specific area locations. To be able to fairly compare all different measurements, areas with similar characteristics were selected. As can be seen in Figure 39, all areas are located at the edge of the fiber tip, so that both the acrylate coating and the silica core are included in the EDS measurements. The most important results are visualized and shown in this chapter, a complete overview of all results is provided in appendix F.

Figure 38 shows the relative presence of different elements on the fiber tip per sample. For each sample, the vast majority of the layer covering the fiber tip consists of carbon, oxygen and silicium. Except for pie chart D, all other elements are represented by 'other'. The results provided in appendix F show which 'other' elements are present exactly. From these results, it is observed that the distinctive element for pork belly samples is magnesium, while for liver samples it is iron and cupper. When the influence of cutting duration is researched, it is obvious that the distinctive elements of 5-seconds-samples are chloride, copper and zinc, while the distinctive elements of 30-seconds-samples are calcium and magnesium.

On the basis of the pie charts shown in Figure 38, some interesting observations can be made. First of all, it is seen that the amount of carbon increases over time for both tissues (with the exception of L30), although the increase rate for pork belly is higher than for liver. In contrast to carbon, both the amount of oxygen and the amount of silicium decrease over time (again with the exception of L30). Furthermore, compared to the unused fiber, the amount of 'other' elements has increased after 5 seconds of cutting

but decreases again after 30 seconds. Also, cutting in porcine liver, generally results in a higher percentage of 'other' elements detected on the fiber tip compared to pork belly.

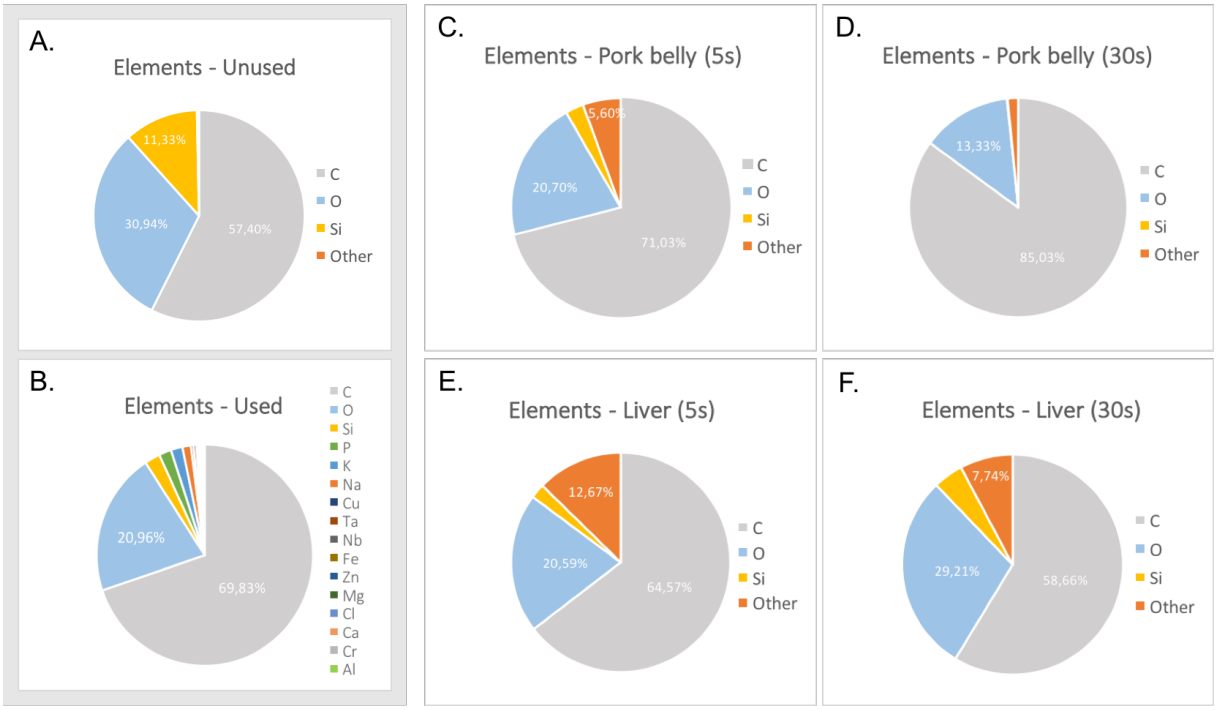

Figure 38: The EDS results summarized in six pie charts showing the relative amounts of different elements per sample. All elements other than carbon, oxygen or silicium are represented by 'other'. Note that pie chart D shows the total percentages of elements present on all five samples.

Figure 39 provides EDS images showing the distribution of carbon, silicium and oxygen particles on a specific area of an unused and a used fiber tip. A complete overview of all EDS images is provided in appendix F.

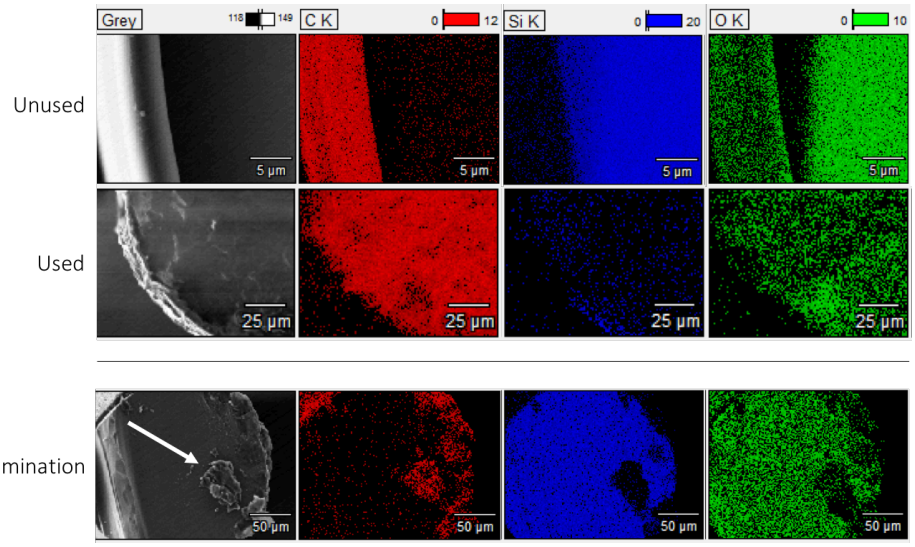

Figure 39: EDS images showing the distribution of the carbon, silicium and oxygen particles per sample. It is observed that carbon and silicium are complementary.

The images of the unused fiber tip clearly show that all carbon is located at the acrylate coating only, all silicium is located at the fiber core only and oxygen is located at both. However, the images of the used

fiber tips show that after electrosurgical use, carbon is no longer only located at the coating, but at the fiber core as well. As a result, the amount of silicium particles decreases wherever the amount of carbon particles increases. In other words, the more carbon is present at a specific location, the less silica is detected. This observation is amplified by the third row of EDS images provided in Figure 39. The grey picture clearly shows a contamination part sticking to the surface of the fiber tip (indicated by the white arrow). In the corresponding EDS images, carbon particles are observed at the location of the contamination, while silicium and oxygen particles are observed everywhere except for the location of the contamination.

9.3.1.3 Conclusion and discussion

The results from the EDS analysis provided in the previous section show which elements are present on the surface of a DRS fiber tip used for *smart* electrosurgery. In order to explain the observations based on these results, it is important to know where all elements originate from. Originally, four different materials were involved in the interaction between the DRS fiber and the tissue: acrylate ($C_3H_3O_2$) [161], fluorine (F), pure silica (SiO_2) [162, 163] and porcine tissue (mainly containing: O, C, H, N, Ca, P, K, S, Na, Cl, Mg) [164-166]. The elemental compositions of these materials help to explain the images of the unused fiber, where all materials are still intact. The acrylate coating indeed shows presence of carbon and oxygen (hydrogen cannot be detected with EDS because it has no core electrons [167]) and the silica core shows presence of silicium and oxygen. Fluorine is not detected.

However, the different compositions of the materials involved in electrosurgical interaction are affected by a phenomenon called charring (previously referred to as carbonization) [55]. Charring is a chemical process caused by incomplete combustion of organic matter when subjected to heat. At temperatures above 300°C, organic materials undergo a thermal decomposition, which means that all non-carbon elements are stripped from carbon chains and rings and are released to the atmosphere [168]. Subsequently, the carbon elements form a hexagonal, graphite-like structure, which becomes more evident and regular with an increasing temperature. As a result, the material turns into char, which has a dark brown or black color and shows graphite-like characteristics. Especially the optical properties undergo a drastic transformation: for example, the absorption in the visible part of the spectrum increases.

Table 10: All elements found on the samples in order from high to low percentage. The fourth column shows the potential origin of each element based on knowledge found in literature about the composition of the primary materials and charring.

#	Element		%	Origin	Source
1	C	Carbon	67,34%	Fresh tissue/charred tissue/acrylate	[164-166]
2	O	Oxygen	22,96%	Fresh tissue/acrylate/silica	[162-166]
3	Si	Silicium	4,12%	Silica	[162, 163]
4	P	Phosphorus	1,48%	Fresh tissue	[164-166]
5	K	Potassium	1,38%	Fresh tissue	[164-166]
6	Na	Natrium	1,03%	Fresh tissue	[164-166]
7	Cu	Copper	0,38%	Fresh tissue	[164-166]
8	Ta	Tanium	0,34%	Sample contamination	-
9	Nb	Niobium	0,28%	Sample contamination	-
10	Fe	Iron	0,26%	Blood	[169]
11	Zn	Zinc	0,16%	Fresh tissue	[164-166]
12	Mg	Magnesium	0,12%	Fresh tissue	[164-166]
13	Cl	Chlorine	0,07%	Fresh tissue	[164-166]
14	Ca	Calcium	0,05%	Fresh tissue	[164-166]
15	Cr	Chromium	0,03%	Fresh tissue	[164-166]
16	Al	Aluminium	0,01%	Sample contamination	-

Based on this knowledge and on the chemical compositions of the primary materials, Table 10 was composed. This table summarizes all elements present in the samples (ordered from high to low percentage) and their potential origins. With the help of Table 10, it may be concluded that all used fiber tips contain traces of fresh tissue (though in different elemental compositions), acrylate, silica and charred tissue/acrylate. Additionally, besides these materials, all liver samples also contain blood.

Now that the principles of charring are clear, all observations suddenly make sense. Due to charring the involved organic materials (acrylate and porcine tissue), are decomposed under the high electrosurgical temperatures of about 350°C. The non-carbon elements are released into the atmosphere, while the carbon elements start to form char. This explains both the increase of carbon and the decrease of oxygen over time. The 'other' non-carbon tissue elements appear on the fiber tip after first use of the s*mart* electrosurgical knife and are therefore detected on the 5 second samples. Due to charring, this amount decreases again after longer use as detected after 30 seconds. However, the rate of charring seems to be lower for liver samples than for pork belly samples. This could have been caused by a difference in temperature, but since temperatures were not measured, this remains unclear for now. Based on the fact that the amount of silicium decreases over time, it may be concluded that the surface of the silica core gets covered with carbon in the form of char. The images shown in Figure 39 confirm this conclusion.

However, some remarks have to be made regarding the reliability of the EDS results. Only the area shown on the microscopic picture is subject to EDS analysis, which makes the EDS result highly dependent on the specific location selected. In the case of this research, the location has not been chosen deliberately constant enough, what has been at the expense of the comparability of the results. In order to achieve more reliability, the samples should have been placed under the microscope in exactly the same position and with the same magnification. Furthermore, sample L30 seems to be an exception for three different observations. It is highly likely that the divergent results of this sample are also caused by inconstant localization. The same applies to the results of the unused fiber. Considering the core/coating ratio of the fiber tip, the carbon percentage should have been much lower. If this EDS experiment is to be repeated, one should pay attention to positioning the samples as constant as possible. In addition, the reliability of the results can be even further increased by analyzing more samples.

9.3.2 Raman spectroscopy

The first technique that is used to investigate the composition of the contamination layer is called Raman spectroscopy. Raman spectroscopy is a spectroscopic technique used to observe rotational, vibrational and other low-frequency modes in a sample [170]. This technique relies on inelastic scattering, called Raman scattering, coming from a laser light source in the visible, near infrared or near ultraviolet range [171]. The Raman scattered light is detected as a Raman spectrum, creating a characteristic fingerprint pattern. This unique pattern makes it possible to identify substances based on the position and shape of the peaks in the spectrum. Raman spectroscopy is non-destructive, it measures both organic and inorganic substances in various states and it does not require any sample preparation. This makes Raman spectroscopy a very suitable technique for the investigation of the DRS fiber tips.

9.3.2.1 Materials and methods

Equipment

Again, five different sample were used: 1) Fiber used on pork belly - 5 seconds, 2) fiber used on pork belly – 30 seconds, 3) fiber used on liver – 5 seconds, 4) fiber used on liver – 30 seconds, and 5) unused fiber. These samples were also created beforehand as described in paragraph 9.2. For this specific analysis, the DRS fibers were again disconnected from the blades to make sure they could be placed

under the lens of the microscope. A confocal Raman microscope (inVia, Renishaw plc., United Kingdom) was connected to a computer and both were used to collect data about the composition. Furthermore, a little piece of clay was used to keep the samples in place.

Setup and methods

Figure 40 shows a schematic representation of the setup of the Raman analysis. The experiment took place at the faculty of Aerospace Engineering at the TU Delft, where the device was located.

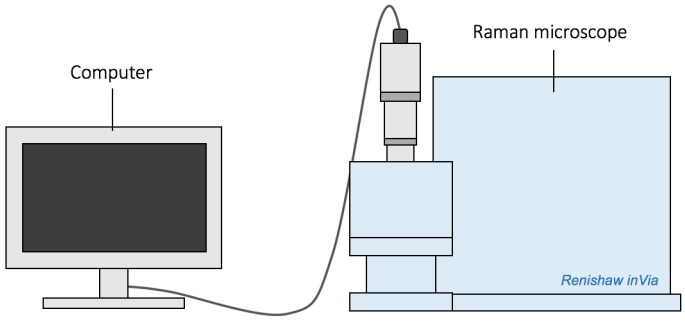

Figure 40: Experimental setup of the Raman analysis, including the Raman microscope and a computer. The samples are placed inside the device under the microscope.

First, with the help of a piece of clay, the samples were placed inside the Raman device under the microscope one by one. A laser light of 532 nm was used to produce the clearest Raman spectrum. A magnification of 50x was used to focus on the surface of the fiber tip. Per fiber, three specific areas of interest were selected for Raman analysis.

9.3.2.2 Results

The Raman analysis has provided results containing information about the composition of the layer covering the tip of the fiber. Five different samples were supposed to be analyzed. However, Raman spectroscopy did not seem to work on the unused fiber, probably because of its transparency. Furthermore, the device broke down halfway through the experiment, meaning that the two last fibers could not be examined. Therefore, the result of this analysis comprises only two samples: number 1) fiber used on pork belly - 5 seconds, and number 4) fiber used on liver – 30 seconds. Note that the Raman spectrum is based on one very small area only. This area is indicated by the white dashed crossing in the pictures next to the graphs. In total, three measurements were taken per fiber, resulting in six different Raman spectra in total. These spectra are to be found in appendix G. As an example, two spectra are provided in Figure 41 and Figure 42.

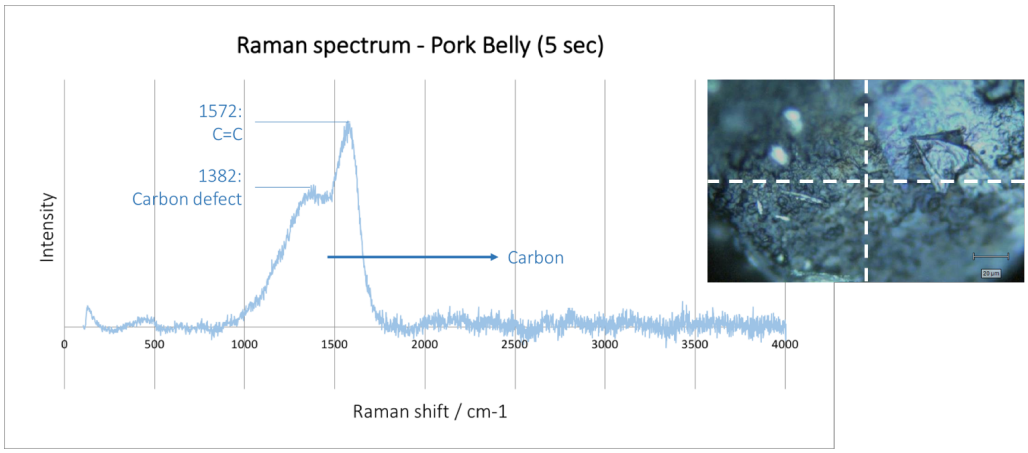

Figure 41: Raman spectrum of surface area #1 of the fiber tip used on pork belly for 5 seconds.

Figure 41 shows the Raman spectrum of a small surface area of the fiber tip used on pork belly for 5 seconds. This spectrum clearly shows peaks at 1382 cm^{-1} and 1572 cm^{-1}. When comparing these specific peaks to reference data found in literature, it turns out that these peaks together indicate the presence of carbon [172-174]. Since no other peaks are detected, it seems as if only carbon is present in this specific area. The other two Raman measurements performed on this fiber (provided in appendix G) show similar results.

Figure 42 shows the Raman spectrum of a small surface area of the fiber tip used on porcine liver for 30 seconds. This spectrum shows peaks at 489 cm^{-1}, 1603 cm^{-1} and 2936 cm^{-1}. Again, when comparing these peaks to reference data found in literature, it is suspected that this spectrum indicates the presence of silica [175], carbon [172-174] and acrylate [174] respectively. The supporting picture next to the graph shows that his specific measurement was performed at the edge of the fiber tip surface. The other two measurements (provided in appendix G) were both performed in the middle of the fiber surface and show deviating results. Although area #1 appears to be black, the corresponding spectrum shows the presence of silica only. The spectrum of area #3 indicates silica, a little bit of carbon and a lot of acrylate.

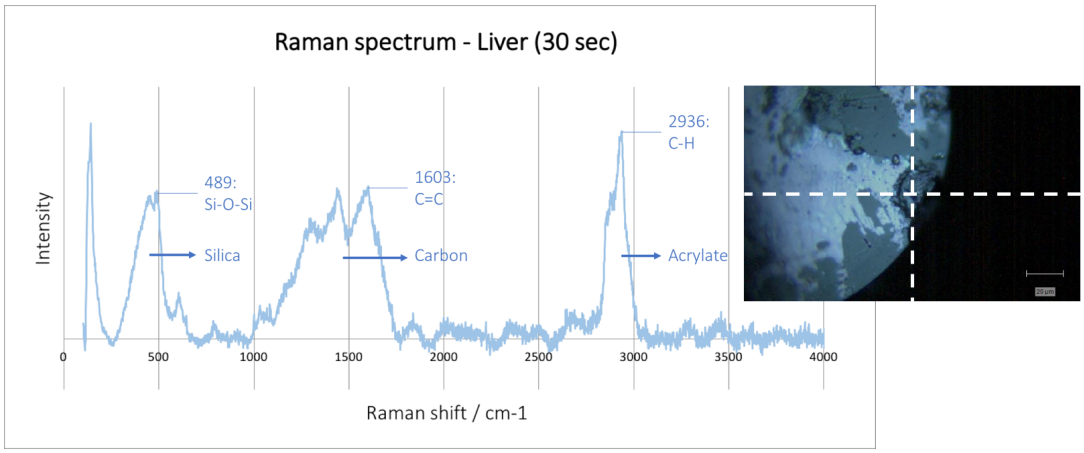

Figure 42: Raman spectrum of surface area #2 of the fiber tip used on porcine liver for 30 seconds.

9.3.2.3 Conclusion and discussion

Based on the results received from the Raman analysis, it may be concluded that fiber tips used on pork belly for only 5 seconds are completely covered with a layer of carbon. It is very likely that this carbon layer causes DRS signal deterioration during smart electrosurgery. In contrast pork belly fibers, fiber tips used on liver for 30 seconds seem to be partly clean (showing silica) and partly covered with both carbon and acrylate. Again, this layer of carbon and acrylate could cause DRS signal deterioration during smart electrosurgery.

However, these conclusions are based on only six small areas located on the surfaces of only two samples. This rather low quantity makes the results somewhat unreliable. Also, it should be noted that the results are highly dependent on the location of the specific areas that were selected for the Raman analysis. The Raman spectra provided in this report do not cover the entire fiber tip surfaces. Additional analysis is required to obtain more extensive and detailed information about the complete layer covering the fiber tip. Furthermore, it remains unclear where the carbon, present on the surface of both fiber tips, originates from. It is suspected that the carbon formation is either caused by burnt tissue, burnt acrylate coating or both. Additional research should clarify this issue.

9.4 Discussion and conclusion

The goal of this chapter was to investigate the morphology and composition of optical fiber tips used for smart electrosurgery on pork belly and porcine liver for both 5 and 30 seconds. In order to examine the influence of smart electrosurgery on the morphology of optical fiber tips, optical microscopy and SEM analyses were performed. For the examination of the influence of smart electrosurgery on the composition of the fiber tip surface, EDS and Raman spectroscopy were used.

For all these different analyses, it should be taken into account that inaccuracies might have taken place. In some cases, the images being compared had different magnifications and scales were set manually, which both might have influenced the observations. Due to overexposure, some EDS images were less usable and less reliable. Also, it should be taken into account that the composition results were highly dependent on the specific locations selected for analysis. Furthermore, for some of the analyses, very few samples were used. During follow-up studies, the reliability of the results could be increased by increasing the total quantity of the samples. It should also be considered that the same samples were used for each different analysis. Although it was tried to handle the samples as carefully as possible, complete quality preservation can unfortunately not be guaranteed. For example, fibers could have been damaged during their removal from the tubes or during transfer from one method to another.

Nevertheless, overall it might be concluded that two different factors seem to have a significant influence on DRS signal deterioration during smart electrosurgery. First, the results of the analyses described in this chapter have shown that the tip of an optical fiber used for smart electrosurgery gets covered by a layer of contamination called tissue debris. This tissue debris layer contains traces of fresh tissue, blood, acrylate and charred tissue/acrylate, of which the latter turned out to be the main component. Presence of the so-called char results from a chemical process called charring. Due to high electrosurgical temperatures (up to 350°C) and incomplete combustion, all organic materials (acrylate and porcine tissue) are thermally decomposed. The non-carbon elements are stripped from carbon chains and rings and are released into the atmosphere, while carbon elements themselves start to form char. This material has a dark brown or black color and shows graphite-like characteristics. Together with fresh tissue, blood and acrylate, char contaminates the tip of the optical fiber, inhibiting light transport through the fiber, leading to signal deterioration. However, it remains unclear whether the char is caused by the melting acrylate coating, by the porcine tissue or by both. This should still be clarified by additional tests.

The results of the analyses described in this chapter indicate a second factor influencing DRS signal deterioration during smart electrosurgery. Images clearly show that, due to high electro-surgical temperatures, the acrylate coating protecting the silica core, melts and undergoes charring. It seems as if this process has two different consequences. First, a small part of the nearby coating is displaced to the upper surface of the fiber tip, blocking the sight of the fiber. Second, the remaining part of the nearby acrylate coating melts away and turns into char, leading to damage to the core and its cladding. As a result, the intensity of the DRS signal deteriorates.

In order to confirm the influence of both tissue debris contamination and heat affected optical fibers on signal deterioration during smart electrosurgery, additional research is required. The remainder of this report therefore focusses on testing different concepts solving these two issues.

10. Design concepts

This chapter describes three different design concepts that could potentially solve DRS signal deterioration during smart electrosurgery. In order to come up with concepts that have enough potential to solve DRS deterioration in the context of smart electrosurgery, a list of requirements was composed. This list contains all requirements that should eventually be met in the future by the final solution for DRS signal deterioration. Based on this list, the concepts described in paragraph 10.2, 10.3 and 10.4 were selected.

10.1 List of requirements

In this paragraph both an extensive list of requirements and a shortlist of requirements are provided. The extensive list names all criteria that the final (future) solution should meet, while the shortlist summarizes all criteria that were used in the first search for possible solutions for DRS signal deterioration during smart electrosurgery.

10.1.1 Extensive list of requirements

The extensive list of requirements contains all important characteristics that the final design solution must have in order to be successful. The list concretely describes all design objectives that can be used to select the most promising ideas and design proposals [131]. The different requirements are drafted on the basis of all information gathered on the design problem. New perspectives on the design problem often lead to the discovery of new requirements. Therefore, the list of requirements was constantly updated over the course of this master thesis. In order to guarantee completeness and to make sure no essential requirements were missed, the basic structure provided in the Delft Design Guide was used to set up this list of requirements [131]. The standard list of requirements is explained in appendix H.

1. Performance

1.1 The solution must enable constant DRS measurements during the entire use of the smart electrosurgical knife.

2. Environment

2.1 The solution must be able to withstand the effects of electrical current.

2.2 The solution must be able to withstand biological fluids.

3. Life in service

3.1 The solution must be functional for as long as the smart electrosurgical knife is used.

3.2 The solution should be functional for at least 10 minutes of effective cutting time per surgery [9].

4. Maintenance

4.1 The solution must be able to withstand all different kinds of cleaning used to remove tissue debris from the blade during smart electrosurgery [9].

5. Target product cost

5.1 The solution should not cause extensive additional costs on top of the total costs of the smart electrosurgical knife.

6. Quantity

6.1 It should be possible to produce quantities large enough to cover the total number of electrosurgical knives currently used in oncological surgery.

7. Production facilities

7.1 Implementation of the solution must fit within the production facilities of Philips and/or the Delft University of Technology.

8. Size and weight

8.1 Both the size and the weight of the solution must not influence the current workflow of the electrosurgical knife.

9. Materials

9.1 The materials used must be able to withstand temperatures up to 350°C [59].

9.2 The materials used must be bioinert.

9.3 The materials used must be able to withstand standard cleaning procedures.

10. Standards, rules and regulations

10.1 The solution must comply with the Conformité Européenne (CE) regulations for medical devices.

11. Ergonomics

11.1 The solution must influence the current electrosurgical workflow as little as possible.

11.2 Handling of the solution must be self-evident, in order to prevent unintended use.

12. Reliability

12.1 If the solution fails during use, the user must be notified in order to prevent false margin assessment indications.

13. Safety

13.1 If the solution fails during use, the user must be notified in order to prevent damage in any form.

14. Installation and initiation of use

14.1 The solution must complement the traditional electrosurgical knife.

14.2 Initial use of the solution must require as little instructions as possible.

15. Reuse

15.1 The solution must last for at least ten surgeries.

10.1.2 Shortlist of requirements

In order to search for potential solutions for the problem of DRS signal deterioration during smart electrosurgery, the extensive list of requirements from the previous paragraph was summarized to a shortlist of requirements in order of importance. The list contains only the most important criteria that a solution should meet in order be considered for further development. During further development, the extensive list might be consulted to understand what additional features should complement the primary solution to make it even more suitable.

1. Performance

1.1 The solution must enable constant DRS measurements during the entire use of the smart electrosurgical knife.

2. Materials

2.1 The materials used must be able to withstand temperatures up to 350°C [59].

2.2 The materials used must be bioinert.

3. Ergonomics

3.1 The solution must influence the current electrosurgical workflow as little as possible.

4. Production facilities

4.1 Implementation of the solution must fit within the production facilities of Philips and/or the Delft University of Technology.

5. Target product cost

5.1 The solution should not cause extensive additional costs on top of the total costs of the smart electrosurgical knife.

10.2 Design concepts

Three different design concepts were selected as potential solutions for DRS signal deterioration during smart electrosurgery. As a starting position, the design of the smart electrosurgical knife of Adank was used [7], since this design has been proven to work and influences the current electrosurgical workflow as little as possible. Adaptions to this design were made based on findings from the optical fiber tip analysis as described in chapter 9 and on the shortlist of requirements provided in the previous paragraph.

10.2.1 Design concept 1: Anti-adhesive coating

The focus of this design concept is on the first factor found to influence DRS signal deterioration during smart electrosurgery: tissue debris contamination. Chapter 9 has shown that a mix of fresh tissue, blood, acrylate and char forms a layer covering the tip of the optical fiber, blocking all passage of light. This means a solution is required that prevents all these different components from forming a layer on the surface of the optical fiber tip. Chapter 8 has shown some examples of tissue engineering preventing materials from sticking to a surface. One of the easiest methods to apply surface engineering to a delicate substrate such as the optical fiber, is the use of a coating. In this case, a coating is required of which the main feature is to make a surface anti-adhesive. Some additional criteria were listed as well in order to systematically search literature for coatings with potential solving debris contamination.

Table 11: Design criteria for an anti-adhesive coating used to prevent tissue debris contamination on the tip of the DRS fiber of the smart electrosurgical knife. The third column shows which design criteria are met by the PTFE coating, within this master thesis selected as the most promising, feasible option for the first design concept [176].

#	Coating design criteria	PTFE coating
1	The coating must have an anti-adhesive effect	✓
2	The coating must enable constant DRS measurements (e.g. transparency)	✓
3	The coating must be thermally stable up to 350°C	265°C max
4	The coating must be bioinert	Chem. resistance
5	The coating must be applicable on glass substrate	✓
6	The costs of the coating must be as low as possible	✓
7	The coating must be easy to apply (at Philips or TU Delft)	✓

Together, those criteria represent the minimum set of properties a coating must possess (Table 11). There is some overlap between these coating design criteria and the list of requirements described in paragraph 10.1. However, the coating design criteria provided below are a more detailed, whereas the list of requirements is a bit more general. On the basis of this list, literature was thoroughly searched for suitable coatings meeting all design criteria. Some very interesting research papers were found,

describing coatings that ticked off most boxes [177, 178]. An overview of the comparison of these coatings is to be found in appendix I. However, it turned out to be much harder than expected to find a coating that has all required features and, at the same time, is cheap and easy to apply. For this master thesis, the latter two were very important, since the selected coating was supposed to be tested in practice. Due to a lack of expertise and a lack of time, it was therefore chosen to come up with a design concept that does not meet all design criteria yet. This design concept will thus not be suitable as a final solution, but it will provide a strong first indication about the potential of using an anti-adhesive coating to prevent DRS signal deterioration. The coating, theoretically showing the most potential so far, is polytetrafluoroethylene (PTFE or 'Teflon'). This coating has been described before in the prior literature study [55].

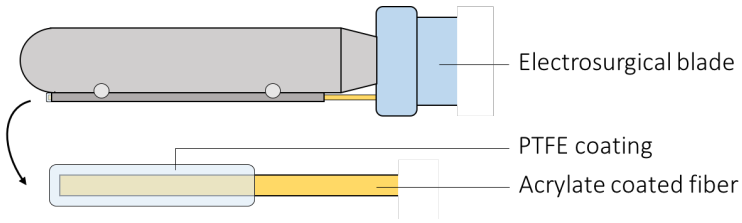

Figure 43: Optical fiber provided with PTFE coating to prevent tissue debris adhesion, leading to DRS signal deterioration.

PTFE is a plastic polymer consisting of long chains of carbon and fluorine atoms and the bonds between those atoms are tremendously strong [179]. The carbon-carbon bonds form the spine of the polymer chain and the fluorine atoms function as a protective sheath covering the carbon spine. This protects the molecule from any chemical attacks, making it chemical inert to the harshest organic and inorganic chemicals. Although PTFE is considered a thermoplastic, it only softens at its melting temperature of approximately 327°C. However, when the maximum operating temperature of 265°C is exceeded, PTFE might thermally degrade. Furthermore, the fluorine sheath reduces the surface energy, which results in outstanding non-stick properties and a very low friction coefficient. The extremely strong interatomic cohesive bonds cause the chains to firmly stick together. In contrast, there are practically no adhesive forces between PTFE chains and other materials, which prevents any material from sticking to PTFE. This principle is shown in Figure 44 [123-125, 179].

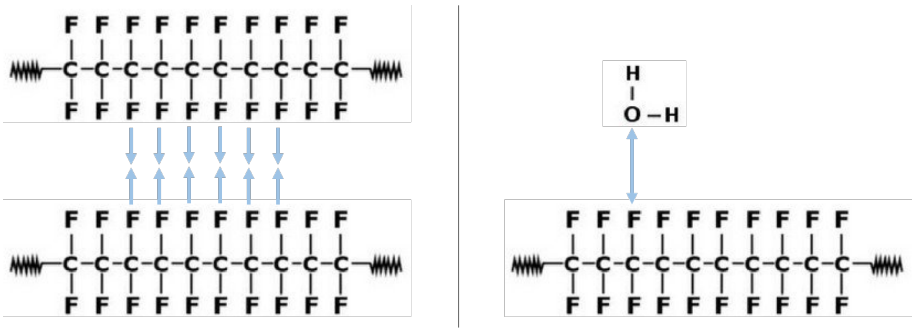

Figure 44: The non-stick principle of PTFE: fluorine atoms prefer their own kind and are drawn to each other (left), while they repel any other kind of molecule, like for example water (right) [125].

Based in this information, it is suspected that testing a PTFE coating could be a very strong starting point, from where further coating development might set off. The third column of Table 11 shows which design criteria are theoretically met by PTFE and which ones still fall short. Eventually, experimental testing of this design concept must reveal how well PTFE coating does in practice.

10.2.2 Design concept 2: Heat-resistant fiber

The focus of this design concept is on the second factor thought to influence DRS signal deterioration: fiber damage. In order to prevent fiber damage, the solution should be able to withstand temperatures up to 350°C. The operating temperature of the originally used fiber was limited by the low melting temperature of the acrylate coating protecting the silica core. Therefore, this design concept needs to get rid of the acrylate coating. One option would be to replace the acrylate coated fiber with an aluminium coated fiber, which increases the maximum operating temperature to 400°C (Figure 45). Detailed specifications of this aluminium coated fiber are to be found in appendix J. Preventing the outer coating from melting should keep the silica core intact, leading to less signal loss during smart electrosurgery.

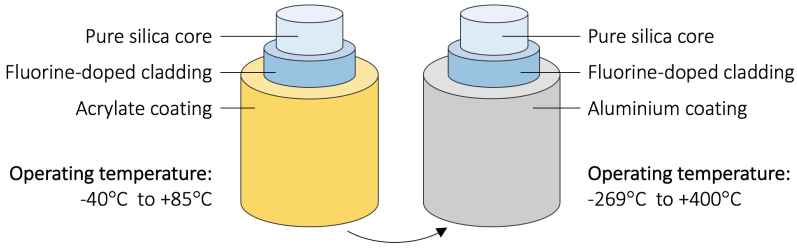

Figure 45: The acrylate coated fiber (left) with a low operating temperature and the aluminium coated fiber (right) with a high operating temperature.

However, the only manufacturer able to supply aluminium coated fiber is located in the USA, which obstructs easy delivery. Due to time, money and legal constrictions, it was chosen to first try out a simpler solution. A simple solution could provide a first indication of the effect of elimination of the acrylate coating on DRS signal deterioration. If this effect turns out to be positive, the use of a heat-resistant fiber might be considered again.

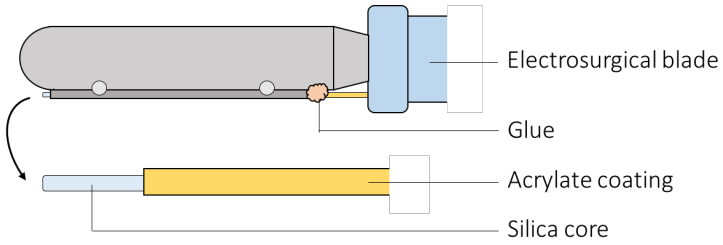

Figure 46: The optical fiber partly stripped from its acrylate coating to avoid thermal degradation effects, leading to DRS signal deterioration. The fiber is attached to the tube with the help of glue at the end of the tube.

Instead of using a different, heat-resistant coating, the acrylate coated fiber is simply transformed to a heat-resistant fiber by stripping off the acrylate coating. In this way, there is no coating left to damage the remaining part of the fiber under the influence of high temperatures. However, as mentioned before, the outer coating of an optical fiber is applied in order to protect the silica core and its cladding. Although the silica core is able to withstand high temperatures, as soon as the whole coating disappears, the core and cladding get exposed and become very vulnerable to other external influences, risking mechanical and chemical damage. This damage may result in a change of the refractive index of the medium, leading to light scattering and significant signal loss [155, 156]. Therefore, the stripped silica core is put into the small metal tube (attached to the electrosurgical blade) for protection and is attached to this tube by using a bit of glue at the back to make sure it is unable to move (Figure 46). This should minimalize the risk on mechanical damage.

10.2.3 Design concept 3: Anti-adhesive coating & heat-resistant fiber

The third design concept is a combination of the first two design concepts. In this concept, both a heat-resistant fiber and an anti-adhesive coating are used to prevent DRS signal deterioration during smart electrosurgery. In order to achieve this, the optical fiber is stripped to get rid of the acrylate coating. Subsequently, PTFE coating is applied to the stripped part of the fiber. This method should eliminate the damaging effect of the degrading acrylate coating and prevent the contaminating effect of tissue debris adhesion.

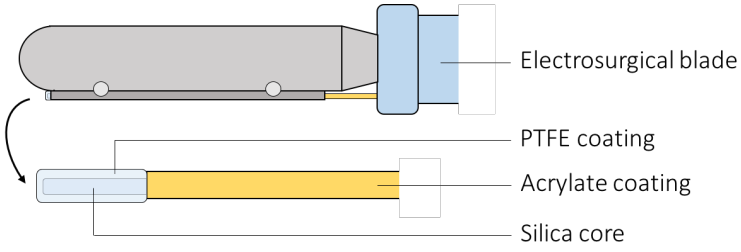

Figure 47: Optical fiber partly stripped from its acrylate coating to avoid thermal degradation effects and also provided with PTFE coating to prevent tissue debris adhesion, both leading to DRS signal deterioration.

10.3 Discussion and conclusion

The goal of this chapter was to describe three different design concepts that all improve DRS measurements during smart electrosurgery. Design concept 1 focusses on the problem of tissue debris adhesion, which blocks the tip of the optical fiber during use. To prevent this from happening, a PTFE coating is applied to the acrylate coated fiber. The most interesting properties of this coating are its non-stick effect, its transparency, its bioinertness and its thermal stability. However, the latter still raises questions, since the maximum operating temperature of PTFE is only 265°C, while tissue temperatures can be as high as 350°C during electrosurgery. Experimental testing still need to indicate whether this causes any problems in practice. Also, the amount of influence of tissue debris contamination on signal deterioration still needs to be confirmed. Results of experimental testing of the PTFE coating should reveal whether the application of an anti-adhesive coating is enough to solve the DRS signal deterioration problem or that additional steps need to be taken.

On the other hand, design concept 2 focusses on the problem of the thermally degraded acrylate coating, both blocking and damaging the fiber tip during use. To prevent this from happening, the acrylate coating is stripped off the optical fiber, exposing the silica core and its cladding. By placing the core in the metal tube, it is thought to have enough protection from external influences other than temperature. However, it remains unclear whether eliminating the acrylate coating has a positive effect that is high enough to improve DRS measurements. Experimental testing should reveal how far-reaching the positive effect of acrylate elimination is in practice.

The third design concept focusses on both problem mentioned above. This means that a stripped optical fiber and the application of a PTFE coating are combined. Theoretically this should result the elimination of the damaging effect of the degrading acrylate coating and prevention of the contaminating effect of tissue debris adhesion. Whether this concept shows the best results in practice as well, still needs to be confirmed by experimental testing.

Overall, it may be concluded that theoretically all three concepts seem promising in solving DRS signal deterioration during smart electrosurgery. However, experimental testing is required to show whether either implementation of one solution is enough to improve DRS measurements or that implementation of two solutions is needed to solve the problem. In order to find out which design concept shows the most promising results; all three concepts are experimentally tested in research phase 3.

IV. RESEARCH PHASE 3

CONCEPT TESTING

The goal of the third phase of this research is to test the design concepts that were described previously. Three different analyses are used to compare these concepts to the traditional smart electrosurgical knife. Chapter 11 describes the entire process of concept testing. The last paragraph of this chapter reveals which concept shows most potential.

11. Concept testing

This chapter describes three different analyses that were performed in order to test the design concepts provided in the previous chapter. Comparing the results of these design concepts to the results of the traditional concept, should indicate the influence of the different modifications on DRS signal deterioration during use of the electrosurgical knife.

11.1 Sample preparation

The goal of this paragraph is to create used optical fiber tip samples in which all three design concepts were implemented, so that the influence of each design concept can be analyzed. This influence analysis will be done in paragraphs following 11.1.

11.1.1 Materials and methods

Equipment
The equipment used for this experiment was very similar to the equipment used for the sample preparation in chapter 9.1. The same ESK (Hangzhou Valued MedTech Co., China), electrosurgical unit (Valleylab, Boulder, United States), dispersive pad (Philips In-Body Systems, Eindhoven) and 12 smart electrosurgical blades (composed at the Delft University of Technology) were deployed. Again, 12 non-functional DRS fibers were attached to the blades, which means that the other end of the fiber was not connected to a DRS connector. However, in order to implement the different design concepts, the fibers used for this experiment were pretreated before attachment to the blades. To achieve this, a disinfectant (Dettol, Reckitt Benckiser, England), a stripping tool (Knipex, Germany) and a PTFE coating (Mororex, Switzerland) were used. Furthermore, 0.5 kg pork belly was used to cut in, because this tissue type had previously shown to lead to the most severe signal blocking.

Setup and methods
In order to observe the influence of the three different design concepts, it was decided to create 3 traditional DRS fibers, 3 stripped fibers, 3 PTFE coated fibers and 3 stripped + PTFE coated fibers. First, all 12 fibers were cleaned with disinfectant. The stripped fibers were fabricated by using the stripping tool to carefully strip off about 1 cm of the acrylate coating from the fiber tips. The PTFE coated fibers were fabricated by using the PTFE spray on the complete fibers and let them dry for about 30 minutes. The stripped + PTFE coated fibers were fabricated by first stripping off the acrylate coating and subsequently use the PTFE spray on the fibers and let them dry for about 30 minutes. After drying, all fibers were attached to the smart electrosurgical blades, that were cleaned before with water and soap. During attachment, it was tried to align the tips of the tubes and the fibers as precise as possible, so that only the tip of the fiber comes into contact with the heated tissue and the remaining part is protected by the metal tube. The setup and the settings of the sample creation were similar to the one shown in Figure 22 in chapter 9.1. The cutting duration was held constant for 30 seconds this time, because this duration showed the most severe signal blocking. Again, this experiment took place at the In-Body Systems department of Philips Research in Eindhoven.

11.1.2 Results

After creating used DRS fiber samples, the fibers were taken out of the tubes, so that they could be studied. Figure 48 shows all fiber samples per design concept. It is clearly observed that there is char present on the fiber tips. On average, this char is reaching about 7 mm down from the top of the fiber tip. With the naked eye, no clear differences are observed between the different design concepts.

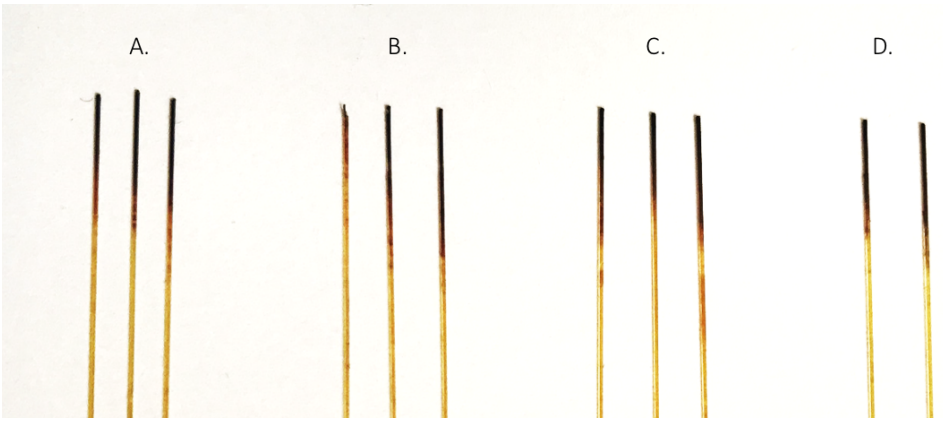

Figure 48: Used fiber tip samples. A) Traditional fiber, B) Design concept 1: stripped fiber, C) Design concept 2: PTFE coated fiber and D) Design concept 3: Stripped + PTFE coated fiber.

11.1.3 Discussion and conclusion

Note that there are only two stripped + PTFE coated fibers (Figure 48-D) provided. Unfortunately, there was a failure during the preparation of the third fiber of that category, causing this fiber to be useless. From the sample preparation and the quick analysis with the naked eye, it may be concluded that there are no clear differences to be observed between the used fiber tips of the different implemented design concepts. All fibers contain a certain amount of char on the fiber tip and both stripping and PTFE coating do not seem to have any influence on that phenomenon. More thorough analyses are required to investigate the influence of the design concepts on signal deterioration in more detail.

11.2 Light intensity analysis

In order to measure the influence of the different design concepts on signal deterioration during use of the smart electrosurgical knife, the samples created in the previous paragraph are analyzed on their light intensity. Measuring the light intensity coming out of each fiber sample, should indicate whether the design concepts have affected the optical signal, compared to the used traditional fibers.

11.2.1 Materials and methods

Equipment

In order to measure the light intensity of the fiber samples, a light source on one side and a high sensitivity thermal laser sensor (Ophir, Jerusalem, Israel) on the other side were used. The light source was placed on a lab jack (Rudolf Grauer AG, Switzerland). Furthermore, some pipettes, foam rubber and tape were used to connect the fibers to the light source, one by one.

Setup and methods

A schematic representation of the setup of the light intensity analysis is shown in Figure 49. Again, this experiment took place at the In-Body Systems department of Philips Research in Eindhoven. After the setup was prepared, the different fibers were attached to the light source one by one. Before measurement, calibration was performed, which included taking into account the surrounding light and temperature and the heat of the light source. Especially the latter turned out to have a huge influence on the measurements, so calibration was an important part of this experiment. For each category, one unused fiber was measured by means of control. This control provided an indication of the influence of each design concept on the general light transmittance through the optical fiber. Subsequently, all the used fibers were placed into the connection part attached to the light source. The light intensity was read from the display of the high sensitivity thermal laser sensor, measured in power (µW).

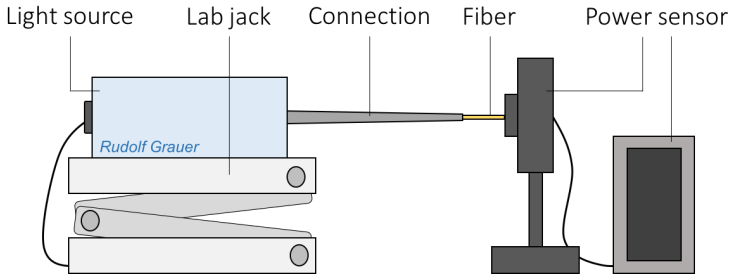

Figure 49: Experimental setup of the light intensity analysis, including light source, lab jack, connection part, and power sensor. One by one, the fiber samples are placed in between the light source and the power sensor.

11.2.2 Results

The results of the light intensity analysis are shown in Table 12 (raw data are provided in appendix K). Column 2 shows the power of the light transmitted through an unused, clean fiber of the specific fiber modification. It is observed that by adding either stripping or PTFE coating to a traditional fiber, the light transmittance of an unused fiber decreases. Adding both stripping and PTFE coating to the traditional fiber, leads to even more power loss. Column 3, 4 and 5 provide the number of samples, the mean power measured and the standard deviation per fiber modification. Column 6 provides the absolute signal loss with respect to the unused fiber and column 7 provides the relative signal loss as a percentage of the power intensity of the unused fiber for each modification.

Table 12: Results of the light power intensity analysis showing the absolute and relative signal loss per modified fiber.

Fiber modification	Unused	N	Mean	SD	Absolute signal loss	Relative signal loss
A. Traditional	12 µW	2	6.5 µW	0.7	5.5 µW	45.8%
B. Stripped	11 µW	3	7.0 µW	1.9	4.0 µW	36.4%
C. PTFE coated	11 µW	3	5.7 µW	0.6	5.3 µW	48.5%
D. Stripped + PTFE coated	10 µW	2	6.0 µW	0.0	4.0 µW	40.0%

When comparing the means of the used fibers with the intensities of the unused fibers, it can be seen that unfortunately all fibers lost signal power. This is confirmed by the absolute signal loss in column 6. This column shows that the traditional fiber has lost the most power. However, relative to the power intensities of the unused fibers, this is not the case. The traditional fiber lost 45.8% of its initial power, while fibers B, C and D lost 36.4%, 48.5% and 40.0% respectively. So, compared to the traditional fiber, the PTFE coated fiber lost more signal power and the stripped fiber and the stripped + PTFE coated fiber lost less signal intensity. In other words, stripping the traditional fiber seems to decrease signal loss, while adding a PTFE coating seems to increase signal loss.

11.2.3 Discussion and conclusion

Although the means in column 4 of Table 12 show some clear differences in light power intensity between the different fiber conditions, the standard deviation confirms that the differences are mainly caused by one or two outliers. Comparing the standard deviations with the differences between means, shows that the numbers provided in Table 12 are not that reliable. Also, the total number of samples (N) is quite low, decreasing the reliability of the results even more. For fiber modification A and D there were only two instead of three samples. One sample broke down during preparation and the other was too short to fit the intensity measurement setup.

However, when conclusions have to be drawn based on these results, it may be concluded that adding PTFE coating to traditional fiber leads to additional signal loss. In contrast, stripping the fiber from its acrylate coating leads to less signal loss compared to the traditional fiber. So, according to this scenario, making the optical fiber resistant to the extreme heat occurring during electrosurgery, seems as the most promising design concept to improve DRS signal deterioration. Due to the unreliability of these results, additional analyses will have to be performed to check whether this indeed is the case.

11.3 Morphology analysis

In order to measure the influence of the different design concepts on signal deterioration during use of the smart electrosurgical knife, the samples created in the first paragraph of this chapter are analyzed on their morphology. The morphology of the used modified fibers will therefore be compared to the morphology of the used traditional fibers. This is done by using the Keyence optical microscope to create detailed images of the fiber tips. This method was used before in paragraph 9.2.1.

11.3.1 Materials and methods

The materials and methods used for this analysis were exactly the same as those described in paragraph 9.2.1.1. The experiment took place at the faculty of Mechanical Engineering at the TU Delft and a schematic representation of this analysis is shown in Figure 24. In total, 15 samples were analyzed, of which 4 were unused fibers, each with a different modification (traditional, stripped, PTFE coated and stripped + PTFE coated) and the remaining 11 were used fibers with the same modifications. One by one, the samples were studied and pictures were taken both in top and in side view. Again, the software ImageJ (Image Processing and Analysis in Java) was used to measure certain distances within the images obtained with optical microscopy.

11.3.2 Results

An overview of all results is provided in appendix L. Figure 50 shows top view images of the samples, obtained with the Keyence optical microscope. The upper row represents unused fibers under different conditions, while the lower row represents used fibers under the same conditions.

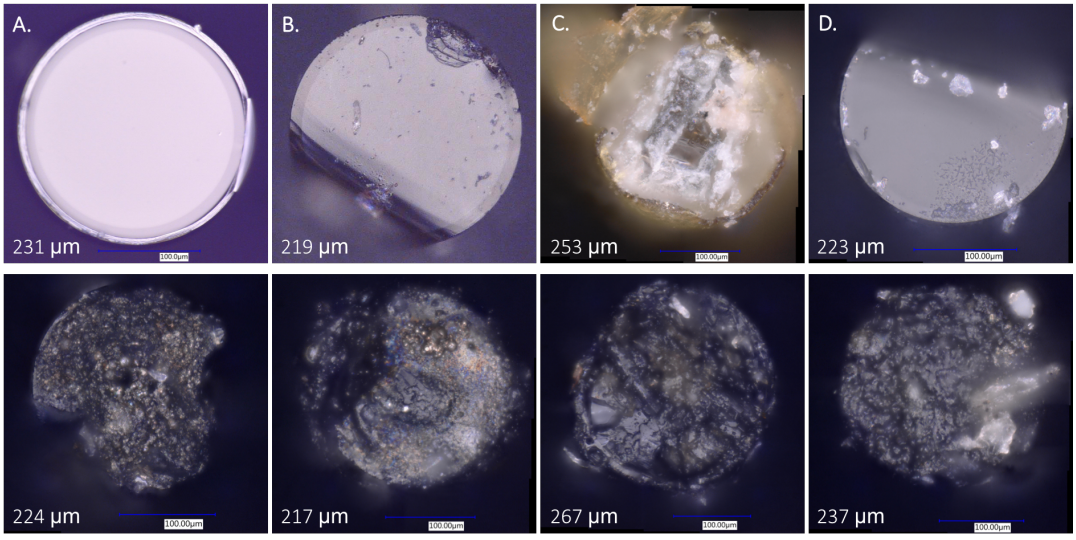

Figure 50: Keyence optical microscope images in top view of unused (upper) and used (lower) fibers with: A) Traditional fiber, B) Stripped fiber, C) PTFE coated fiber, and D) Stripped + PTFE coated fiber.

For each sample, the outer diameter (in µm) is shown. For the unused fibers, these diameters are based on one sample only, while for the used fibers, these diameters are based on the average of two samples. The outer diameters provide indications about what happens to the different modified fiber layers

during smart electrosurgery. It is observed that the acrylate coating of the traditional fiber (A) partly disappears during use, just like has been observed before. The outer diameter of the stripped fiber (B) is equal to the diameter of the core and cladding of the traditional fiber. This diameter does not change during use, which indicates that all layers are remained. The outer diameter of the unused PTFE coated fiber (C) is larger than the outer diameter of the traditional fiber, which can be explained by the additional layer of PTFE coating that has been applied. This diameter has increased after use, which might be caused by differences in PTFE coating thickness. The fact that this outer diameter has not decreased after use, indicates that the PTFE coating protects the acrylate coating. The outer diameter of the stripped + PTFE coated fiber (D) has increased as well after use, which is probably also caused by PTFE coating differences.

It is suspected that the bright, white pieces of material observed on C and D represents PTFE coating. The unused fiber tip of C is completely covered with this material, while it seems as if there is hardly any PTFE coating attached to the unused fiber of D. This could explain the big difference in outer diameter between the unused and used D fibers. Some small pieces of PTFE coating are detected on the used fibers, which indicates that this coating has prevented tissue debris adhesion a little. Furthermore, a difference is observed in the structure of the tissue debris layers covering the used tips. The structure of A and B fibers looks more refined and smooth, while the structure of C and D looks a bit rougher.

The white PTFE coating pieces are also to be found in the side views of the coated fibers (C and D) in Figure 51. However, compared to A and B, the surfaces of the C and D look more contaminated and rougher. For the traditional fiber, it is observed that the acrylate coating indeed has melted away again. For the stripped fiber, some cracks are observed, which could have been caused by a lack of protection by the acrylate coating.

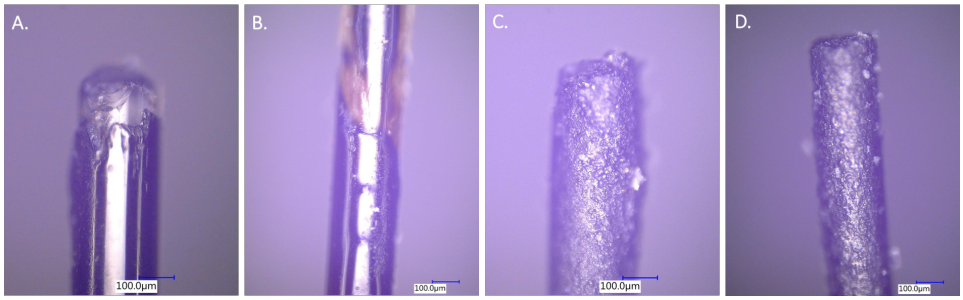

Figure 51: Keyence optical microscope images in side view of used fibers with: A) Traditional fiber, B) Stripped fiber, C) PTFE coated fiber, and D) Stripped + PTFE coated fiber.

11.3.3 Discussion and conclusion

From the results provided in the previous paragraph conclusions can be drawn. However, there are some uncertainties that need to be taken into account. First of all, the unused fibers of this analysis were not exactly the same fibers that were used to cut tissue. Therefore, the differences in shape, structure and measurements cannot only be explained by electrosurgical use. Furthermore, in contrast to the fiber samples created in chapter 9.1, these fiber tips were not polished before use. In general, material sticks to rough surfaces easier than to smooth surfaces. Therefore, the results obtained in this chapter cannot be compared with the results of chapter 9. This also explains why some sample parts are either deformed or missing. Also, all fibers were manually placed inside and attached to the tubes of the smart blades. It was tried to align the tips of the tube and the fiber as precise and constant as possible, however, this might not always have worked out just as well. The position of the fiber with respect to the tube, could influence the effect of heat on the fiber tip.

Overall, it may be concluded that the PTFE coating used for this experiment does not seem the be able to completely prevent tissue debris from sticking to the surface of the optical fiber tip. This is probably caused by the limited operating temperature of this particular coating (265°C). The fact that the electrosurgical temperature exceeds the maximum operating temperature of the PTFE coating, has probably led to thermal degradation of the coating. In general, this leads to a deformed, rougher surface, that facilitates easier tissue debris adhesion. This effect is indeed observed on the surfaces of the used PTFE coated fiber tips. Another cause for the failure of the PTFE coating to completely prevent tissue debris adhesion, could be the weak binding between the coating and the fiber surface. It is generally known that the binding between a substrate and a coating gets stronger when they are baked in the oven at high temperatures after application. This has not been the case in this research. A strong binding between the fiber and a coating is suspected to positively influence its anti-adhesive function and its heat-resistance. Furthermore, it might be concluded that, initially, a PTFE coating is able to protect an acrylate coating against the high tissue temperatures that occur during smart electrosurgery. However, after the PTFE coating itself degrades due to extreme heat, this will probably no longer be the case. This should be investigated during further research for the effect of heat on the optical fiber. The images of the side view of the stripped fiber samples, show that stripping the fiber leads to an increased risk of fiber damage due to a lack of protection. It is therefore suggested to repeat this experiment with a heat-resistant fiber, subsequently covered with a more advanced non-stick coating that is sure to adhere well to the optical fiber.

From this morphology analysis, it has not become clear whether the amount of char on top of the modified fibers has decreased compared to traditional fiber. It is suspected that a composition analysis might be able to reveal more information concerning the amounts of element present on the tip of the fiber. This analysis is described in the next paragraph.

11.4 Composition analysis

In order to measure the influence of the different design concepts on signal deterioration during use of the smart electrosurgical knife, the layer covering the tips of the samples created in the first paragraph of this chapter are analyzed on their composition as well. Just like in paragraph 9.3.1, this is done by using EDS.

11.3.1 Materials and methods

The materials and methods used for the EDS analysis were exactly the same as those described in paragraph 9.3.1.1. The experiment took place at the faculty of Aerospace Engineering at the TU Delft and a schematic representation of this analysis is shown in Figure 37. In total 6 samples were analyzed, of which 4 were used fibers, with different modifications (traditional, stripped, PTFE coated and stripped + PTFE coated) and the remaining 2 were unused fibers (PTFE coated and stripped + PTFE coated). One by one, pictures of the samples were taken and the different compositions were studied. While taking a picture, it was tried to depict the entire fiber tip at a magnification of 400x, in order to be able to compare the different results.

11.3.2 Results

The EDS analysis has provided interesting results containing information about the composition of the layer covering the tip of the optical fiber. A complete overview of the results is to be found in appendix M. Figure 52 shows the results of three different kinds of unused fibers. Compared to the traditional unused sample, the amount of carbon has increased at the coated sample, which can be explained by the composition of PTFE coating (C_2F_4), covering the tip of this fiber. This composition also explains the presence of fluorine (F) at both the PTFE coated samples. In contrast, the amount of carbon has decreased at the stripped + PTFE coated sample, while a lot of silica is detected at this sample. Furthermore, a high amount of calcium is detected at the unused PTFE coated sample.

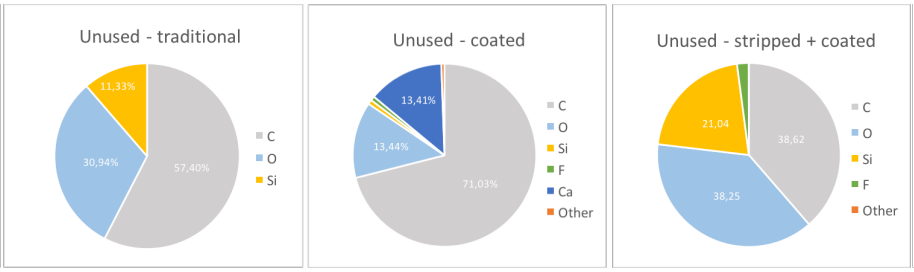

Figure 52: EDS results showing the relative amounts of elements present at the tips of three different unused fibers. The result of the unused traditional fiber was copied from the previous EDS experiment.

Figure 53 shows the results of four different kinds of used fiber tips. Compared to the traditional used fiber, the amount of carbon on the stripped fiber has decreased, while the number of other elements (indicating fresh tissue) has increased.

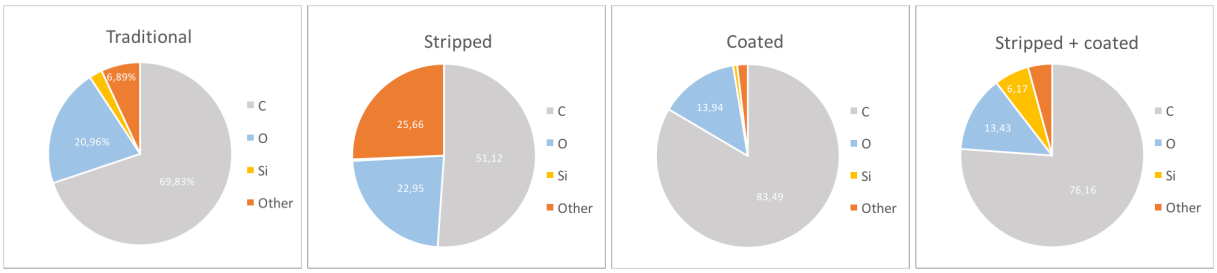

Figure 53: EDS results showing the relative amounts of elements present at the tips of four different used fibers. The result of the traditional fiber was established by taking the average of all used fiber tips analyzed in this report.

Part of the carbon decrease is caused by the elimination of acrylate. However, the combination of carbon decrease and the increase of other elements, could also indicate that, compared to the traditional used sample, the tissue debris covering the stripped fiber tip contains less char and more fresh tissue. The amount of carbon on the coated sample has increased. This increase is partly caused by the addition of PTFE coating, but it is also suspected that degradation of this PTFE coating under the high electrosurgical temperatures leads to even more char and tissue debris adhesion. In other words, it is suspected that the application of a PTFE coating leads to worse signal deterioration. Furthermore, the result of the stripped + PTFE coated fiber lies in between the results of the two previous samples, which seems logical because this fiber is a combination of those two. However, it is observed that more carbon is present on this fiber, compared to the traditional fiber. This indicates that the negative effect of the PTFE coating is larger than the positive effect of stripping.

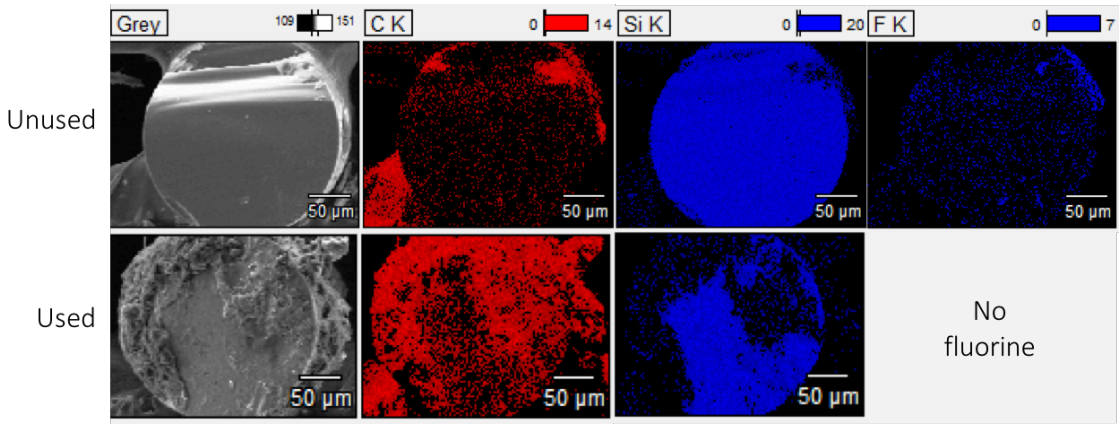

Figure 54: Images of an unused fiber (stripped + PTFE coated) and a used fiber (stripped + PTFE coated).

Figure 54 shows images of an unused fiber (stripped + PTFE coated) and a used fiber (stripped + PTFE coated). In red it is observed that most of the carbon detected in the image of the unused fiber originates from a small piece of dirt and from the glue at the background that was used to keep the samples in place. In contrast, the used fiber seems to be covered with carbon for a large part. This is confirmed by the decreasing amount of silica shown in this image. Lastly, this figure shows that fluorine was detected on the unused fiber, spread over the surface of the tip. However, after use no fluorine was detected anymore.

11.3.3 Discussion and conclusion

The results provided in the previous section show some uncertainties that need to be taken into account. It is suspected that the low amount of carbon at the unused stripped + PTFE coated fiber is partly caused by a rather weak binding between this specific fiber and the PTFE coating. The latter is amplified by the fact that, despite the application of a PTFE coating, a lot of silica is detected at this sample. Furthermore, the high amount of calcium at the unused PTFE coated sample is remarkable. Based on the picture of this fiber tip, showing some kind of pollution, and on the fact that calcium was not found at any of the other samples, it is assumed that this sample was contaminated. Also, it should be mentioned again that the fiber tips were not polished before use, leading to more and a different kind of tissue debris adhesion. Therefore, the results obtained in this chapter cannot be fairly compared with the results of chapter 9. This also explains why some sample parts are either deformed or missing. Also, all fibers were manually placed inside and attached to the tubes of the smart blades. It was tried to align the tips of the tube and the fiber as precise and constant as possible, however, this might not always have worked out just as well. The position of the fiber with respect to the tube, could have influenced the composition of the layer covering the fiber tip.

Both the increase of the amount of carbon and the complete disappearance of fluorine after use of the PTFE coated fibers, indicate that the electrosurgical temperatures are too high for PTFE coating and that the coating might even undergo charring as well. This makes sense when the maximum operating temperature of PTFE (265°C) is compared to the electrosurgical temperature (350°C). Beforehand it was chosen to try out the PTFE coating anyway, because it was unclear whether the non-stick effect would outweigh the temperature limitation. It has now become clear that it does not and that using PTFE under the extreme heat of smart electrosurgery leads to the opposite effect of non-sticking. Literature states that at temperatures above 260°C the quality of PTFE may deteriorate and loose its non-stick quality and that the melting temperature of PTFE is 327°C [180]. In addition, melting and deterioration of the PTFE coating leads to a rougher surface, which in turn leads to increased tissue debris adhesion. However, according to literature, the coating will not show significant decomposition unless temperatures exceed about 349°C. Since this temperature lies very close to the temperature that is assumed to be reached during smart electrosurgery (based on literature), it remains unclear whether PTFE undergoes charring during electrosurgery. In order to find out whether this is the case, further research should focus on the exact temperatures that occur during smart electrosurgery and its effect on optical fiber.

Since the stripped fiber has shown a decrease in the relative amount of carbon, it is assumed that less charring occurs during smart electrosurgery with a stripped fiber. However, the relative amount of fresh tissue has increased at the stripped fiber, compared to the traditional fiber. This indicates that elimination of the acrylate coating influences the amount of charring positively, leading to less char, while it seems to be unable to prevent tissue debris adhesion. Further research should investigate the effects of different char-tissue debris ratios. It could very well be, that the less char is present in tissue debris, the less problematic tissue debris adhesion is for DRS signal deterioration.

11.5 Discussion and conclusion

Based on the results provided in this chapter, some indications can be given about reducing DRS signal deterioration during use of the smart electrosurgical knife. However, it is important to note that the results are somewhat unreliable and that additional research is required to confirm the findings in this chapter. First of all, more reliable results might be obtained by increasing the number of samples. Also, all fiber tips need to be polished before use in order to be able to compare the different samples equally. In addition, to be able to compare the unused and used fibers fairly, the same physical fibers should be used for both the 'before' and 'after' analyses. Furthermore, it should be taken into account that all fibers were manually attached to the tubes of the smart blades. It was tried to align the tips of the tube and the fiber as equal as possible, however, this might not always have worked out that well. The position of the fiber tip with respect to the tube, could influence the effect of heat on the fiber tip.

Nevertheless, some findings do contribute to determining the direction of the next steps of this research. Before use of the modified fibers, it was observed that both fiber stripping and PTFE coating application reduce general transmittance of light through the acrylate coated optical fiber. After use, it is observed that all fiber tips have undergone charring regardless of which fiber modification was applied. This indicates that both fiber stripping and PTFE coating application are not able to completely prevent signal deterioration.

The electrosurgical temperature (350°C) exceeds the maximum operating temperature of the PTFE coating (265°C), which leads to thermal degradation and non-stick quality loss. In addition, melting and degradation of a coating leads to a rougher surface, which facilitates tissue debris adhesion even more. Together, the coating quality loss and the facilitation of debris adhesion result in the complete opposite effect of non-sticking, leading to increased DRS signal deterioration. This indicates that the high tissue temperatures that occur during smart electrosurgery should not be underestimated, because extreme heat turns out to have more influence on signal deterioration than was thought so far. Further research should investigate the exact temperatures that occur during smart electrosurgery and its (tissue independent) effect on the optical fiber. This information is thought to be important input for both the cause of signal deterioration and the selection of a suitable solution for this problem.

Unfortunately, stripping off the acrylate coating from a traditional optical fiber has also turned out to be unable the completely prevent DRS signal deterioration. However, the results of the light intensity test indicate that a stripped fiber does result in a decrease of signal loss compared to the traditional fiber. This positive effect could have been caused by the divergent char-fresh tissue ratio detected in tissue debris covering this specific fiber tip. Relatively, less char was detected, while more fresh tissue was found. It is therefore suggested that the smaller the proportion of char present in tissue debris (regardless of the amounts of other tissue debris components), the less problematic tissue debris adhesion is for DRS signal deterioration during use of the smart electrosurgical knife. This suggestion needs further investigation and might therefore be subject to further research. However, the side view images of the stripped fiber samples, show that stripping the fiber does lead to an increased risk of fiber damage due to a lack of protection. It is therefore recommended to implement a heat-resistant protection coating (like suggested in paragraph 10.2.2), instead of stripping off the outer coating, to make the optical fiber resistant to the extreme electrosurgical heat.

Overall, it might be concluded that the problem of signal loss during smart electrosurgery requires a solution that combines extreme heat-resistance with anti-adhesiveness. It is suggested to achieve this by applying a heat-resistant, anti-adhesive coating on a heat-resistant optical fiber, both thermally stable up to at least 350°C. In addition, this coating should meet all coating design criteria as listed in Table 11.

V. EVALUATION

The evaluation consists of two important chapters. Chapter 12 contains the final discussion and recommendations for further research, while chapter 13 contains the final conclusion based on the findings of this research.

12. Discussion & recommendations

This chapter contains the overall discussion of this master thesis and the recommendations for further research based on the findings obtained in this thesis.

12.1 Discussion

The goal of the final discussion is to briefly touch upon all the findings obtained in this master thesis, to reflect on the results and to determine the research contribution and the actual value of this research. First the most important results will be summarized and compared to literature, subsequently the research limitations will be discussed.

12.1.1 Most important results

12.1.1.1 Factors influencing DRS signal deterioration

Overall, it was observed that two different factors influence DRS signal deterioration during smart electrosurgery. First, the tip of the optical fiber gets covered by a layer of contamination called tissue debris. This tissue debris layer contains traces of fresh tissue, blood, acrylate and char, of which the latter turned out to be the main component. Char is the result of a chemical process called charring. Due to high electrosurgical temperatures (up to 350°C) and incomplete combustion, all organic materials are thermally decomposed. Carbon elements start to form char, which together with fresh tissue, blood and acrylate, contaminates the tip of the optical fiber, leading to signal deterioration. The presence of char, fresh tissue and blood corresponds with the hypothesis that was conducted in the literature study prior to this master thesis [55].

The presence of acrylate however, was unexpected and has indicated a second factor influencing DRS signal loss. Research results clearly showed that, due to extreme heat, the acrylate coating has melted and degraded. This process has two different consequences. First, a small part of the coating is displaced to the upper surface of the fiber tip, blocking the sight of the fiber together with tissue debris and leading to signal loss. Second, the remaining part of the acrylate coating has melted away, leading to core and cladding damage. As a result, the intensity of the DRS signal deteriorates. This observation matches statements found in literature saying that the maximum operating temperature of the acrylate coated optical fiber is 85°C and the maximum operating temperature of acrylate itself is 80°C, after which it degrades [153, 154].

12.1.1.2 Concepts solving DRS signal deterioration

Three different design concepts were created in order to respond to the two factors influencing DRS signal deterioration. Design concept 1 was meant to solve tissue debris adhesion, by applying a PTFE coating on the surface of the traditional fiber. Design concept 2 was meant to solve the low heat-resistance of the optical fiber, by stripping off the acrylate coating, exposing the high heat-resistant silica core and its cladding to the tissue. The third design concept focused on both problems, by combining a stripped optical fiber with the application of a PTFE coating. Testing these design concepts, led to some interesting findings that contribute to determining the direction of the next steps of this research. First of all, it was observed that all fiber tips had undergone charring regardless of which fiber modification was applied. This indicates that both fiber stripping and the application of a PTFE coating are not able to completely prevent signal deterioration during use of the smart electrosurgical knife.

The electrosurgical temperature (350°C) exceeded the maximum operating temperature of the PTFE coating (265°C), which has led to thermal degradation and non-stick quality loss. In addition, melting and degradation of the coating has led to a rougher surface, which generally facilitates tissue debris adhesion even more. These observations are both confirmed by literature describing the thermal effects on PTFE [180]. Together, the coating quality loss and the facilitation of debris adhesion results in the complete opposite effect of non-sticking, leading to increased DRS signal deterioration. This indicates that the high tissue temperatures that occur during smart electrosurgery should not be underestimated. Extreme heat turns out to have more influence on signal deterioration than was thought so far.

Unfortunately, stripping off the acrylate coating from a traditional optical fiber has also turned out to be unable to completely prevent DRS signal deterioration. However, the results of the light intensity test indicate that a stripped fiber does result in a decrease of signal loss compared to the traditional fiber. This positive effect could have been caused by the divergent ratio of char and fresh tissue detected in tissue debris covering this specific fiber tip. Relatively, less char was detected, while more fresh tissue was found. It was therefore suggested that the smaller the proportion of char present in tissue debris, the less problematic tissue debris adhesion is for DRS signal deterioration during use of the smart electrosurgical knife. However, this effect was not described in literature before and therefore more research is required to validate this statement. Furthermore, side view images of the stripped fiber samples (Figure 51), show that stripping the fiber leads to an increased risk of fiber damage due to a lack of protection. This observation is confirmed by Thorlabs, the manufacturer of the acrylate coated optical fibers used in this research [156].

12.1.2 Research limitations

Although useful results were obtained during this master thesis, a few critical notes have to be placed on the reliability and execution of this research.

12.1.2.1 General reliability

Overall, the reliability of the results obtained in this research could have been higher if more samples were used. Conclusions drawn in this master thesis were often based on one or two samples, which makes these conclusions less valid. In addition, the different analyses could have been repeated more often to improve the reliability of the results. Furthermore, for sample preparation porcine tissue was used, while the instrument will eventually be used on humans. The differences between porcine and human tissue need to be taken into account when studying the results in detail.

Also, most experiments were performed manually, which generally leads to a human error. For example, samples were created manually and observations were done based on common sense. However, all experiments were performed by one and the same person, eliminating interobserver error. In addition, all samples were used for multiple analyses and therefore have had a lot to endure. Although samples were handled with care, complete quality preservation could not be guaranteed. For example, fibers could have been damaged during their removal from the tubes or during transfer from one method to another.

Furthermore, it should be taken into account that most results obtained in this research consist of subjective observations that were highly dependent on one (or two) person's opinion and expertise. This has caused a certain unreliability, that could have been prevented by implementing a higher level of quantification. This would have led to more objective results that generally enable clear analysis, strong comparison and higher reliability.

12.1.2.2 Time and resource restrictions

Furthermore, in chapter 7 different design directions were described. One of these design directions was chosen as the most promising one and was therefore selected to continue the rest of this research

with. However, this leaves the other two design directions unexplored, while there might be some interesting solutions to be found in these directions as well. This issue actually applies to all decisions made during this research, but choices do have to be made in order to move forward.

Moreover, some decisions were based on either time or resource restrictions. Especially the choices concerning the design concepts were strongly influenced by these restrictions. It was known in advance that none of the three concepts were going to solve DRS signal loss, because none of them met all requirements that were listed before. However, both time and resource restrictions obstructed the implementation of more advanced solutions within this master research. It was therefore chosen to continue with simpler design concepts that could at least provide some indications on the most interesting directions for follow-up research.

Another decision that was made based on time restrictions concerns concept testing. During this phase, the goal was to determine the influence of different modifications on DRS signal deterioration. However, during the entire research the actual DRS signal intensity was never measured. Instead, all conclusions were based on analyses indirectly indicating whether the signal deterioration of a specific fiber had increased or decreased. In order to validate these conclusions, actual DRS measurements still need to be performed. Furthermore, during the first sample preparation both pork belly and porcine liver were used to see whether there would be a difference in tissue debris between those two tissue types. When it turned out, after the analyses described in chapter 9, that there were no considerable differences, it was decided to continue concept testing with pork belly only. This decision was again also based on time and resource restrictions. However, the influence of blood on the results of the modified fibers was therefore not investigated.

12.1.2.3 Validation

The contact angle analysis, that was performed in chapter 8, revealed that the surface of the traditional fiber tip was hydrophilic. By applying a PTFE coating, it was tried to make the surface superhydrophobic, which is preferred when a non-stick effect is desired. However, after applying the coating, it was never verified whether this indeed led to a superhydrophobic fiber tip surface. Moreover, the complete interaction between the PTFE coating and the optical fiber was never analyzed in detail. It therefore remains unclear whether, for example, the specific coating used for this experiment attaches well to the optical fiber. In other words, the validation of the practical interaction between the two materials should have been more extensive.

12.2 Recommendations

This paragraph describes the recommendations for further research, based on the findings of this master thesis, structured according to three main topics interesting for follow-up research.

12.2.1 Analyze electrosurgical heat

This research has shown that the extreme electrosurgical heat has more influence on the smart electrosurgical knife than was thought before. It has turned out to be the main cause for tissue debris formation, tissue debris adhesion and optical fiber quality deterioration. However, so far, the actual temperatures have not been measured yet and remain unclear. Further research should therefore investigate the exact temperatures that occur during smart electrosurgery and their effects on the optical fiber. This information is thought to be important for both the cause of signal deterioration and the selection of a suitable solution. Questions that need to be answered are: how does the temperature change over time? Where are the different temperatures located? What are the (isolated) effects of these temperatures on optical fiber and how may these be prevented? Based on the results of this research, it is suggested that the problem of signal loss during smart electrosurgery requires a solution that combines extreme heat-resistance with anti-adhesiveness. It is suggested to achieve this by

applying a heat-resistant, anti-adhesive coating on a heat-resistant optical fiber, both thermally stable up to at least 350°C. The coating should meet all coating design criteria as listed in Table 11 and the optical fiber could be the aluminium coated one that was suggested in chapter 10.2.2.

12.2.2 Explore char

During the course of this master thesis, it has become clear that the chemical process charring occurs during smart electrosurgery and that this process leads to char formation, which is the main component of the tissue debris layer covering the optical fiber tip. However, it remains unclear what causes the stubborn adhesive effect of this char, which makes it hard to find out how to prevent the adhesion of char on optical fiber tips. Furthermore, it was suggested that the smaller the proportion of char present in tissue debris, the less problematic tissue debris adhesion is for DRS signal deterioration during use of the smart electrosurgical knife. However, this suggestion needs further investigation and might therefore be subject to further research.

12.2.3 Focus on signal loss

The focus of this research has been on decreasing DRS signal deterioration. However, it remains unclear how much the signal loss should be reduced. Of course, the ultimate goal is to completely prevent all signal loss, but for the time being this seems unfeasible. This raises the question what maximum amount of signal loss is satisfying within the context of smart electrosurgery. This is a question that needs to be answered during follow-up research.

12.2.4 Select most suitable tissue

Furthermore, so far, *ex vivo* porcine tissue has been used to create used optical fiber samples. However, eventually the smart electrosurgical knife will be used on human tissue *in vivo*. It is therefore recommended to perform all future experiments on tissue that is as close to *in vivo* human tissue as possible. In general, the main difference between those two tissues is the amount of blood, which in this case could have a large influence on research results.

13. Conclusion

In the introduction of this report, the main research question and sub questions were provided. The goal of this master thesis was to eventually be able to answer the main research question: how can deterioration of the diffuse reflectance spectroscopy signal during use of the smart electrosurgical knife be prevented? Answering the sub questions, automatically answers the main research question as well.

13.1 What is the influence of smart electrosurgery on optical fibers?

Previous research has shown that, during use of the smart electrosurgical knife, deterioration of DRS signal intensity occurs, obstructing proper functioning of the device. A layer covering the fiber tip has been observed and is thought to influence transmittance of the DRS signal. Therefore, this master thesis has focused on the influence of smart electrosurgery on both the morphology and composition of the outer surface of optical fiber tips. The results of this research showed that extreme heat is the main factor influencing changes in morphology and composition. Tissue underneath the tip of the electrosurgical blade can heat up to temperatures of at least 350°C, clearly affecting the morphology and composition of the outer surface of the optical fiber. The fiber tip gets soiled by a layer of tissue debris covering the tip, and gets damaged due to melting of the outer acrylate coating.

13.2 What causes the DRS signal to deteriorate?

The changes described above, both have a negative influence on DRS signal transmittance during use of the smart electrosurgical knife. Especially the layer of tissue debris covering the tip of the fiber, has found to lead to signal loss. Tissue debris contains traces of fresh tissue, blood and mainly char. Together these components contaminate the tip of the optical fiber, inhibiting light transport through the fiber, leading to signal deterioration.

The second cause of signal loss has turned out to be the lack of a proper coating protecting the silica core and its fluorine-doped cladding. Despite protecting metal tubes surrounding the optical fiber, acrylate coating degrades under the high temperatures of electrosurgery. Part of the coating is displaced to the upper surface of the fiber tip, blocking light transmittance together with tissue debris. The remaining part of the acrylate coating melts away, leading to damage to the core and cladding. As a result, the DRS signal deteriorates even more.

13.3 How should an optical fiber be modified in order to decrease DRS signal deterioration during smart electrosurgery?

In order to eliminate the two main factors influencing signal loss, two different surface modifications were tested: stripping off the acrylate coating to prevent melting damage, and applying a PTFE coating to prevent tissue debris adhesion. Unfortunately, both modifications were unable to completely prevent signal loss. However, eliminating the acrylate coating has shown to reduce signal loss from 45.8% to 36.4%, compared to the traditional optical fiber. Nevertheless, microscopic side view images show this modification does lead to an increased risk of fiber damage due to a lack of physical protection of the core and cladding. In order to minimize signal loss, it is therefore suggested to apply a heat-resistant outer coating instead of stripping off the acrylate coating. This will protect the fiber from both heat and other external damage.

In contrast, the application of a PTFE coating has shown to slightly increase signal loss from 45.8% to 48.5%, compared to the traditional optical fiber. Research results indicate that exceeding the maximum operating temperature of the coating leads to the opposite effect of non-sticking, resulting in additional

tissue debris adhesion. However, based on literature it still seems as if the application of a coating is a very reliable and often used method to prevent all different kinds of adhesion, provided that the maximum operating temperature is not exceeded. Besides thermal stability and anti-adhesiveness, other important requirements need to be met as well. Table 11 describes the minimum set of properties a coating must possess in order to solve DRS signal loss during smart electrosurgery. This set should be kept close when searching for a suitable coating to prevent tissue debris adhesion.

Based on the results of this research, it is suggested that the optimal solution for signal loss during use of the smart electrosurgical knife should respond to optical fiber damage and tissue debris adhesion, both caused by extreme tissue heat. Overall, it can be concluded that this extreme heat has been underestimated so far and should be one of the main points of focus in improving DRS signal deterioration. Therefore, this research credits the most potential to the implementation of a heat-resistant optical fiber provided with an advanced heat-resistant, anti-adhesive coating.

Bibliography

1. *Breast cancer: prevention and control*. 2018 [cited 2018.

2. Chiappa, C., et al., *Surgical margins in breast conservation.* International Journal of Surgery, 2013. **11**: p. S69-S72.

3. O'Kelly Priddy, C.M., V.A. Forte, and J.E. Lang, *The importance of surgical margins in breast cancer.* Journal of surgical oncology, 2016. **113**(3): p. 256-263.

4. Fleischer, J.C., *Integration of tissue-sensing into electrosurgical instruments*. 2015, Delft University of Technology.

5. Fleischer, J.C., *Diffuse Reflectance Spectroscopy for Intraoperative Tumor Margin Assessment: Workflow Analysis and Effect of Coagulation on Tissue Sensing*. 2015, Delft University of Technology.

6. Adank, M.W., *Assessing the added value of diffuse reflectance spectroscopy in electrosurgery*. 2017, Delft University of Technology.

7. Adank, M.W., *Evaluation of a smart electrosurgical knife – assessing the feasibility of tumor detection with diffuse reflectance spectroscopy in breast conserving surgery*. 2017, Delft University of Technology.

8. Mollerus, F.C.S., *The integration of diffuse reflectance spectroscopy into the electrosurgical knife used during breast-conserving surgery*. 2018, Delft University of Technology.

9. Mollerus, F.C.S., *The integration of Diffuse Reflectance Spectroscopy into the electrosurgical knife used for Breast-Conserving Surgery - Determining and overcoming the challenge of tissue debris adhering to the 'smart' electrosurgical knife*, in *Biomechanical Engineering*. 2018, Delft University of technology.

10. Hay, D.J., *Electrosurgery.* Surgery-Oxford International Edition, 2008. **26**(2): p. 66-69.

11. Advincula, A.P. and K. Wang, *The evolutionary state of electrosurgery: where are we now?* Current Opinion in Obstetrics and Gynecology, 2008. **20**(4): p. 353-358.

12. Gallagher, K., B. Dhinsa, and J. Miles, *Electrosurgery.* Surgery-Oxford International Edition, 2011. **29**(2): p. 70-72.

13. McCauley, G., *Understanding electrosurgery.* Bovie Med Corp, 2010. **4**: p. 4-15.

14. Meeuwsen, F.C., et al., *The Art of Electrosurgery: Trainees and Experts.* Surgical Innovation, 2017. **24**(4): p. 373-378.

15. *NCI Dictionary of Cancer Terms*. [cited 2018; Available from: https://www.cancer.gov/.

16. Sharma, V., et al., *Auto-fluorescence lifetime and light reflectance spectroscopy for breast cancer diagnosis: potential tools for intraoperative margin detection.* Biomedical optics express, 2012. **3**(8): p. 1825-1840.

17. Fajdic, J., et al., *Criteria and Procedures for Breast Conserving Surgery.* Acta Inform Med, 2013. **21**(1): p. 16-9.

18. *Breast cancer*. 2012 [cited 2018; Available from: https://richtlijnendatabase.nl/.

19. Thill, M., *MarginProbe: intraoperative margin assessment during breast conserving surgery by using radiofrequency spectroscopy.* Expert Rev Med Devices, 2013. **10**(3): p. 301-15.

20. *Surgical margins*. 2017 [cited 2018; Available from: http://www.breastcancer.org/.

21. Krekel, N.M., et al., *Ultrasound-guided breast-sparing surgery to improve cosmetic outcomes and quality of life. A prospective multicentre randomised controlled clinical trial comparing ultrasound-guided surgery to traditional palpation-guided surgery (COBALT trial).* BMC surgery, 2011. **11**(1): p. 8.

22. Bydlon, T.M., *Intra-operative Assessment of Breast Tumor Margins Using Diffuse Reflectance Spectroscopy*. 2012.

23. Evers, D.J., et al., *Diffuse reflectance spectroscopy: towards clinical application in breast cancer.* Breast cancer research and treatment, 2013. **137**(1): p. 155-165.

24. Yu, B., et al., *Emerging optical techniques for detection of oral, cervical and anal cancer in low-resource settings.* Austin J. Biomed. Eng, 2014. **1**(2): p. 1007.

25. De Boer, L., et al., *Fat/water ratios measured with diffuse reflectance spectroscopy to detect breast tumor boundaries.* Breast cancer research and treatment, 2015. **152**(3): p. 509-518.

26. Vieweg, U., *Electrosurgery*, in *Manual of Spine Surgery*. 2012, Springer. p. 63-67.

27. Vilos, G.A. and C. Rajakumar, *Electrosurgical generators and monopolar and bipolar electrosurgery.* Journal of minimally invasive gynecology, 2013. **20**(3): p. 279-287.

28. Munro, M.G., *Fundamentals of electrosurgery Part I: Principles of radiofrequency energy for surgery*, in *The SAGES Manual on the Fundamental Use of Surgical Energy (FUSE)*. 2012, Springer. p. 15-59.

29. Fleischer, J., *Diffuse Reflectance Spectroscopy for Intraoperative Tumor Margin Assessment: Workflow Analysis and Effect of Coagulation on Tissue Sensing*. 2015, Delft University of Technology.

30. Rey, J.F., et al., *European Society of Gastrointestinal Endoscopy (ESGE) guideline: the use of electrosurgical units.* Endoscopy, 2010. **42**(9): p. 764-72.

31. Lepock, J.R., *Cellular effects of hyperthermia: relevance to the minimum dose for thermal damage.* International Journal of Hyperthermia, 2003. **19**(3): p. 252-266.

32. Fischer-Cripps, A.C., *The electronics companion*. 2004: CRC Press.

33. M Jawad, M., et al., *An overview of laser principle, laser–tissue interaction mechanisms and laser safety precautions for medical laser users.* International Journal of Pharmacology, 2011. **7**(2): p. 149-160.

34. Daniel Dargent, M.a.S.S., MD, *Physical bases of electrosurgery.* Modern Medicine Network, 2011.

35. Thomsen, S. and J.A. Pearce, *Thermal damage and rate processes in biologic tissues*, in *Optical-thermal response of laser-irradiated tissue*. 2010, Springer. p. 487-549.

36. Goldberg, S.N., et al., *Radiofrequency tissue ablation: importance of local temperature along the electrode tip exposure in determining lesion shape and size.* Academic radiology, 1996. **3**(3): p. 212-218.

37. Goldberg, S.N., *Radiofrequency tumor ablation: principles and techniques.* European Journal of Ultrasound, 2001. **13**(2): p. 129-147.

38. Waye, J.D., D.K. Rex, and C.B. Williams, *Colonoscopy: principles and practice*. 2008: John Wiley & Sons.

39. Wright, N.T., *Quantitative Models of Thermal Damage to Cells and Tissues*, in *Heat Transfer and Fluid Flow in Biological Processes*. 2015, Elsevier. p. 59-76.

40. *Protein Refolding*, in *BIC: Biologics International Corp*, P. Refolding, Editor., BIC: biologicscorp.com.

41. Massarweh, N.N., N. Cosgriff, and D.P. Slakey, *Electrosurgery: history, principles, and current and future uses.* Journal of the American College of Surgeons, 2006. **202**(3): p. 520-530.

42. Yarmolenko, P.S., et al., *Thresholds for thermal damage to normal tissues: an update.* International Journal of Hyperthermia, 2011. **27**(4): p. 320-343.

43. Soderstrom, R.M., B.S. Levy, and T. Engel, *Reducing bipolar sterilization failures.* Obstetrics and gynecology, 1989. **74**(1): p. 60-63.

44. Bowers, C.A., et al., *Comparison of tissue effects in rabbit muscle of surgical dissection devices.* International Journal of Surgery, 2014. **12**(3): p. 219-223.

45. Dodde, R.E., et al., *Monopolar electrosurgical thermal management for minimizing tissue damage.* IEEE Transactions on biomedical engineering, 2012. **59**(1): p. 167-173.

46. Taheri, A., et al., *Electrosurgery: part I. Basics and principles.* Journal of the American Academy of Dermatology, 2014. **70**(4): p. 591. e1-591. e14.

47. Thomsen, S. *Targeted thermal injury: mechanisms of cell and tissue death*. in *Energy-based Treatment of Tissue and Assessment V*. 2009. International Society for Optics and Photonics.

48. Gomel, V. and A. Brill, *Reconstructive and reproductive surgery in gynecology*. 2010: CRC Press.

49. Haak, D. *Eschar: Definition, Formation & Treatment*. [cited 2018.

50. Hampton, S.C., F., *Tissue Viability: The prevention, treatment and management of wounds*. 2004: Whurr Publishers.

51. Ma, F., *Accumulative eschar after burn.* Clin Case Rep, 2016. **4**(2): p. 151-3.

52. Osguthorpe, J.D., *Head and neck burns.* Arch Otolaryngol Head Neck Surg, 1991. **117**: p. 969-74.

53. Thomas, A.M., K.G. Harding, and K. Moore, *The structure and composition of chronic wound eschar.* J Wound Care, 1999. **8**(6): p. 285-7.

54. Heim, W.P., S.A. Miller III, and J.L. Brassell, *Electrosurgical system for reducing/removing eschar accumulations on electrosurgical instruments*. 2000, Google Patents.

55. Gent, C.M.v., *Exploring methods to prevent tissue debris adhering to the 'smart' electrosurgical knife*, in *Biomedical Engineering*. 2018, Delft University of Technology.

56. Ansari, M.A., M. Erfanzadeh, and E. Mohajerani, *Mechanisms of laser-tissue interaction: II. Tissue thermal properties.* Journal of lasers in medical sciences, 2013. **4**(3): p. 99.

57. Schneider, A. and H. Feussner, *Biomedical engineering in gastrointestinal surgery*. 2017: Academic Press.

58. Speight, J.G., *Chapter 3 - Industrial Organic Chemistry*, in *Environmental Organic Chemistry for Engineers*, J.G. Speight, Editor. 2017, Butterworth-Heinemann. p. 87-151.

59. Zheng, L., et al., *Effect of high-frequency electric field on the tissue sticking of minimally invasive electrosurgical devices.* Royal Society Open Science, 2018. **5**(7): p. 180125.

60. Ruoslahti, E. and B. Öbrink, *Common principles in cell adhesion.* Experimental cell research, 1996. **227**(1): p. 1-11.

61. Horbett, T.A., *The role of adsorbed proteins in animal cell adhesion.* Colloids and Surfaces B: Biointerfaces, 1994. **2**(1-3): p. 225-240.

62. Vitte, J., et al., *Is there a predictable relationship between surface physical-chemical properties and cell behaviour at the interface.* Eur Cell Mater, 2004. **7**: p. 52-63.

63. Ruoslahti, E. and M.D. Pierschbacher, *New perspectives in cell adhesion: RGD and integrins.* Science, 1987. **238**(4826): p. 491-497.

64. Wahlgren, M. and T. Arnebrant, *Protein adsorption to solid surfaces.* Trends in biotechnology, 1991. **9**(1): p. 201-208.

65. Baier, R.E. and R.C. Dutton, *Initial events in interactions of blood with a foreign surface.* Journal of Biomedical Materials Research Part A, 1969. **3**(1): p. 191-206.

66. Anselme, K., L. Ploux, and A. Ponche, *Cell/material interfaces: influence of surface chemistry and surface topography on cell adhesion.* Journal of Adhesion Science and Technology, 2010. **24**(5): p. 831-852.

67. Rabe, M., D. Verdes, and S. Seeger, *Understanding protein adsorption phenomena at solid surfaces.* Advances in colloid and interface science, 2011. **162**(1-2): p. 87-106.

68. Taubert, A., J.F. Mano, and J.C. Rodríguez-Cabello, *Biomaterials surface science*. 2013: John Wiley & Sons.

69. Dee, K.C., D.A. Puleo, and R. Bizios, *Blood-Biomaterial Interactions and Coagulation.* An introduction to tissue-biomaterial interactions, 2002: p. 53-88.

70. Müller, I., *A history of thermodynamics: the doctrine of energy and entropy*. 2007: Springer Science & Business Media.

71. Gooch, J.W., *Encyclopedic Dictionary of Polymers Springer-Verlag 2007.*

72. Hwang, H. *DLVO theory*. 2011.

73. Andrade, J., V. Hlady, and A. Wei, *Adsorption of complex proteins at interfaces.* Pure and applied chemistry, 1992. **64**(11): p. 1777-1781.

74. Mathes, J., *Protein Adsorption to Vial Surfaces*. 2010, lmu.

75. Koutsoukos, P., W. Norde, and J. Lyklema, *Protein adsorption on hematite (α-Fe2O3) surfaces.* Journal of colloid and interface science, 1983. **95**(2): p. 385-397.

76. Norde, W. *Driving forces for protein adsorption at solid surfaces*. in *Macromolecular Symposia*. 1996. Wiley Online Library.

77. Demanèche, S., et al., *Dissimilar pH-dependent adsorption features of bovine serum albumin and α-chymotrypsin on mica probed by AFM.* Colloids and Surfaces B: Biointerfaces, 2009. **70**(2): p. 226-231.

78. Rabe, M., et al., *Surface organization and cooperativity during nonspecific protein adsorption events.* The Journal of Physical Chemistry B, 2008. **112**(44): p. 13971-13980.

79. Ramsden, J. and J. Prenosil, *Effect of ionic strength on protein adsorption kinetics.* The Journal of Physical Chemistry, 1994. **98**(20): p. 5376-5381.

80. Gao, D., D.-Q. Lin, and S.-J. Yao, *Mechanistic analysis on the effects of salt concentration and pH on protein adsorption onto a mixed-mode adsorbent with cation ligand.* Journal of Chromatography B, 2007. **859**(1): p. 16-23.

81. Xu, L.-C. and C.A. Siedlecki, *Effects of surface wettability and contact time on protein adhesion to biomaterial surfaces.* Biomaterials, 2007. **28**(22): p. 3273-3283.

82. Gessner, A., et al., *Influence of surface charge density on protein adsorption on polymeric nanoparticles: analysis by two-dimensional electrophoresis.* European journal of pharmaceutics and biopharmaceutics, 2002. **54**(2): p. 165-170.

83. Bernabeu, P. and A. Caprani, *Influence of surface charge on adsorption of fibrinogen and/or albumin on a rotating disc electrode of platinum and carbon.* Biomaterials, 1990. **11**(4): p. 258-264.

84. Kapur, R., J. Lilien, and J. Black, *Field-dependent fibroblast orientation on charged surfaces is independent of polarity and adsorbed serum proteins.* Biomaterials, 1993. **14**(11): p. 854-860.

85. Gray, J.J., *The interaction of proteins with solid surfaces.* Current opinion in structural biology, 2004. **14**(1): p. 110-115.

86. Lyklema, J., *Fundamentals of interface and colloid science: soft colloids*. Vol. 5. 2005: Elsevier.

87. Lee, J.H., et al., *Interaction of fibroblasts on polycarbonate membrane surfaces with different micropore sizes and hydrophilicity.* Journal of Biomaterials Science, Polymer Edition, 1999. **10**(3): p. 283-294.

88. Judd, S., *The MBR book: principles and applications of membrane bioreactors for water and wastewater treatment*. 2010: Elsevier.

89. Law, K.-Y., *Definitions for hydrophilicity, hydrophobicity, and superhydrophobicity: getting the basics right*. 2014, ACS Publications.

90. Palacio, L., et al., *Contact angles and external protein adsorption onto UF membranes.* Journal of membrane science, 1999. **152**(2): p. 189-201.

91. Ito, Y., *Surface micropatterning to regulate cell functions.* Biomaterials, 1999. **20**(23-24): p. 2333-2342.

92. Scopelliti, P.E., et al., *The effect of surface nanometre-scale morphology on protein adsorption.* PloS one, 2010. **5**(7): p. e11862.

93. Atluri, P., *The Surgical Review: An Integrated Basic and Clinical Science Study Guide*. 2006: Lippincott Williams & Wilkins.

94. Qiu, Y., et al., *Platelet mechanosensing of substrate stiffness during clot formation mediates adhesion, spreading, and activation.* Proceedings of the National Academy of Sciences, 2014. **111**(40): p. 14430-14435.

95. Li, Z., et al., *Signaling during platelet adhesion and activation.* Arteriosclerosis, thrombosis, and vascular biology, 2010. **30**(12): p. 2341-2349.

96. Packham, M.A., *The behavior of platelets at foreign surfaces.* Proceedings of the Society for Experimental Biology and Medicine, 1988. **189**(3): p. 261-274.

97. Marieb, E.N. and K. Hoehn, *Human anatomy & physiology*. 2007: Pearson Education.

98. Carver, C. *Knowing the difference between scabs and eschar*. 2016 [cited 2018.

99. Zhang, Z., et al., *Blood compatibility of surfaces with superlow protein adsorption.* Biomaterials, 2008. **29**(32): p. 4285-4291.

100. Koh, L.B., I. Rodriguez, and S.S. Venkatraman, *The effect of topography of polymer surfaces on platelet adhesion.* Biomaterials, 2010. **31**(7): p. 1533-1545.

101. Chen, H., et al., *Biocompatible polymer materials: role of protein–surface interactions.* Progress in Polymer Science, 2008. **33**(11): p. 1059-1087.

102. Slaughter, M.S., et al., *Evaluation of new Forcefield technology: Reducing platelet adhesion and cell coverage of pyrolytic carbon surfaces.* Journal of Thoracic and Cardiovascular Surgery, 2011. **142**(4): p. 921-925.

103. Sivaraman, B. and R.A. Latour, *The relationship between platelet adhesion on surfaces and the structure versus the amount of adsorbed fibrinogen.* Biomaterials, 2010. **31**(5): p. 832-839.

104. O'Brien, J.R., *The adhesiveness of native platelets and its prevention.* J Clin Pathol, 1961. **14**: p. 140-9.

105. Ishihara, K., et al., *Modification of polysulfone with phospholipid polymer for improvement of the blood compatibility. Part 2. Protein adsorption and platelet adhesion.* Biomaterials, 1999. **20**(17): p. 1553-1559.

106. Lindon, J.N., et al., *Does the conformation of adsorbed fibrinogen dictate platelet interactions with artificial surfaces?* Blood, 1986. **68**(2): p. 355-362.

107. Sunny, S., et al., *Transparent antifouling material for improved operative field visibility in endoscopy.* Proc Natl Acad Sci U S A, 2016. **113**(42): p. 11676-11681.

108. *An unobstructed view into the human body*. 2016 [cited 2018; Available from: https://wyss.harvard.edu/an-unobstructed-view-into-the-human-body/.

109. Hamming, L.M. and P.B. Messersmith, *Fouling resistant biomimetic poly (ethylene glycol) based grafted polymer coatings.* Mater. Matters, 2008. **3**(52).

110. Chen, S., et al., *Surface hydration: principles and applications toward low-fouling/nonfouling biomaterials.* Polymer, 2010. **51**(23): p. 5283-5293.

111. *What is spectranetics?* 2018 [cited 2018.

112. Buch, E., N.G. Boyle, and P.H. Belott, *Pacemaker and defibrillator lead extraction.* Circulation, 2011. **123**(11): p. e378-e380.

113. Rawlins, J., et al., *Coronary intervention with the excimer laser: Review of the technology and outcome data.* Interventional Cardiology Review, 2016. **11**(1): p. 27.

114. Tian, Y., et al., *Adhesion and friction in gecko toe attachment and detachment.* Proceedings of the National Academy of Sciences, 2006. **103**(51): p. 19320-19325.

115. Bixler, G.D. and B. Bhushan, *Fluid drag reduction with shark-skin riblet inspired microstructured surfaces.* Advanced Functional Materials, 2013. **23**(36): p. 4507-4528.

116. Peng, Y.L., C.G. Lin, and L. Wang. *The preliminary study on antifouling mechanism of shark skin*. in *Advanced Materials Research*. 2009. Trans Tech Publ.

117. Damodaran, V.B. and N.S. Murthy, *Bio-inspired strategies for designing antifouling biomaterials.* Biomater Res, 2016. **20**: p. 18.

118. Bixler, G.D. and B. Bhushan, *Biofouling: lessons from nature.* Phil. Trans. R. Soc. A, 2012. **370**(1967): p. 2381-2417.

119. Ensikat, H.J., et al., *Superhydrophobicity in perfection: the outstanding properties of the lotus leaf.* Beilstein J Nanotechnol, 2011. **2**: p. 152-61.

120. Yu, M., et al., *Why a lotus-like superhydrophobic surface is self-cleaning? An explanation from surface force measurements and analysis.* Langmuir, 2014. **30**(45): p. 13615-21.

121. Forbes, P., *Self-cleaning materials.* Scientific American, 2008. **299**(2): p. 88-95.

122. Cheng, Y.T., et al., *Effects of micro-and nano-structures on the self-cleaning behaviour of lotus leaves.* Nanotechnology, 2006. **17**(5): p. 1359.

123. Cheng, S.K., *Cooking pans*. 1988, Google Patents.

124. Woodford, C., *Nonstick pans.* 2017.

125. Ashokkumar, S. and J. Adler-Nissen, *Evaluating non-stick properties of different surface materials for contact frying.* Journal of food engineering, 2011. **105**(3): p. 537-544.

126. Selim, M., et al., *Recent progress in marine foul-release polymeric nanocomposite coatings.* Progress in Materials Science, 2017. **87**: p. 1-32.

127. Yebra, D. and C. Weinell, *Key issues in the formulation of marine antifouling paints*, in *Advances in Marine Antifouling Coatings and Technologies*. 2009, Elsevier. p. 308-333.

128. *What is fouling release?* 2018.

129. *Innovations in Anti-fouling Coatings and Surfaces for Heat Exchangers - Advanced Coatings & Surface Technology TOE*. 2016 [cited 2018.

130. Jung, C., *Press Release - Hannover Messe*, L.I.f.N. Materials, Editor. 2016, INM: www.leibniz-inm.de.

131. van Boeijen, A., et al., *Delft design guide: Design methods*. 2014: BIS publishers.

132. Dee, K.C., D.A. Puleo, and R. Bizios, *An introduction to tissue-biomaterial interactions*. 2003: John Wiley & Sons.

133. Falde, E.J., et al., *Superhydrophobic materials for biomedical applications.* Biomaterials, 2016. **104**: p. 87-103.

134. Roach, P., D. Farrar, and C.C. Perry, *Surface tailoring for controlled protein adsorption: effect of topography at the nanometer scale and chemistry.* Journal of the American Chemical Society, 2006. **128**(12): p. 3939-3945.

135. Zhang, X., L. Wang, and E. Levänen, *Superhydrophobic surfaces for the reduction of bacterial adhesion.* Rsc Advances, 2013. **3**(30): p. 12003-12020.

136. Scardino, A., E. Harvey, and R. De Nys, *Testing attachment point theory: diatom attachment on microtextured polyimide biomimics.* Biofouling, 2006. **22**(1): p. 55-60.

137. Adlhart, C., et al., *Surface modifications for antimicrobial effects in the healthcare setting: a critical overview.* Journal of Hospital Infection, 2018.

138. Jooyoun Kim, S.-O.C., *11 - Superhydrophobicity*, in *Waterproof and Water Repellent Textiles and Clothing*. 2018, The Textile Institute Book Series: ScienceDirect.

139. Busscher, H., et al., *Adhesion and spreading of human fibroblasts on superhydrophobic FEP-Teflon.* Cells and Materials, 1991. **1**(3): p. 5.

140. Hou, X., et al., *Preparation of polypropylene superhydrophobic surface and its blood compatibility.* Colloids and Surfaces B: Biointerfaces, 2010. **80**(2): p. 247-250.

141. Sun, T., et al., *No platelet can adhere—largely improved blood compatibility on nanostructured superhydrophobic surfaces.* Small, 2005. **1**(10): p. 959-963.

142. Zhou, M., et al. *Blood platelet's behavior on nanostructured superhydrophobic surface*. in *Journal of Nano Research*. 2008. Trans Tech Publ.

143. Huang, Q., et al., *Reduced platelet adhesion and improved corrosion resistance of superhydrophobic TiO2-nanotube-coated 316L stainless steel.* Colloids and Surfaces B: Biointerfaces, 2015. **125**: p. 134-141.

144. Nokes, J.M., et al., *Reduced Blood Coagulation on Roll-to-Roll, Shrink-Induced Superhydrophobic Plastics.* Advanced healthcare materials, 2016. **5**(5): p. 593-601.

145. Nishimoto, S. and B. Bhushan, *Bioinspired self-cleaning surfaces with superhydrophobicity, superoleophobicity, and superhydrophilicity.* Rsc Advances, 2013. **3**(3): p. 671-690.

146. Mattox, D.M., *Handbook of physical vapor deposition (PVD) processing*. 2010: William Andrew.

147. Ohgaki, M., et al., *Manipulation of selective cell adhesion and growth by surface charges of electrically polarized hydroxyapatite.* Journal of Biomedical Materials Research: An Official Journal of The Society for Biomaterials, The Japanese Society for Biomaterials, and The Australian Society for Biomaterials and the Korean Society for Biomaterials, 2001. **57**(3): p. 366-373.

148. Cloutier, M., D. Mantovani, and F. Rosei, *Antibacterial coatings: challenges, perspectives, and opportunities.* Trends in biotechnology, 2015. **33**(11): p. 637-652.

149. Wischerhoff, E., et al., *Controlled cell adhesion on PEG-based switchable surfaces.* Angewandte Chemie International Edition, 2008. **47**(30): p. 5666-5668.

150. Ladd, J., et al., *Zwitterionic polymers exhibiting high resistance to nonspecific protein adsorption from human serum and plasma.* Biomacromolecules, 2008. **9**(5): p. 1357-1361.

151. Israelachvili, J., S. Marčelja, and R.G. Horn, *Physical principles of membrane organization.* Quarterly reviews of biophysics, 1980. **13**(2): p. 121-200.

152. Seed, B., *Silanizing glassware.* Current protocols in protein science, 1998. **13**(1): p. A. 3E. 1-A. 3E. 2.

153. *0.22 NA Silica Core, Glass Clad Multimode Optical Fiber, Step Index*. 2013 [cited 2018.

154. Technologies, P., *Polymer Coatings for Silica Optical Fiber*, Molex, Editor. 2009, Polymicro Technologies.

155. *Cable Basics: Fiber Optic Cable*. 2018.

156. *Sources of Attenuation: Scattering*. 2018; Available from: https://www.thorlabs.com/tutorials.cfm?tabID=789B6970-20AC-47C3-81A9-838CD7594644.

157. Toosi, R. and D. Modarress, *Radiation and temperature survivability of multimode step-index fluorine-doped silica fibers.* IEEE transactions on nuclear science, 1991. **38**(5): p. 985-993.

158. van de Ven, A.L., et al., *Preparation, characterization, and cellular associations of silicon logic-embedded vectors*, in *Methods in enzymology*. 2012, Elsevier. p. 1-16.

159. *Scanning Electron Microscopes (SEM)*. 2017; Available from: https://www.jeol.co.jp/en/science/sem.html.

160. d'Alfonso, A., et al., *Atomic-resolution chemical mapping using energy-dispersive x-ray spectroscopy.* Physical Review B, 2010. **81**(10): p. 100101.

161. Ohara, T., et al., *Acrylic acid and derivatives.* Ullmann's encyclopedia of industrial chemistry, 2000.

162. Iler, R.K., *Chemistry of Silica--Solubility, Polymerization, Colloid and Surface Properties, and Biochemistry.* 1979.

163. Iler, R.K., *The colloid chemistry of silica and silicates*. Vol. 80. 1955: LWW.

164. Nielsen, F.H., *Ultratrace elements in nutrition: current knowledge and speculation.* The Journal of Trace Elements in Experimental Medicine: The Official Publication of the International Society for Trace Element Research in Humans, 1998. **11**(2-3): p. 251-274.

165. Woodard, H. and D. White, *The composition of body tissues.* The British journal of radiology, 1986. **59**(708): p. 1209-1218.

166. Iyengar, G.V., W.E. Kollmer, and H.J.M. Bowen, *The elemental composition of human tissues and body fluids: a compilation of values for adults*. 1978: Vch Pub.

167. Stojilovic, N., *Why can't we see hydrogen in X-ray photoelectron spectroscopy?* Journal of Chemical Education, 2012. **89**(10): p. 1331-1332.

168. Chylek, P., S. Jennings, and R. Pinnick, *AEROSOLS| Soot.* 2015.

169. Cooke, S. *What Element Make Up the Chemical Compound of Blood?* 2016; Available from: https://socratic.org/.

170. Bowley, H.J., et al., *Practical raman spectroscopy*. 2012: Springer Science & Business Media.

171. *What is Raman spectroscopy?* 2016; Available from: https://www.nanophoton.net/raman/raman-spectroscopy.html.

172. Nestler, K., et al., *Thermogravimetric and Raman spectroscopic investigations on different coals in comparison to dispersed anthracite found in permineralized tree fern Psaronius sp.* Journal of Molecular Structure, 2003. **661**: p. 357-362.

173. Li, J.-G., C.-Y. Tsai, and S.-W. Kuo, *Fabrication and characterization of inorganic silver and palladium nanostructures within hexagonal cylindrical channels of mesoporous carbon.* Polymers, 2014. **6**(6): p. 1794-1809.

174. Shamsudin, M., et al. *Micro-raman, optical and impedance characteristics of cnt-substituted acrylate/cnt nanocomposite thin film*. in *Advanced Materials Research*. 2014. Trans Tech Publ.

175. Tsiminis, G., et al., *Identification and quantification of explosives in nanolitre solution volumes by Raman spectroscopy in suspended core optical fibers.* Sensors, 2013. **13**(10): p. 13163-13177.

176. Teflon, P. and P.F. Resin, *Properties handbook.* DuPont Fluoroproducts, Washington, 1996.

177. Li, Z., et al., *Durable Broadband and Omnidirectional Ultra-antireflective Surfaces.* ACS applied materials & interfaces, 2018.

178. Liu, D., et al., *Self-cleaning antireflective coating with a hierarchical texture for light trapping in micromorph solar cells.* Journal of Materials Chemistry C, 2017. **5**(1): p. 103-109.

179. coatings, P. *Technology*. 2016; Available from: http://www.ptfecoatings.com/technology/technology.php.

180. *Teflon Coatings - Six Basic Types*. 2018 [cited 2018.

181. Kulkarni, A. and P. Rao, *Synthesis of polymeric nanomaterials for biomedical applications*, in *Nanomaterials in Tissue Engineering*. 2013, Elsevier. p. 27-63.

182. Zhang, P., et al., *Stable slippery liquid-infused anti-wetting surface at high temperatures.* Journal of Materials Chemistry A, 2016. **4**(31): p. 12212-12220.

183. Hu, Z., et al., *Optically transparent, amphiphilic networks based on blends of perfluoropolyethers and poly (ethylene glycol).* Journal of the American Chemical Society, 2008. **130**(43): p. 14244-14252.

184. *PTFE Coated Medical Components*. 2018; Available from: http://www.surfacesolutionsgroup.com/capabilities/ptfe-medical-components/.

185. Zhang, H. and M. Chiao, *Anti-fouling coatings of poly (dimethylsiloxane) devices for biological and biomedical applications.* Journal of medical and biological engineering, 2015. **35**(2): p. 143-155.

186. Lin, J., et al., *Highly transparent superhydrophobic organic–inorganic nanocoating from the aggregation of silica nanoparticles.* Colloids and Surfaces A: Physicochemical and Engineering Aspects, 2013. **421**: p. 51-62.

187. *Nanotechnology increasingly used in medical devices*. 2015 [cited 2018.

188. Gao, W. and Z. Li, *Nano-structured alloy and composite coatings for high temperature applications.* Materials Research, 2004. **7**(1): p. 175-182.

Appendices

Appendix A: Problem validation

In this appendix, the overall problem of this research is validated. First the main findings of previous master researches on this subject are summarized and discussed and in the second paragraph the former recommendations are evaluated. The goal of this chapter is to create a clear overview of the current state of play and the progress that has been made so far, and to determine the most promising and logical next steps that might be explored in this research.

1. Previous findings

In this paragraph, the main previous findings of Mollerus are summarized. The goal of this paragraph is to create an overview of the experiments that have been performed and the conclusions that were subsequently drawn. This overview should indicate which aspects of this research are not yet explored and which aspects need further investigation. This knowledge will help to determine the most useful direction for the current study.

1.1 Influence of clinical use on tissue debris

This first section covers the main findings up to now concerning the influence of the clinical use of the electrosurgical instrument on tissue debris formation.

Influence of instrument selection on tissue debris

The master thesis of Mollerus investigated the influence of the type of electrosurgical instrument on the formation of tissue debris [9]. She found that most electrosurgical generators used in the Netherlands are produced by the companies Medtronic and ERBE Nederland BV. After a thorough clinical analysis, containing of several interviews with specialists and visits to multiple hospitals, she concludes that it is very hard to make statements about the influence of an electrosurgical instrument on the tissue debris. This is because the electrosurgical outcome (including the amount of tissue debris formation) is highly surgeon dependent. During an interview for the master thesis of Mollerus, a representative of Medtronic states that the main factor influencing the electrosurgical result is represented by the experience of the specialist [9]. Besides, although certain instruments are prescribed to particular procedures, in practice surgeons choose an instrument based on their own preferences and education. Furthermore, an experiment performed by Mollerus shows that there is no significant correlation between the type of electrode and the amount of times the instrument is cleaned because of tissue debris formation during BCS ($r(29) = 0{,}298,\ p = 0{,}109$) [9]. So according to this experiment the choice of instrument does not have any influence on tissue debris formation.

Influence of instrument settings on tissue debris

Just as applies for the choice of instrument, it also appears to be very difficult to make statements about the influence of settings used during electrosurgery [9]. According to literature, using certain electrosurgical settings may lead to more unnecessary tissue debris formation. This could be prevented by having surgeons use the recommended settings for a particular surgery. However, surgeons seem to have their own way of working and are not willing to attend instruction lectures. They are convinced of their own electrosurgical skills and are not aware of any downsides of their technique. In addition, during an interview for the master thesis of Mollerus, two surgeons from the NKI-AvL hospital stated that the magnitude of the prescribed settings does not have noteworthy effects on surgeries encountering lots of fat tissue, like for example BCS [9]. This statement is confirmed by an experiment performed by Mollerus, showing no significant correlation between different settings (within a

recommended range) and the amount of times an electrosurgical instrument needs cleaning due to tissue debris adhesion during BCS (*r(20) = -0,295, p = 0,114 and r(29) = 0,206, p = 0,274*) [9]. So according to this experiment the exact instrument settings do not influence tissue debris formation. This means that the incentive for surgeons to properly adjust the instrument settings is not large enough.

Influence of instrument cleaning on tissue debris
Examples of suggested methods to clean the electrode tip of an electrosurgical knife include moistened sponges and electrode cleaning pads [9, 55]. However, according to literature cleaning the knife by using these existing methods, might cause damage to the blade. Scratches subsequently lead to an abrasive surface, increasing tissue debris adhesion. Debris build-up impedes the desired current flow, which causes the electrosurgical device to function less effectively. In order to compensate for this loss, surgeons tend to adjust the generator settings or substitute their electrode tip. However, contrary to what is stated in literature, an experiment performed by Mollerus shows that the more often the electrosurgical knife was cleaned, the less tissue debris was found on the electrode (*r(14) = -0,610, p = 0,027*) [9]. So according to this experiment cleaning the electrosurgical instrument leads to less tissue debris adhesion.

Influence of surgical parameters on tissue debris
For her master thesis Mollerus investigated the influence of the duration of electrosurgical use, the operation date, the weight of the tumor and the electrosurgical mode on tissue debris formation [9]. A significant correlation was found between the operation date and the amount of tissue debris found on the knife (*r(14) = 0,642, p = 0,10*). This implies that the longer ago the surgery took place, the less tissue debris remains on the electrode. Several studies confirm that breast tissue debris decays over time. All the other parameters seem to have no significant influence on tissue debris formation.

1.2 Influence of tissue debris on smart electrosurgery
This second section covers the main findings up to now concerning the influence of tissue debris on (smart) electrosurgical measurements.

Influence of tissue debris on electrosurgery
The general influence of tissue debris on smart electrosurgery has been widely discussed in previous reports and eventually this phenomenon represents the overall motive of this particular research [9, 55]. Currently, the key challenge within smart electrosurgery is the disturbance of DRS spectra caused by tissue charring and ablation found on both the blade and the optical fibers of the electrosurgical knife. This tissue debris arises from the applied electrical heat, changing both the physical and chemical composition of the tissue. Certain interactions between tissue and foreign surfaces take place and the formation of adhesive bonds between the different materials leads to an adsorbed layer of tissue debris on the electrosurgical knife [9, 55]. The debris layer impedes the desired current flow, which causes the entire electrosurgical device to function less effectively. The resistive heating of the tip increases leading to a worse cutting performance. In addition, some imply that tissue debris on the electrode can cause tissue tearing, which leads to re-bleedings and foreign body responses in the wound. All in all, tissue debris formation has an undesired influence on both the functionality and the efficiency of (smart) electrosurgery.

Influence of tissue debris on DRS measurements
Tissue debris adhesion on the optical surfaces of the DRS fibers comes at the expense of the signal intensity of the DRS spectrum. According to Beer's law, the darker the color of the tissue debris, the more light is absorbed by the debris and the less light is reflected and may be used for DRS measurements. This statement is confirmed by an experiment performed by Mollerus, showing a significant correlation between the amount of tissue debris and DRS intensity (*r(14) = −0,679, up = 0,005*) [9]. Moreover, the average signal obtained after two minutes of cutting from an electrosurgical

blade with tissue debris was only 2% of the normal intensity obtained from a clean blade. In addition, a negative, exponential correlation was found between the power output of the DRS signal and the time. This means that the power output exponentially decreases over time. It is assumed that this decrease is a result of an exponential increase of tissue debris over time.

Influence of optical fiber cleaning on DRS measurements
The same experiment of Mollerus shows the influence of fiber cleaning on the DRS measurements. According to this experiment, cleaning and polishing the fibers leads to a recovery of the maximum power output from 2% to 43%. Cleaning them only once (after two minutes of cutting), leads to a recovery from 2% to 24%. Unfortunately, these percentages are not satisfying enough for proper functioning of the optical fibers. Therefore, cleaning is not a sufficient method for solving the tissue debris adhesion problem.

1.3 Influence of electrosurgery on tissue debris composition
The third section covers the main findings up to now concerning the influence of electrosurgery on the composition of tissue debris.

Influence of electrosurgery on tissue debris composition
In order to explore the influence of electrosurgery on the composition of tissue debris, Mollerus performed a tissue analysis for her master thesis [9]. Both DRS and Fourier Transform – Infrared (FTIR) measurements were used to characterize tissue debris. The shape of a spectrum indicates specific characteristics, and the intensity of a spectrum shows the influence of tissue debris on measurements (as explained in the previous section). So, for characterizing the tissue debris composition the spectrum shape is the most important indicator. The signal shape of the DRS spectrum only showed the presence of water and lipid. Scattering obstructed the ability to draw further conclusions on the weak indications of other constituents. The signal shape of the FTIR spectrum on the other hand, indicated proteins (matching with hemoglobin and hydrolyzed protein) and fatty acid esters. All in all, the tissue analysis performed by Mollerus has shown the presence of at least three different constituents in tissue debris: water, proteins (hemoglobin and hydrolyzed protein) and lipids (fatty acid esters).

2. Previous recommendations
This paragraph summarizes the previous recommendations proposed by Mollerus. Evaluating these recommendations will help to determine the scope of this research and structure the activities ahead, in order to efficiently work towards a solution for the proposed problem.

2.1 Recommendations on experiments
The first section describes the recommendations concerning the experiments that were performed and might be repeated in the future. Most of the experiments performed by Mollerus were done with a limited number of samples coming from a limited amount of attended procedures, which makes the results somewhat unreliable. In order to find more significant correlations, it was therefore recommended to repeat some of the experiments, though with a larger amount of data. During the experiments performed by Mollerus, the amount of debris found on the blade of the electrosurgical knife was measured by the naked eye only, which unfortunately does not result in reliable values. For more precise and reliable data, it is therefore recommended to repeat the concerned experiments, while using an alternative method to measure the exact amounts of tissue debris adhering on the electrosurgical knife. When repeating an experiment, additional influencing factors that are not subject to the correlation of interest, should be kept constant as much as possible. For example: have only one person performing the procedures and make sure the same settings are used for all the procedures. So far, all experiments have been performed *ex* vivo on animal tissue. Eventually, a final prototype should be tested on actual human breast tissue in order to verify whether the smart electrosurgical knife functions as it was intended to.

2.2 Recommendations on design developments

The second section describes the recommendations concerning the further developments of the design of the smart electrosurgical knife. As soon as the tissue debris adhesion problem has been overcome, a next challenge is represented by providing the surgeon with feedback. In order to anticipate his actions to the margin measurements taken during surgery, the surgeon needs to receive some kind of real-time feedback on the values measured. The prototype as created by Mollerus still contains some uncertainties. For example, smoke production during electrosurgery is a common phenomenon. This is an undesired effect and it should be investigated how the smart electrosurgical knife could eliminate this without losing its margin assessment abilities. More accurate measurements could be achieved by integrating more DRS fibers into the design of the electrosurgical knife. This would lead to a greater measurement surface area, leading to more data on the concerned tissue area. The research of Mollerus mainly focused on breast-conserving surgery. However, in other biomedical areas similar issues are going on. These areas might profit from intra-operative margin assessment with the electrosurgical knife as well. Further research should explore these applications.

3. Discussion

This paragraph is about the relevance of all the conclusions and recommendation from previous studies for this particular research. Some of them do not really influence the further course of this research and are therefore less relevant. Others are relevant and need further exploration.

3.1 Excluded topics

This first section describes the topics discussed in previous studies that are no longer relevant for this research and will therefore be excluded.

Influence of clinical use

A large part of the conclusions drawn by Mollerus is about the influence of the clinical use of the electrosurgical knife on tissue debris formation. The influence of surgical parameters, instrument selection, settings and cleaning are all explored and investigated. However, eventually none of these factors enable complete absence of tissue debris adhesion. Instead, when used in the right way, they might at most reduce the amount of tissue debris formation, which is not good enough for solving the complex adhesion problem.

Influence of surgeon behavior

Furthermore, from previous researches and literature studies, it might seem as if changing the behavior of surgeons and improving their electrosurgical skills is an efficient way to decrease tissue debris formation. However, the extent of the intended implementation of this solution is way too big and lies out of the scope of this research. User behavior has turned out to be a very difficult factor to control and both the reliability and functionality of the smart electrosurgical knife cannot be dependent on such an unpredictable factor. Therefore, any method that aims to change the current behavior and/or habits of the medical staff performing electrosurgery, is not considered as a sufficient solution for the tissue debris adhesion problem within the context of this research.

Clinical observations

All in all, a lot of clinical research has been done so far, which has provided this research with a broad knowledge on the clinical workflow during electrosurgery. Currently there is enough information available concerning this aspect and therefore it will not be necessary for the current research to explore this field any further.

3.2 Included topics

The second section describes the topics discussed in previous studies that remain quite relevant for this research and will therefore be included for further investigation.

Tissue debris composition

The findings of Mollerus on the analyzed composition of the tissue debris material partly match the findings of the literature study prior to this research. However, complete reliability of the experiments still lacks. More samples should be investigated in order to draw strong conclusions on the exact tissue debris composition. This composition seems to be crucial information in finding the optimal solution for the tissue debris adhesion problem. Repeating and amplifying this particular experiment might therefore be of great interest for this research.

Breast-conserving surgery

The focus during experiments for this research will be on breast-conserving surgery, just like the focus of previous researches has been. If other surgeries and tissue compositions need to be taken into account as well, all previous findings become useless. Therefore, expanding the field of applications might be an interesting aspect for further research, once the concept of the electrosurgical knife for BCS has turned out to be successful.

Quantifying tissue debris

It might be of added value to have more detailed information on the exact influence of tissue debris on the DRS measurements. This information will help to determine how much of the total amount of tissue debris on the optical fibers should be reduced in order to obtain sufficient DRS measurements. Clarification is needed on the exact threshold for the percentage of the power output enabling sufficient DRS measurements. In other words, should this research aim for a method to prevent 100% tissue debris adhesion or is 80% prevention of tissue debris adhesion enough as well? This characteristic might influence the choice for an optimal solution. When performing experiments concerning this issue, an alternative method should be developed to measure the exact amounts of tissue debris adhering on the electrosurgical knife.

Biomedical coatings on fibers

The use of coatings on the outer surfaces of the optical fibers to prevent tissue debris adhesion was quite easily rejected in previous researches. Mentioned reasons for this were based on experiments captured in literature stating that tissue debris partly remained adhering on the instrument, despite the different coatings used. However, these experiments focused on tissue debris on the blade of the electrosurgical knife, while this research focusses on tissue debris on the optical fibers of the smart electrosurgical instrument. Before ex- or including coatings as a possible solution, experiments should be performed to test their ability to prevent tissue debris adhesion on optical fibers during electrosurgery.

Appendix B: Structure research phases

The research phase of this master thesis report was structured according to Figure 55. The structure is based on two design theories called 'design thinking' and the 'fish trap model' [131]. Figure 55 clearly shows the diverging and converging processes during the course of a design project. By alternating between diverging and converging of choices, direction is provided in the search for a solution. The structure shown in Figure 55 will help to consider all possible choices and to deliberately reach the most optimal solution step by step. The project is started off with a problem statement and after three consecutive evaluations a final solution will eventually be achieved.

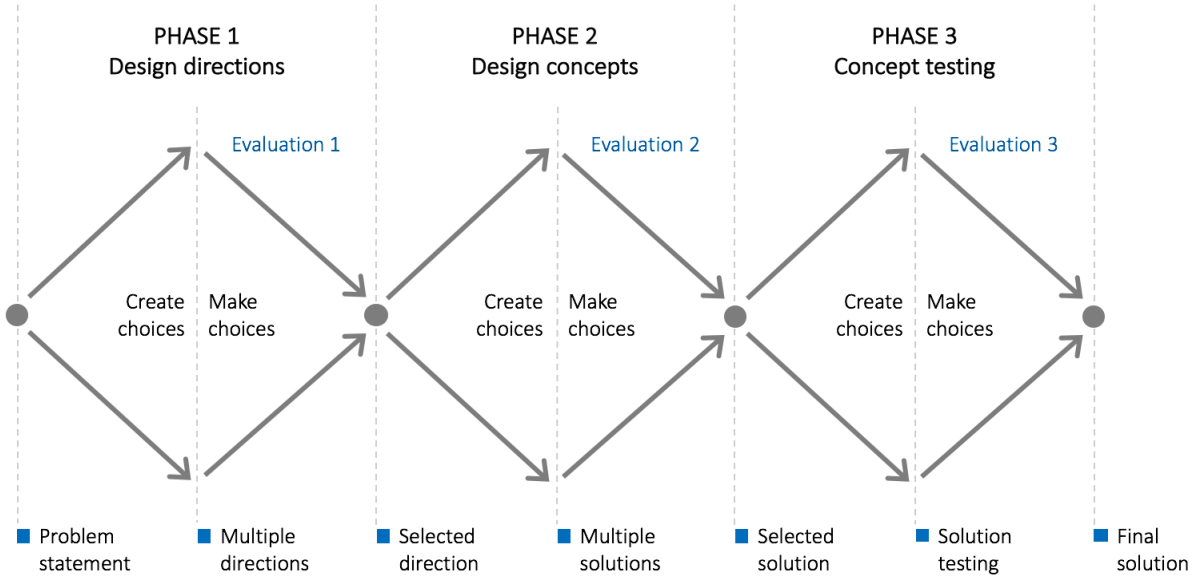

Figure 55: Thesis structure based on design thinking and the fish trap model. Choices are created and after evaluation choices are made. Diverging and converging are alternated [131].

Appendix C: Evaluation of example methods to prevent adhesion

In chapter 6 nine different examples from three different sectors were discussed. Each example describes a specific method to prevent undesired material adhesion during a given process. Each method has a different set of characteristics that makes that method suitable for solving one specific adhesion problem. In order to find an appropriate method to prevent tissue sticking on the optical fibers during smart electrosurgery, a specific set of required characteristics is composed. With the help of these characteristics the methods provided in the previous paragraphs of this chapter can be compared. An overview of these characteristics per method will indicate which aspects of the different methods are worth considering during a follow-up research.

1. Method requirements

Below, the main required characteristics are described of a method that prevents tissue adhesion during smart electrosurgery. The four different requirements are provided in sequence of importance.

I. The method should prevent tissue debris adhesion

First of all, the method should prevent human cells, necrotic tissue and blood from sticking to the surface of the optical fibers on the smart electrosurgical knife. This is the most important requirement the method should meet in order to qualify [7, 8].

II. The method should ensure constant optical measurements after calibration

The second requirement the method should meet is that optical measurements should remain constant after calibration of the sensors. If the spectra change during measurements, the optical fibers lose their reliability and the entire added value of the smart electrosurgical knife disappears [7]. To prevent this, the method should comply to this requirement.

III. The method should be biocompatible

The next requirement concerns biocompatibility. This term is widely described in literature, but in general it is defined as the ability of a biomaterial to optimally perform its desired function with respect to a medical therapy, without falling short by eliciting any unwanted, negative effects at the expense of the treatment outcome [181]. The concept of the smart electrosurgical knife is developed in order to improve patient outcomes during electrosurgery. A non-biocompatible method could lead to the opposite: a worse patient outcome with a risk on infections or follow-up surgery for example. Therefore, it is very important that the tissue sticking prevention method meets biocompatibility.

IV. The method should be functional at temperatures reaching 500℃

During electrosurgery local temperatures at the surgical site are elevated and can occasionally reach 500°C (see chapter 4). The prevention method should be able to cope with these extreme conditions and its functioning should remain stable.

In Table 13 an overview is provided of the four main requirements for the method preventing tissue adhesion during smart electrosurgery.

Table 13: List of main requirements for the method preventing tissue adhesion during electrosurgery.

#	Requirement
1	Method should prevent tissue debris adhesion
2	Method should ensure constant optical measurements after calibration
3	Method should be biocompatible
4	Method should be functional at temperatures reaching 500°C

2. Comparing methods

Based on the required characteristics provided in the previous section, the different prevention methods described in the examples can now be compared. This comparison should clarify which methods are most relevant to the specific smart electrosurgery situation. These methods could potentially be subject to further research.

Requirement fulfillment

Table 14 shows an overview of the different methods, based on the four main requirements. To check whether a method meets the requirements, four questions are being answered in this table: 1) Does this method prevent tissue debris adhesion? 2) Does this method ensure constant optical measurements after calibration? 3) Is this method biocompatible? 4) Is this method functional at temperatures reaching 500°C?

Table 14: Overview of the comparison of the eight prevention methods found in examples, based on the four most important requirements. 'YES' meaning the method meets the requirement, 'NO' meaning the method does not meet the requirement, 'TBD' meaning it is still to be determined whether the requirement is met or not.

Prevention example		Requirement			
Situation	Method	1	2	3	4
Endoscope visibility	Liquid-infused coating	YES [107]	YES [107]	YES [107]	YES [182]
Medical implants	PEG-based coating	YES [109]	YES [183]	YES [110]	TBD
Laser surgery	Cooled catheter	TBD	YES [160]	YES [160]	TBD
Gecko detachment	Contact area decrease	TBD	TBD	TBD	TBD
Shark skin	Surface morphology + chemical agent	TBD	TBD	TBD	TBD
Lotus leaves	Superhydrophobic surface	TBD	TBD	TBD	TBD
Food adhesion	Teflon coating	YES [184]	YES [184]	YES [184]	NO [180]
Marine biofouling	Foul-release coating	TBD	YES [185]	TBD	TBD
Fouling heat exchangers	Nano-coating	TBD	YES [186]	YES [187]	YES [188]

Table 14 shows that a lot of information still lacks, which makes it difficult to properly compare the different methods. For most methods holds that there is some information available with regard to the requirements, but that the amount and the quality of the information is not sufficient. In these cases, 'to be determined' means that more information is needed before concrete conclusions on requirement fulfillment can be drawn. Therefore, a less binary method is needed to compare the different methods.

Harris Profile

Based on the information we do have available in this research, it is possible to work with a more nuanced method that shows the relative strengths and weaknesses with respect to the predefined requirements in a more visual way. For this purpose, the graphic representation of the Harris Profile is used. In general, the Harris Profile is used to evaluate concepts and facilitate decisions on which concepts to continue with in a design process. The main requirements are ranked in order of importance and each of them is evaluated on the basis of an even number of scores (--/-/+/++) to prevent neutral scoring. By analyzing in which direction the 'tower of colored blocks' would fall, it can be made clear which methods have the most potential [131]. The scores are based on the information provided in this research. However, measurable scores have not been allocated yet and therefore this performance assessment is typically an intuitive prediction with relatively low reliability [131].

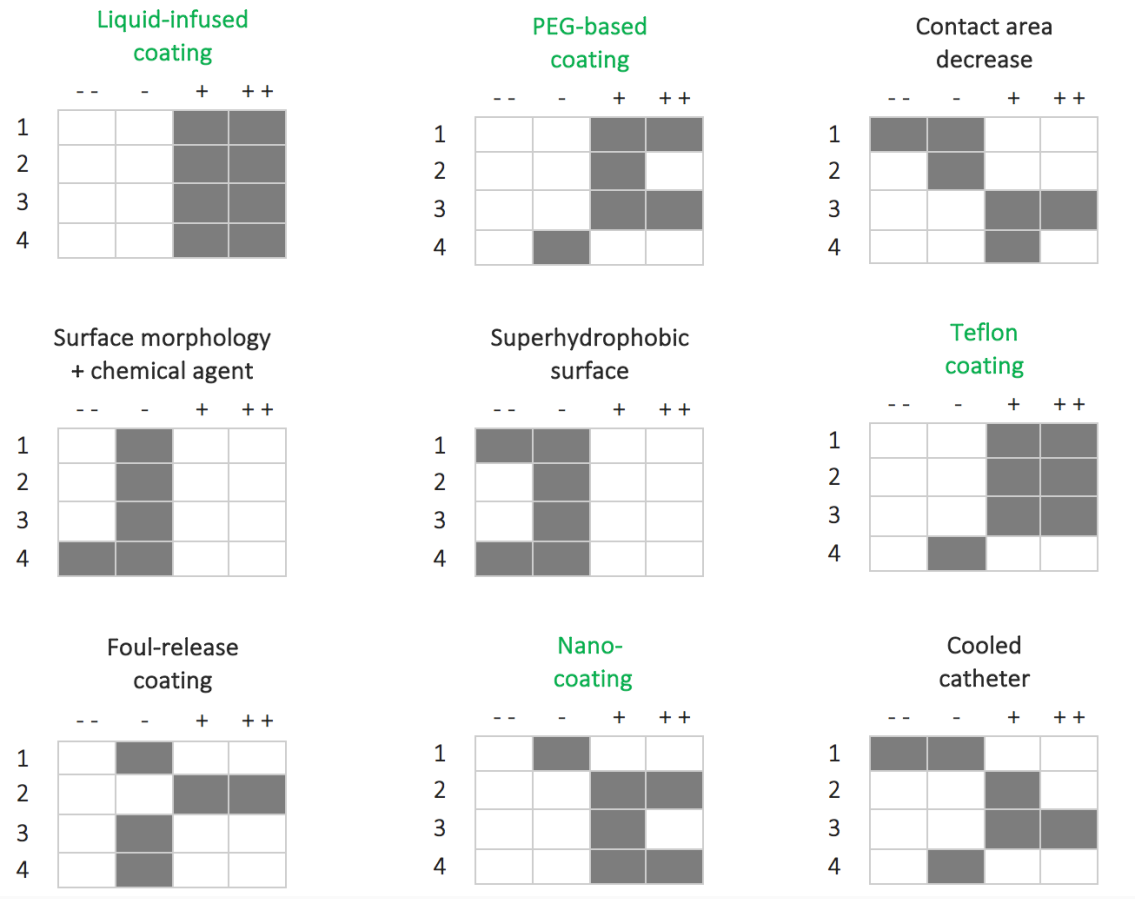

Figure 56: An overview of the different Harris Profiles of all methods based on the four main requirements: 1 = preventingtissue adhesion, 2 = constant optical measurements, 3 = biocompatibility and 4 = functional at temperatures reaching 500℃

Figure 56 shows four 'towers of colored blocks' that would tilt towards the positive side: liquid-infused coating used for endoscope visibility, PEG-based coating used for medical implants, Teflon coating used for cookware and nano-coating used for heat exchangers. These four methods are potentially eligible for solving the tissue adhesion problem during smart electrosurgery.

Appendix D: Results - Exploring electrosurgical settings

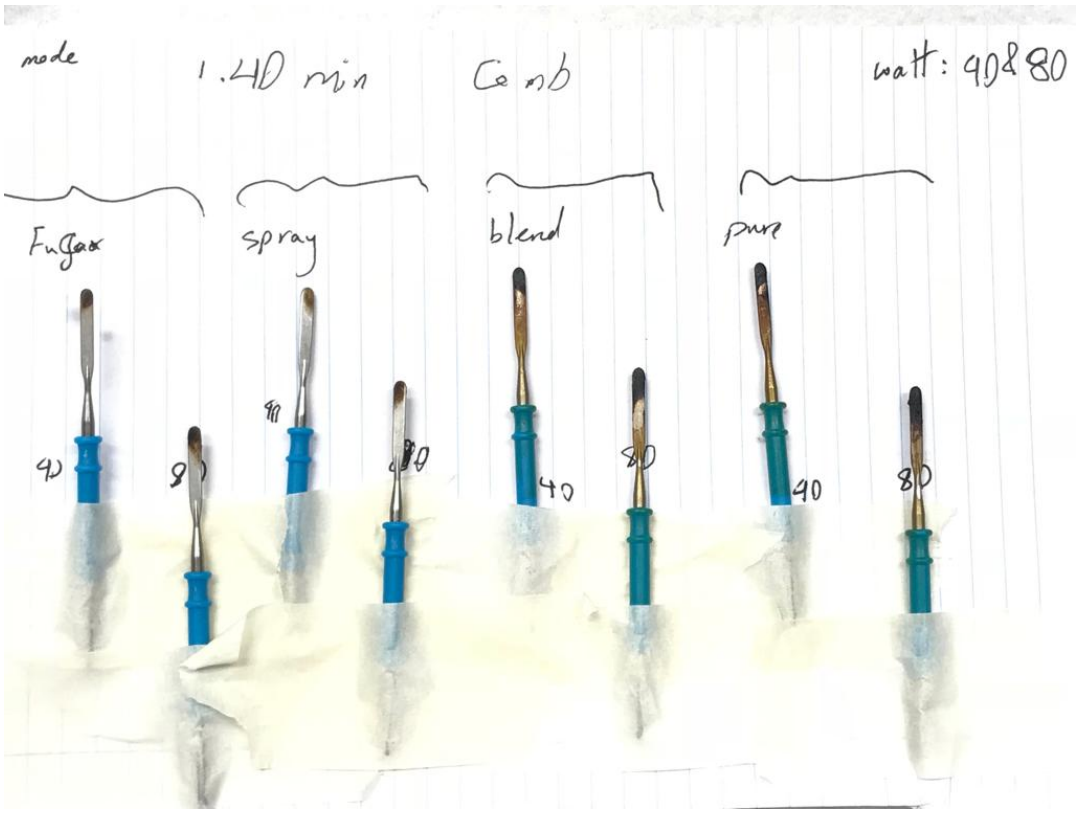

Figure 57: Influence of different settings (cutting mode and watts) on amount of tissue debris after 1.33 minutes of cutting.

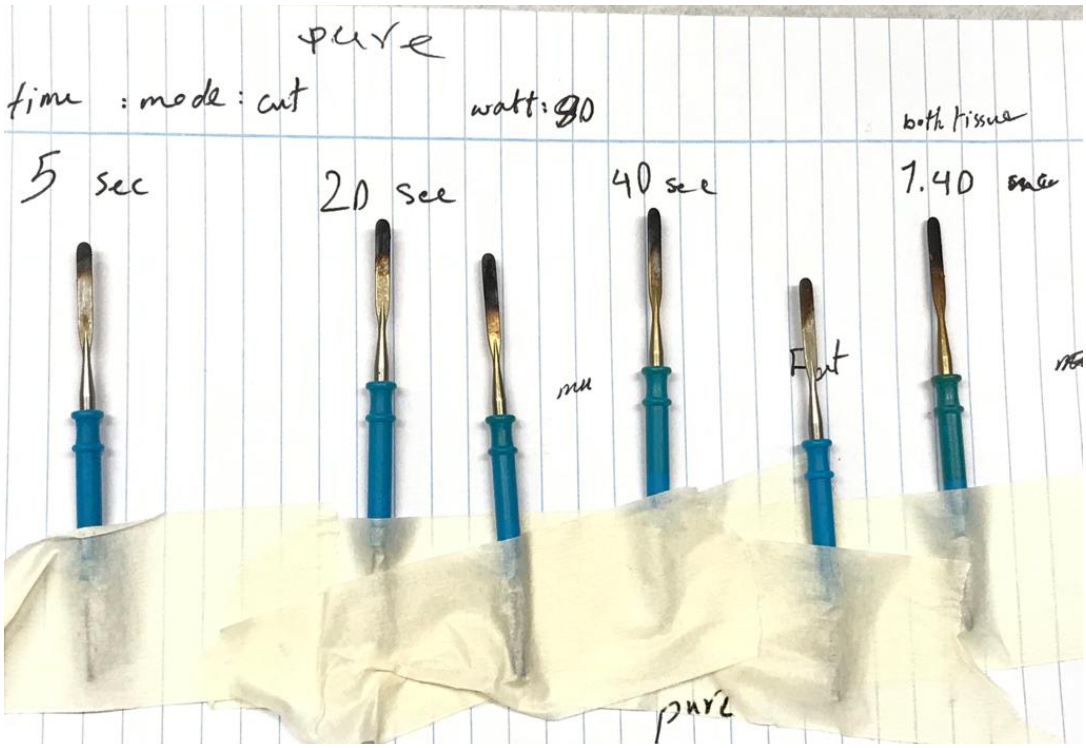

Figure 58: Influence of cutting duration on amount of tissue debris while using pure cutting mode and 80 watts.

Appendix E: Results - Optical microscope

This appendix shows all the images obtained with digital optical microscopy. The caption underneath each image explains what exactly is shown in the picture.

1. Blade tips (side view)

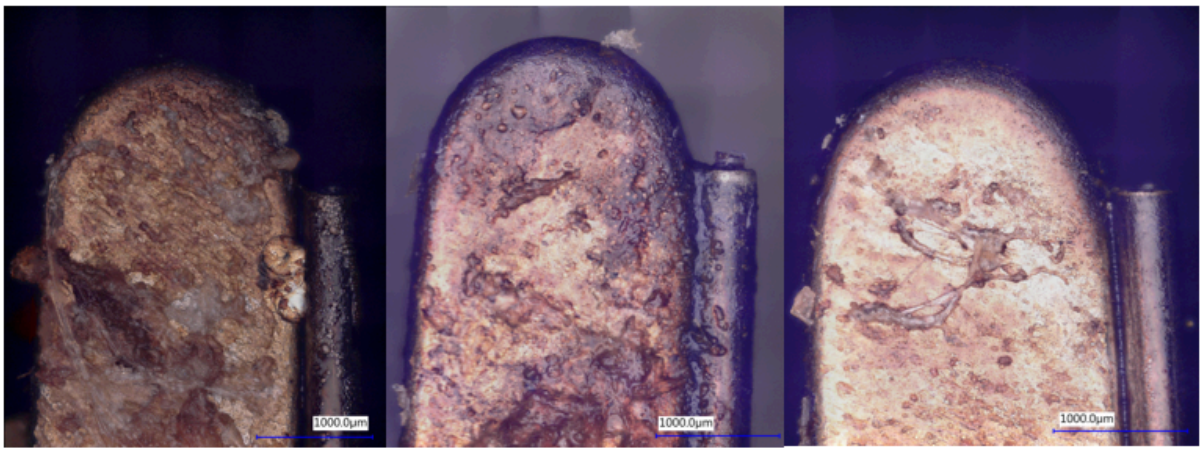

Figure 59: Three blade tips used on pork belly for 5 seconds. Magnification 250x.

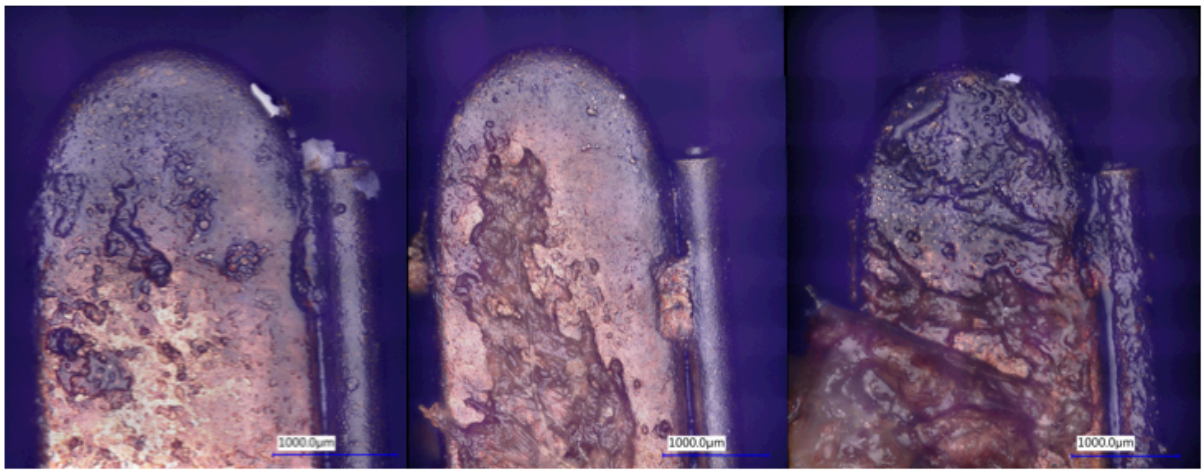

Figure 60: Three blade tips used on pork belly for 30 seconds. Magnification 250x.

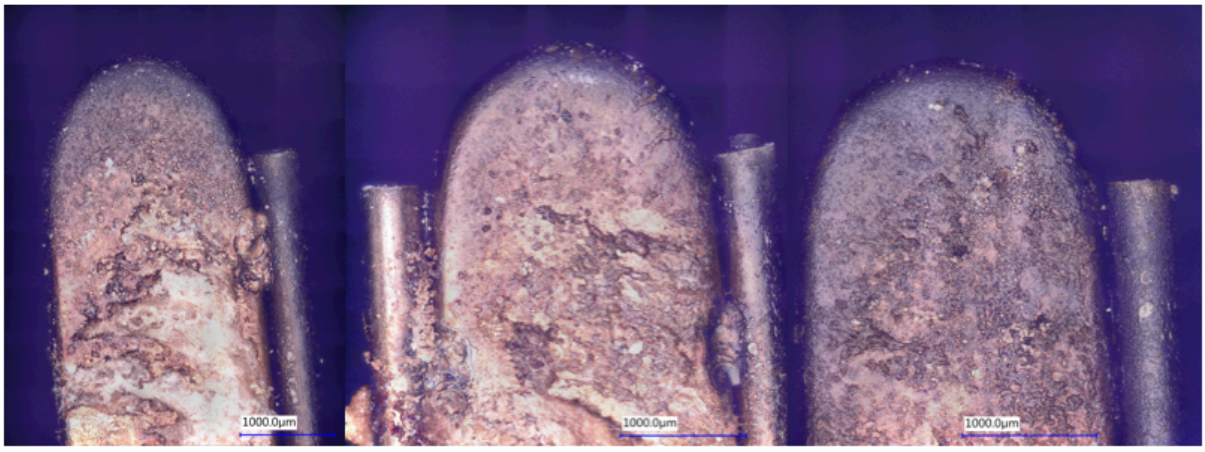

Figure 61: Three blade tips used on porcine liver for 5 seconds. Magnification 250x.

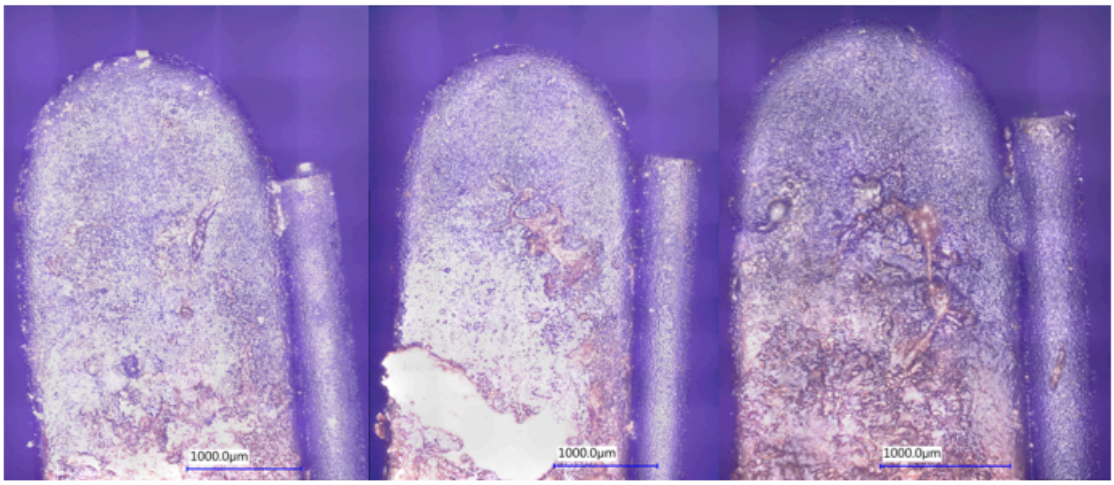

Figure 62: Three blade tips used on porcine liver for 30 seconds. Magnification 250x.

2. Tube/fiber tips (side view)

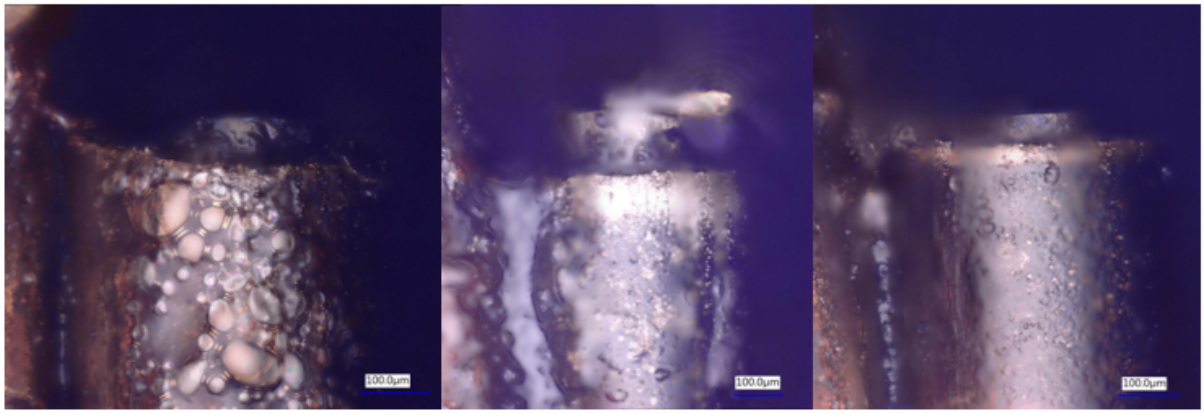

Figure 63: Three tube/fiber tips used on pork belly for 5 seconds. Magnification 1000x.

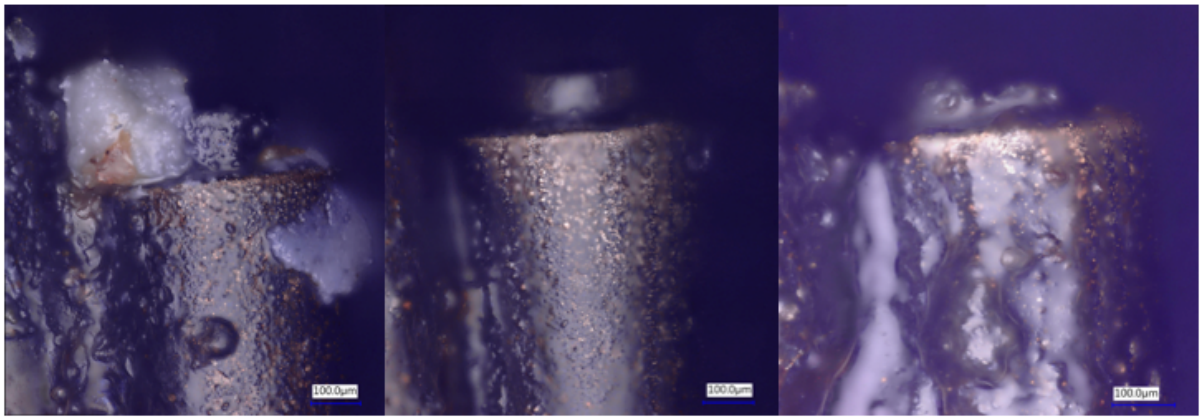

Figure 64: Three tube/fiber tips used on pork belly for 30 seconds. Magnification 1000x.

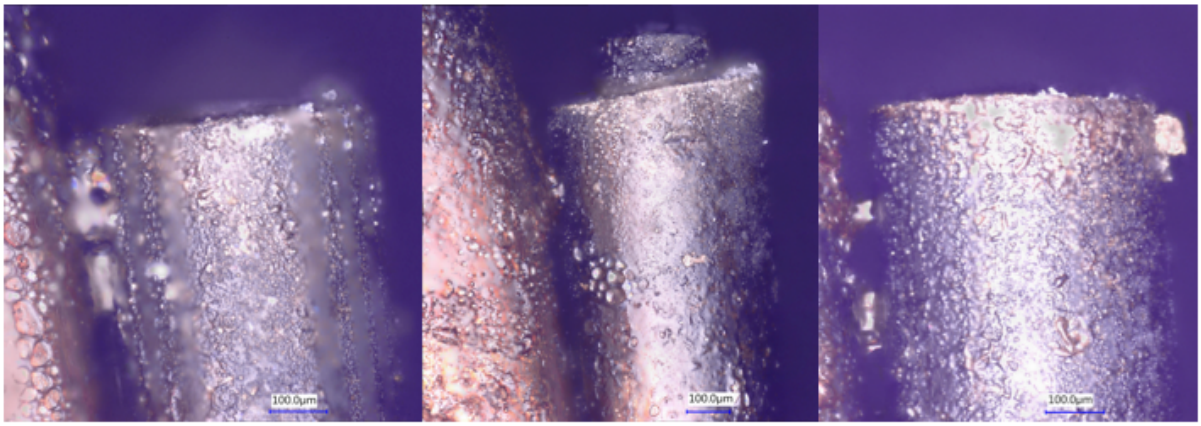

Figure 65: Three tube/fiber tips used on porcine liver for 5 seconds. Magnification 1000x.

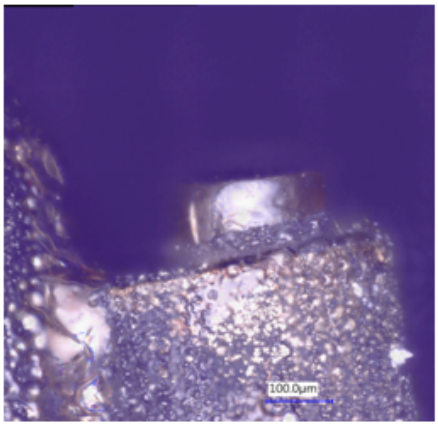

Figure 66: One tube/fiber tip used on porcine liver for 30 seconds. Magnification 1000x.

3. Fiber tips (side view)

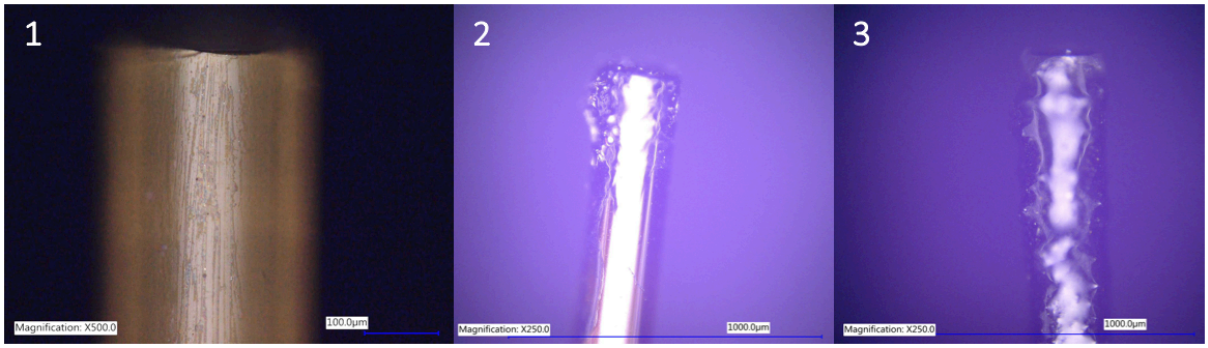

Figure 67: Three different fiber tips. 1 = Unused, polished fiber tip (magnification 500x), 2 = fiber tip used on porcine liver for 5 seconds (magnification 250x), 3 = fiber tip used on pork belly for 30 seconds (magnification 250x).

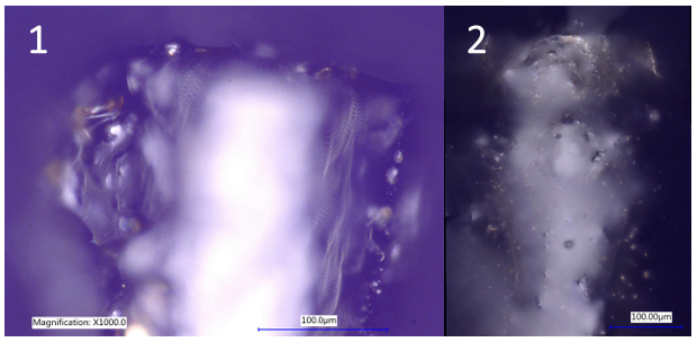

Figure 68: Two different fiber tips. 1 = Fiber tip used on porcine liver for 5 seconds (magnification 1000x), 2 = fiber tip used on pork belly for 30 seconds (magnification 2000x).

4. Fiber tips (top view)

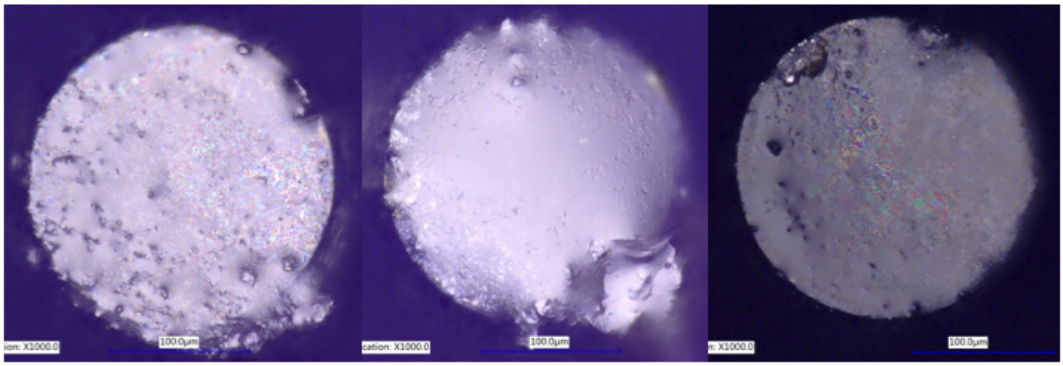

Figure 69: Three fiber tips used on pork belly for 5 seconds. Magnification 1000x.

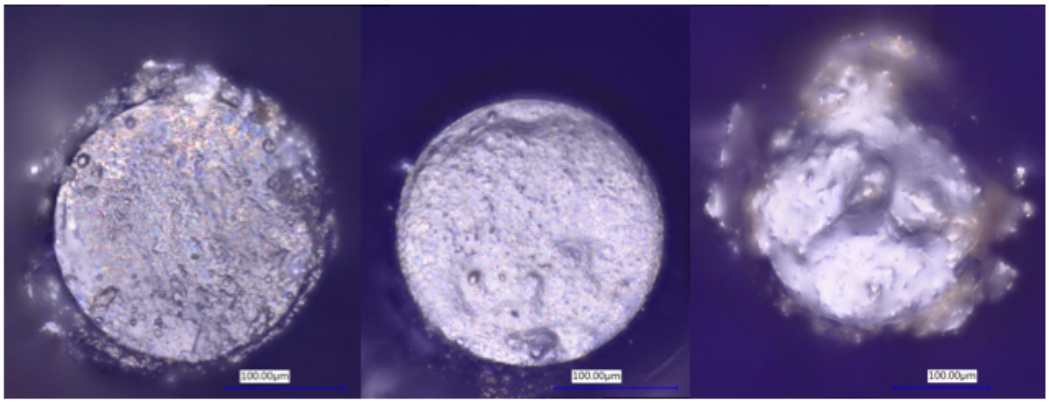

Figure 70: Three fiber tips used on pork belly for 30 seconds. Magnification 1000x.

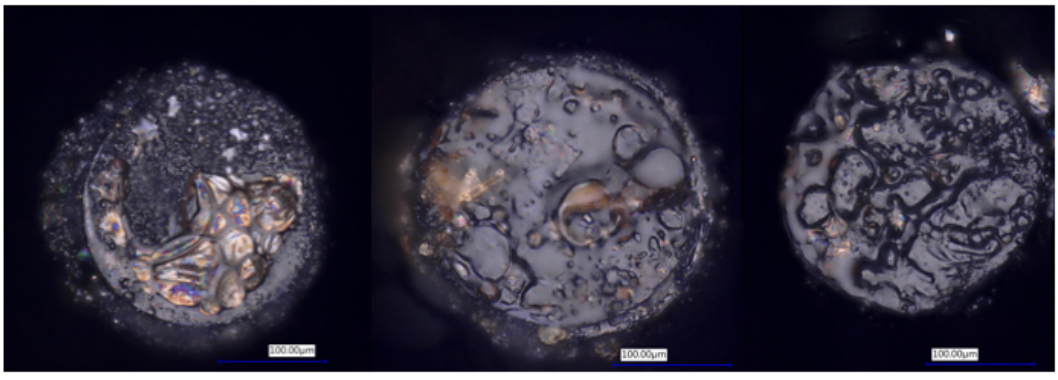

Figure 71: Three fiber tips used on porcine liver for 5 seconds. Magnification 1000x.

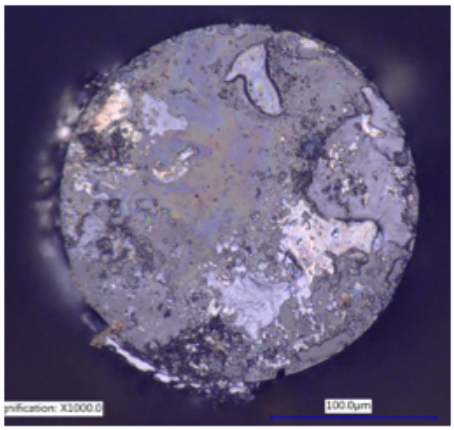

Figure 72: Fiber tip used on porcine liver for 30 seconds. Magnification 1000x.

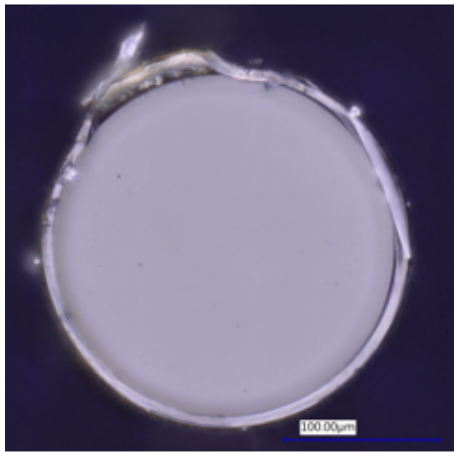

Figure 73: Unused, polished fiber tip. Magnification 1000x.

5. Fiber tips (3D)

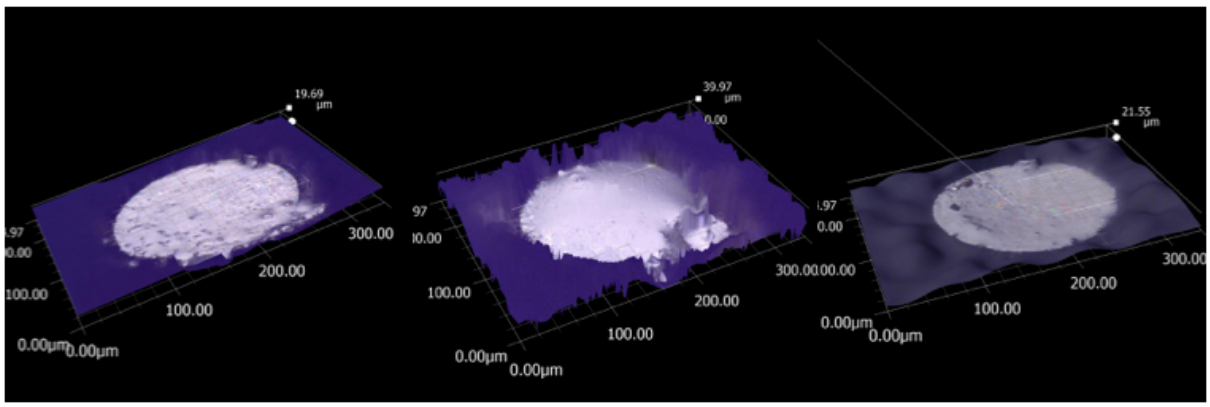

Figure 74: 3D representation of three fibers used on pork belly for 5 seconds.

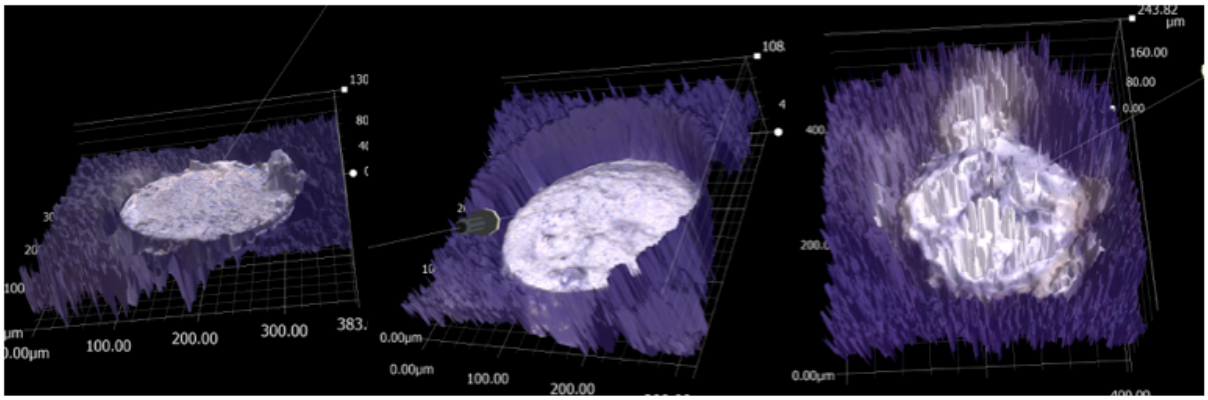

Figure 75: 3D representation of three fibers used on pork belly for 30 seconds.

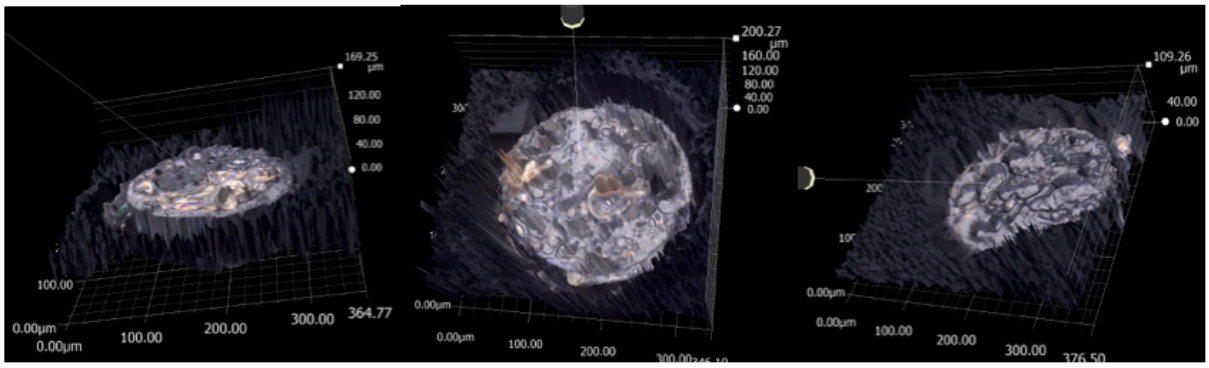

Figure 76: 3D representation of three fibers used on porcine liver for 5 seconds.

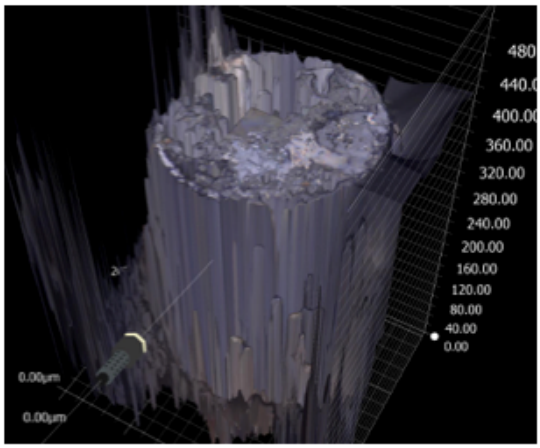

Figure 77: 3D representation of a fiber used on porcine liver for 30 seconds.

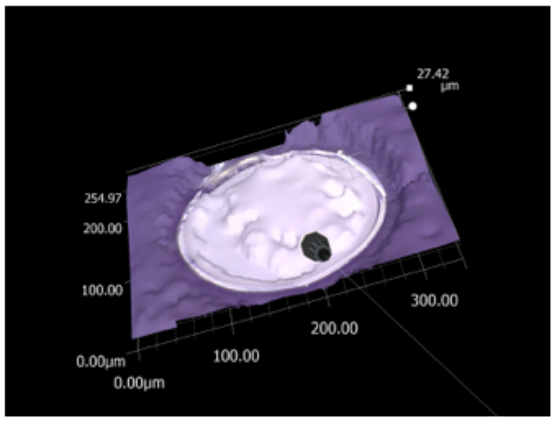

Figure 78: 3D representation of an unused, polished fiber.

Appendix F: Results - Energy-dispersive spectroscopy

1. EDS images

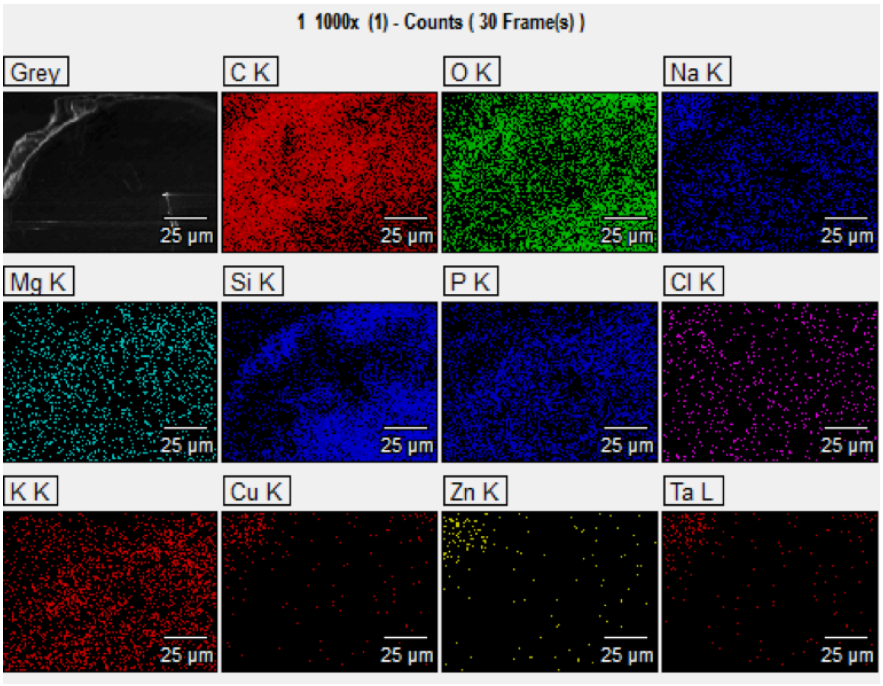

Figure 79: EDS images showing the different elements present on a fiber tip used on pork belly for 5 seconds.

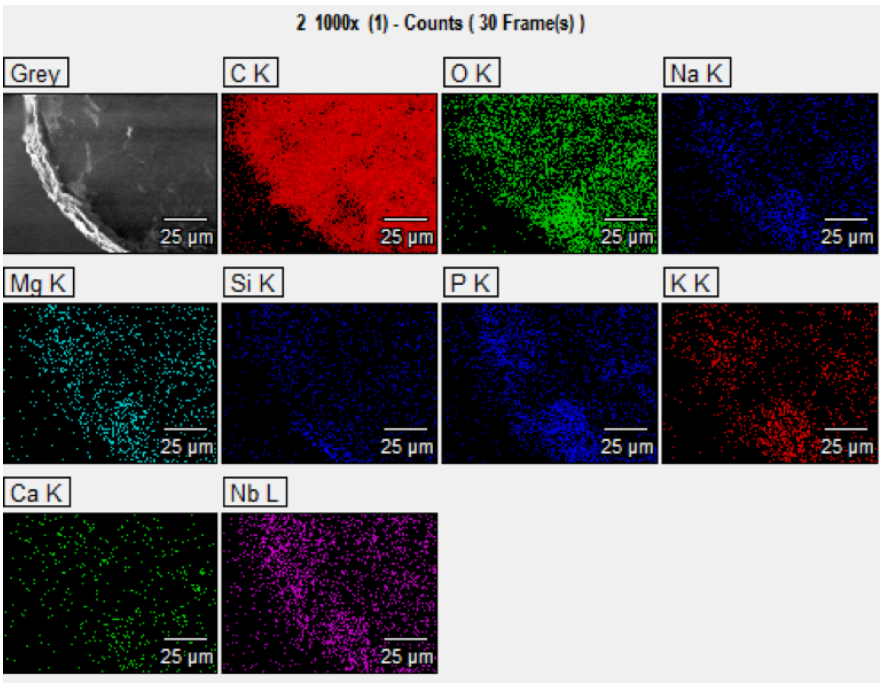

Figure 80: EDS images showing the different elements present on a fiber tip used on pork belly for 30 seconds.

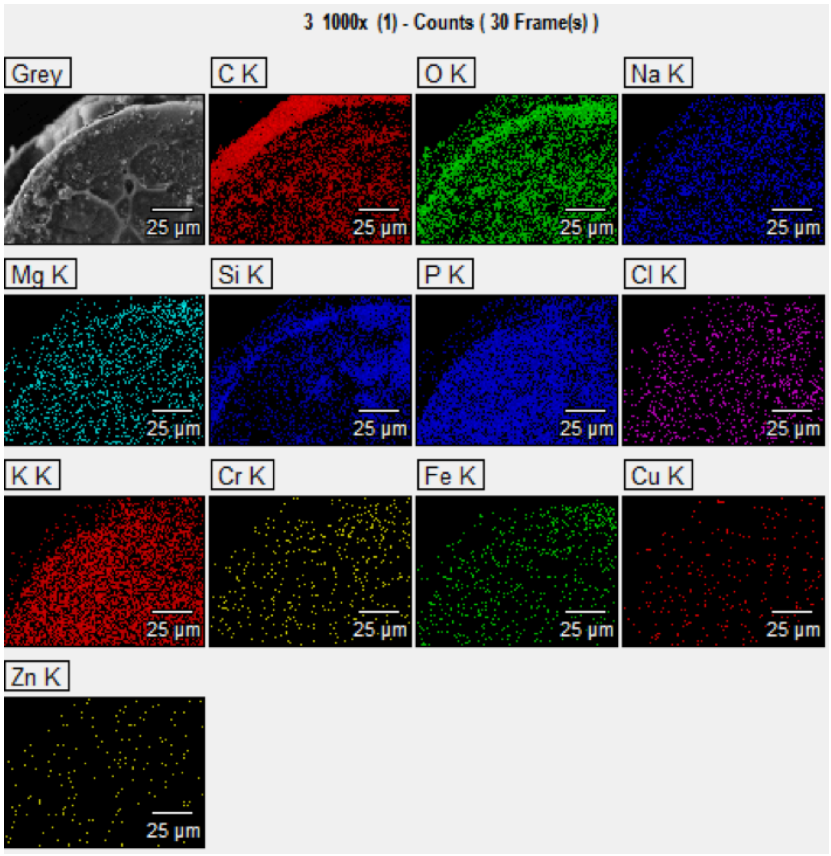

Figure 81: EDS images showing the different elements present on a fiber tip used on porcine liver for 5 seconds.

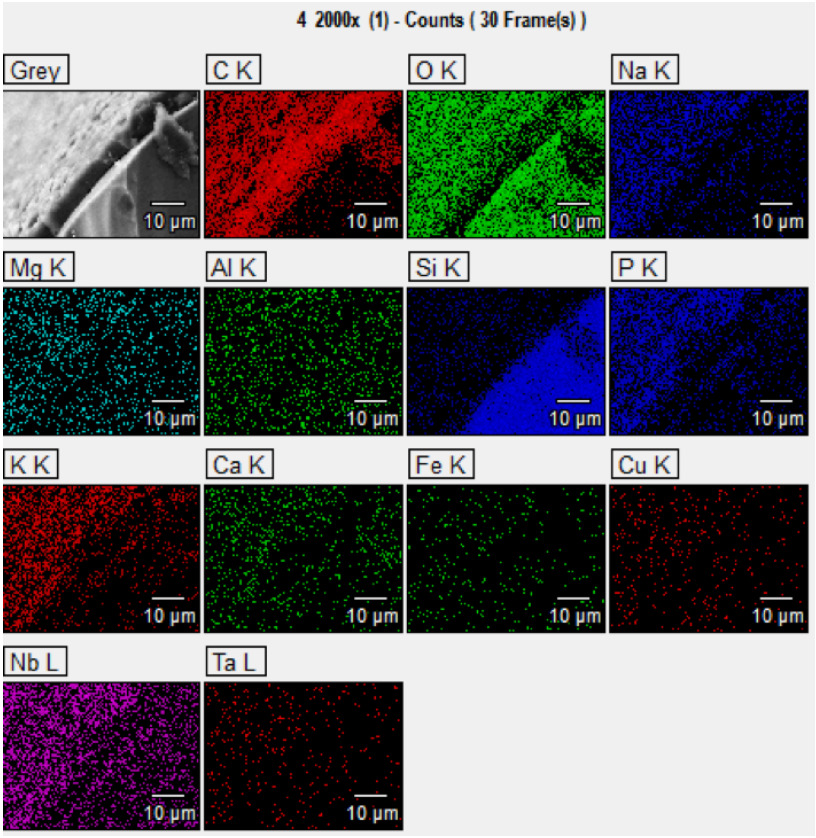

Figure 82: EDS images showing the different elements present on a fiber tip used on porcine liver for 30 seconds.

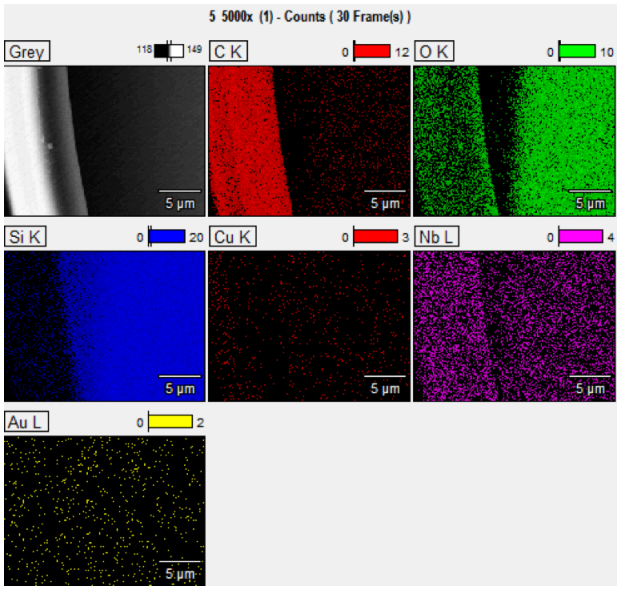

Figure 83: EDS images showing the different elements present on an unused, polished fiber tip.

2. EDS spectra

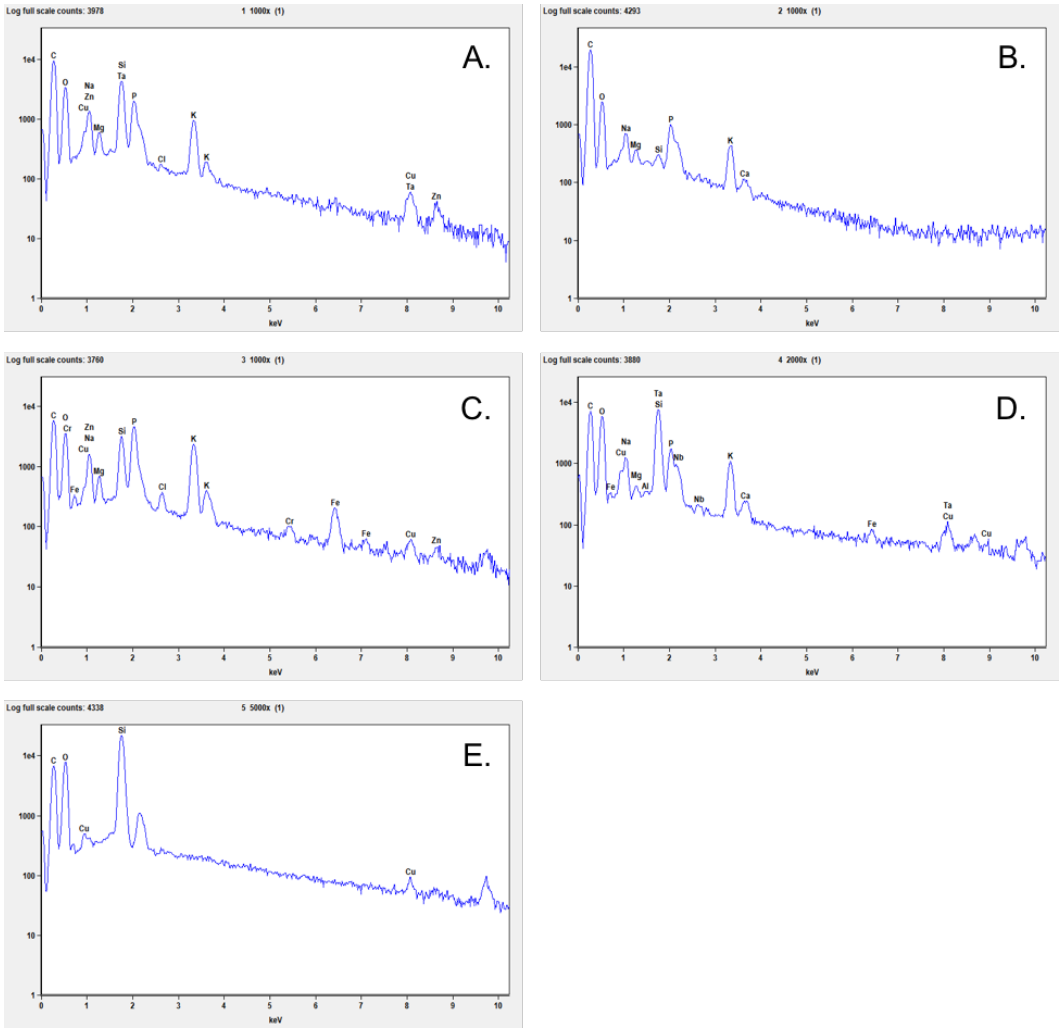

Figure 84: EDS spectra showing peaks for the different element present. A) Pork belly - 5 sec, B) Pork belly – 30 sec, C) Porcine liver – 5 sec, D) Porcine liver 30 sec.

3. EDS elements

Table 15: Elements detected with EDS on the fiber tip used on pork belly for 5 seconds.

#	Element Line	Weight %	Weight % Error	Atom %	Atom % Error
1	C	71,03%	± 0.32	79.18	± 0.36
2	O	20,70%	± 0.21	17.33	± 0.18
3	Si	2,66%	± 0.15	1.27	± 0.07
4	Na	1,49%	± 0.02	0.87	± 0.01
5	K	1,30%	± 0.02	0.44	± 0.01
6	P	1,29%	± 0.03	0.56	± 0.01
7	Cu	0,50%	± 0.05	0.10	± 0.01
8	Zn	0,41%	± 0.06	0.08	± 0.01
9	Ta	0,35%	± 0.17	0.03	± 0.01
10	Mg	0,23%	± 0.01	0.13	± 0.00
11	Cl	0,03%	± 0.01	0.01	± 0.00
	Total	100,0%		100.00%	

Table 16: Elements detected with EDS on the fiber tip used on pork belly for 30 seconds.

#	Element Line	Weight %	Weight % Error	Atom %	Atom % Error
1	C	85,03%	± 0.28	88.84	± 0.29
2	O	13,33%	± 0.20	10.46	± 0.15
3	Si	0,08%	± 0.01	0.04	± 0.00
4	Na	0,51%	± 0.02	0.28	± 0.01
5	K	0,50%	± 0.02	0.16	± 0.01
6	P	0,42%	± 0.02	0.17	± 0.01
7	Mg	0,07%	± 0.01	0.04	± 0.01
8	Ca	0,06%	± 0.01	0.02	± 0.00
	Total	100,0%		100.00%	

Table 17: Elements detected with EDS on the fiber tip used on porcine liver for 5 seconds.

#	Element Line	Weight %	Weight % Error	Atom %	Atom % Error
1	C	64,57%	± 0.34	75.60	± 0.40
2	O	20,59%	± 0.30	18.10	± 0.26
3	Si	2,15%	± 0.02	1.08	± 0.01
4	P	4,30%	± 0.04	1.95	± 0.02
5	K	3,82%	± 0.04	1.37	± 0.01
6	Na	1,86%	± 0.03	1.14	± 0.02
7	Fe	1,16%	± 0.07	0.29	± 0.02
8	Cu	0,45%	± 0.06	0.10	± 0.01
9	Zn	0,39%	± 0.08	0.08	± 0.02
10	Cl	0,32%	± 0.02	0.13	± 0.01
11	Mg	0,20%	± 0.02	0.12	± 0.01
12	Cr	0,17%	± 0.02	0.05	± 0.01
	Total	100,0%		100.00%	

Table 18: Elements detected with EDS on the fiber tip used on porcine liver for 30 seconds.

#	Element Line	Weight %	Weight % Error	Atom %	Atom % Error
1	C	58,66%	± 0.30	69.35	± 0.35
2	O	29,21%	± 0.24	25.92	± 0.21
3	Si	4,39%	± 0.08	2.22	± 0.04
4	P	1,38%	± 0.02	0.63	± 0.01
5	Nb	1,38%	± 0.05	0.21	± 0.01
6	Ta	1,34%	± 0.19	0.10	± 0.01
7	Na	1,27%	± 0.02	0.79	± 0.01
8	K	1,27%	± 0.01	0.46	± 0.01
9	Cu	0,64%	± 0.06	0.14	± 0.01
10	Ca	0,19%	± 0.01	0.07	± 0.00
11	Fe	0,14%	± 0.03	0.04	± 0.01
12	Mg	0,09%	± 0.01	0.05	± 0.00
13	Al	0,04%	± 0.01	0.02	± 0.01
	Total	100,0%		100.00%	

Table 19: Elements detected with EDS on the unused, polished fiber tip.

#	Element Line	Weight %	Weight % Error	Atom %	Atom % Error
1	C	57,40%	± 0.32	67.11	± 0.37
2	O	30,94%	± 0.19	27.15	± 0.17
3	Si	11,33%	± 0.03	5.66	± 0.02
4	Cu	0,33%	± 0.05	0.07	± 0.01
	Total	100,0%		100.00%	

Origin different elements:

- Charred tissue (C)
- Non-charred tissue (C, O, P, K, Na, Mg, Cu, Cl, Zn, Ca)
- Charred acrylate (C)
- Non-charred acrylate (C, O)
- Silica (O, Si)
- Blood (Fe)

Appendix G: Results - Raman spectroscopy

1. Pork belly – 5 seconds

The Raman spectra provided below belong to the specific areas indicated by the white, dashed crossing in the supporting picture. All areas are located on the surface of a fiber tip used on pork belly for 5 seconds. Although three quite different areas are analyzed, the corresponding spectra are obviously very similar. According to reference data found in literature, the two peaks around 1500 cm^{-1} indicate the presence of carbon.

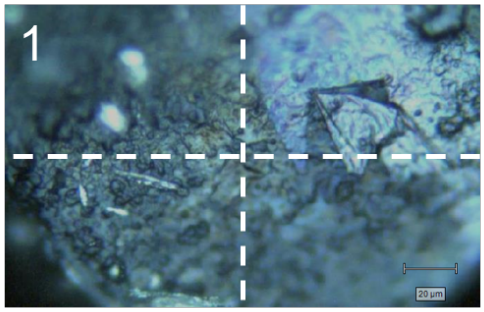

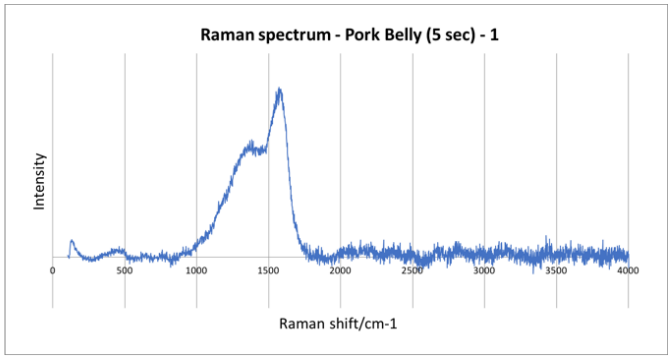

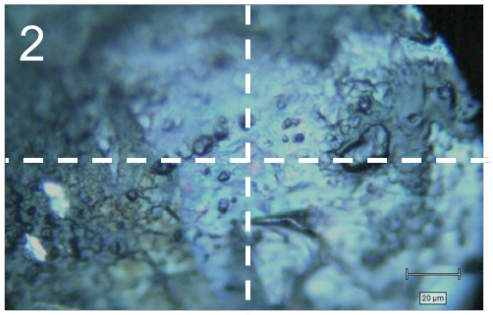

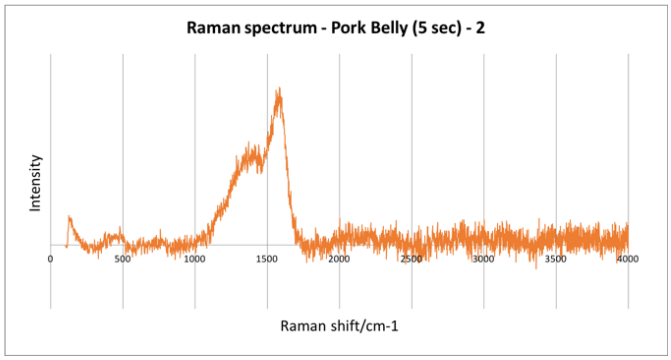

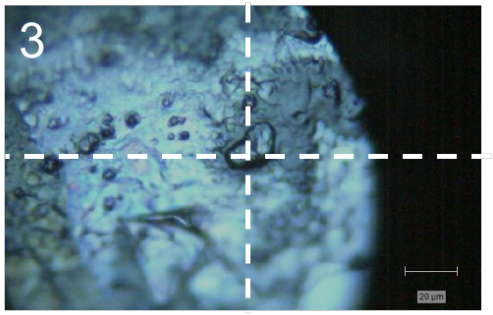

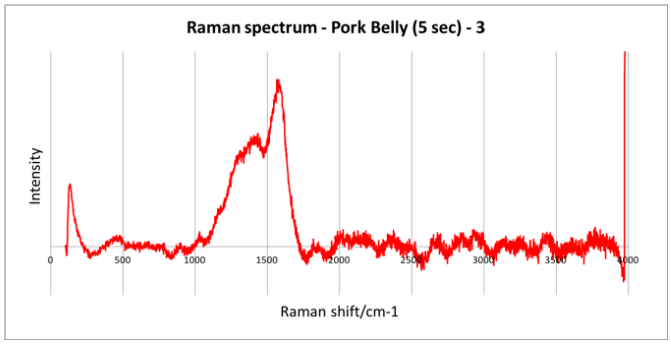

2. Porcine liver – 30 seconds

The Raman spectra provided below belong to the specific areas indicated by the white, dashed crossing in the supporting picture. All areas are located on the surface of a fiber tip used on porcine liver for 30 seconds. Three quite different areas are analyzed, obviously resulting in three quite different Raman spectra as well. According to reference data found in literature, the peak around 500 cm^{-1} indicates the presence of silica (location 1, 2 and 3), the two peaks around 1500 cm^{-1} indicate carbon (location 2 and 3) and the peak around 3000 cm^{-1} indicates acrylate (location 2 and 3).

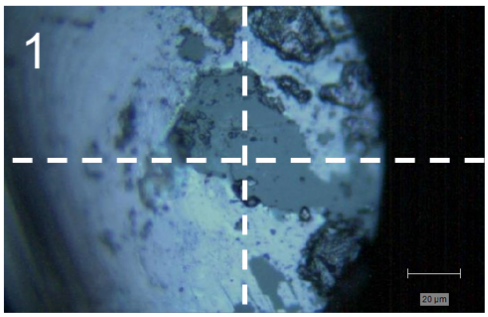
1
20 µm

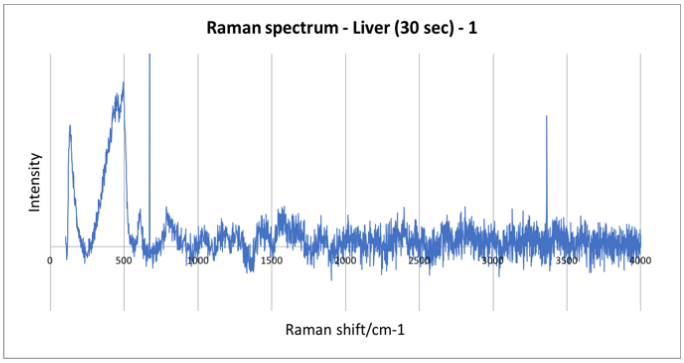
Raman spectrum - Liver (30 sec) - 1
Intensity
0
500
1000
1500
2000
2500
3000
3500
4000
Raman shift/cm-1

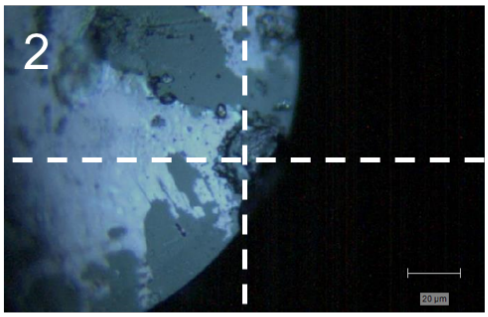
2
20 µm

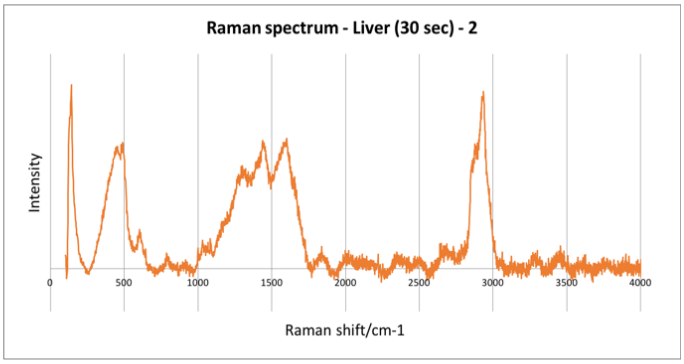
Raman spectrum - Liver (30 sec) - 2
Intensity
0
500
1000
1500
2000
2500
3000
3500
4000
Raman shift/cm-1

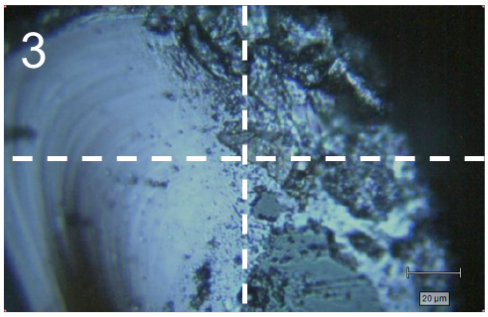
3
20 µm

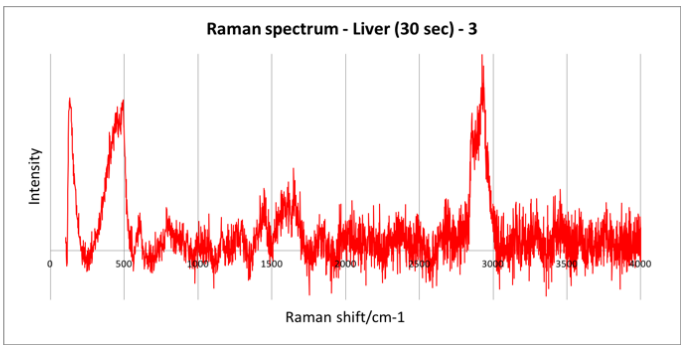
Raman spectrum - Liver (30 sec) - 3
Intensity
0
500
1500
3000
Raman shift/cm-1

Appendix H: Explanation of list of requirements

1. Performance

Describes the main functions the design solution needs to fulfil, in terms of functional properties (speed, power, strength, precision, capacity).

2. Environment

Describes the environmental influences the design solution needs to withstand during production, transport and use (temperature, vibrations, moisture).

3. Life in service

Describes the intensity the design solution is used with and for how long this should last.

4. Maintenance

Describes the necessity of maintenance.

5. Target product cost

Describes a realistic price for the design solution considering similar products. Also, a corresponding margin is provided that needs to be delivered.

6. Transport

Describes the requirements concerning transport of the product solution during production and to the location of usage.

7. Quantity

Describes the requirements concerning the quantity that needs to be produced.

8. Production facilities

Describes to which production facilities the design solution is limited.

9. Size and weight

Describes the boundaries to the size and weight of the solution.

10. Materials

Describes the requirements concerning that must or cannot be used.

11. Product life span

Describes how long the design solution is expected to be produced and sold.

12. Standards, rules and regulations

Describes the standards, rules and regulations (national and international) that apply to the product and the production process.

13. Ergonomics

Describes the requirements that result from observing, understanding, handling and operating the product.

14. Reliability

Describes what chance of failure is acceptable and what kind of failure should be avoided at all cost.

15.Testing
Describes the quality tests that are conducted on the design solution.

16.Safety
Describes the specific precautions that must be taken because of the safety of users and non-users.

17.Product policy
Describes the requirements resulting from the company's product portfolio.

18.Installation and initiation of use
Describes the requirements that result from installation, connecting to other systems and learning how to handle and operate the design solution.

19.Reuse
Describes requirements concerning reuse of the design solution.

Appendix I: Overview coatings from literature

Name	Anti-adhesive	Transparency	Thermal stability	Bio-compatibility	Other stability	Substrate material	Costs	Fabrication	Suggested application
Xu, 2014 High fabrication temperature	Super-hydrophobic	Broadband antireflective	300◦C max	Unknown	Strong acid, strong alkali, water drop impact, sand impact. 3H pencil hardness test	Glass	Unknown	Reproducible, dip-coating 550◦C – 5hrs 550◦C – 3hrs 720◦C – 135s	Windshields, eyeglasses, solar cells, windows
Guldin, 2013 Wrong application	Self-cleaning: photocata-lytic TiO2	Broadband antireflective	Unknown	Unknown	UV, mechanical impact, stearic acid	Glass, flexible plastic	Low	Reproducible	Flexible plastics
Faustini, 2010	Water repellent, anti fogging, photocata-lytic TiO2	Broadband antireflective	Unknown	Unknown	Mechanical and chemical	Glass	Low	Reproducible, dip-coating 450◦C – 10min 70◦C – 2hrs 500◦C – 5min	Solar cells
Yang, 2014 Low operation temperature	Superhydro-phobic, self-cleaning	Broadband antireflective	Unknown	Unknown	Mechanical	Dielectric surfaces	Unknown	Reproducible	Biological and optoelectronic
Mahadik, 2012	Super-hydrophobic	Transparent	200◦C max	Unknown	Unknown	Glass	Unknown	Reproducible, spray coating 100◦C – 3min 150◦C – 2hrs 550◦C – 1hr	Industrial scale-up and high-technology fields

Name	Anti-adhesive	Transparency	Thermal stability	Bio-compatibility	Other stability	Substrate material	Costs	Fabrication	Suggested application
Luo, 2019	Superhydro-philic self-cleaning, moth-eye (cu)	Omnidirect-ional and broadband antireflection	Unknown	Unknown	Mechanical durability	Glass	Low	Thermal dewetting 400-600◦C – 10-60min 150◦C – 5min 450◦C – 3hrs	Solar cells
Li, 2018 High thermal stability	Superhydro-phobic self-cleaning, silanized silica	Omnidirect-ional and broadband antireflection, transparent	High	Unknown	Mechanical durability	Glass and others	Low	PS spheres 90◦C – 3min 400-800◦C	Solar cells, displays, optical lenses, optoelectronic devices
Fan, 2018 Wrong substrate	Hyper-hierarchical, superhydro-phocib self-cleaning	Hyper-hierarchical broadband antireflection	250◦ max	Unknown	Structural robustness	Metals	Unknown	Unknown	Light harvesting
Jia, 2018 Too much unknown	Hydrophobic self-cleaning	Gradient refractive index antireflection	Unknown	Unknown	Unknown	Glass	Unknown	Dip-coating	Unknown
Tao, 2018 High fabrication temperature	Hydrophilicity	TiO2-SiO2 broadband antireflection	High	Unknown	Favourable robustness	Glass	Low	Dip-coating, 550◦C – 3hrs	Lenses, solar cells

Name	Anti-adhesive	Transparency	Thermal stability	Bio-compatibility	Other stability	Substrate material	Costs	Fabrication	Suggested application
Tan, 2017 Wrong substrate	Fluoroalkyl hydrophobic coating	Broadband, moth-eye antireflection	Unknown	Unknown	Mechanically robust, flexible	Flexible substrate	Unknown		Flexible displays
Bao, 2017 Fabrication is difficult	Superhydro-phobic (PFOTES modified)	Double-layer broadband antireflective coating	Unknown	Unknown	Mechanical robustness	Glass	Unknown	Dip-coating, takes 2wks, 400◦C – 2hrs 150◦C – 2hrs (2x) 160◦C – 1.5h	Solar cells
Jin, 2017 High fabrication temperature	Photocatalytic self-cleaning, durable superhydro-phobicity	TiO2-SiO2 broadband antireflection	Unknown	Unknown	Mechanical robustness and functional durability	Glass	Unknown	60◦C – 20hrs 550◦C – 3hrs 60◦C – 10hrs 550◦C – 3hrs (2x)	Optical devices, display devices, solar cells
Liu, 2017 Heat resistant?	Hierarchical texture hydrophobi-city and self-cleaning	Hierarchical texture broadband antireflection	Unknown	Unknown	Unknown	Glass	Low	Al anodization 0◦C – 3min 45◦C – 55min 90◦C – 24hrs	Solar cells

Gouda, 2016 Not hydro-phobic enough	Hydrophobic self-cleaning	Asymmetric silicon nanocones, broadband antireflection	Unknown	Unknown	Unknown	Hydrophilic silicon surface	Unknown		Solar cells

Name	Anti-adhesive	Transparency	Thermal stability	Bio-compatibility	Other stability	Substrate material	Costs	Fabrication	Suggested application
Gouda, 2016 (2)	Hydrophobic self-cleaning	Random textured silicon nanocones, broadband antireflection	Unknown	Unknown	Unknown	Silicon	Low		Solar cells, optoelectronic applications
Leem, 2016 Low operating temperature	Hydrophobic self-cleaning	Broadband antireflection	180◦ max	Unknown	Unknown	ITO glass, PET	Unknown		Flexible and rigid optical, optoelectronic systems
Fuerst, 2016 Hydrophilic	TiO2 hydrophilic self-cleaning	TiO2-Silicone broadband antireflection	Stable	Unknown	Mechanical robustness	Flexible PET, FTO glass solar cells	Unknown		Flexible solar cells
Chen, 2015 Polymer	Superhydro-phobic self-cleaning	Cicada wings nanostructure broadband antireflection	Unknown	Unknown	Unknown	Polymer	Unknown		Optical devices, solar cells, protective coatings
Aytug, 2015 Wrong application (temp)	Chemically modified self-cleaning	Nanostruc-tured glass coating broad-band anti-reflection	Unknown	Unknown	Mechanical robustness	Glass	Unknown		Optical devices

Name	Anti-adhesive	Transparency	Thermal stability	Bio-compatibility	Other stability	Substrate material	Costs	Fabrication	Suggested application
Ye, 2015	Superhydro-phobic, self-cleaning	Silicon random grass, broadband antireflection	Unknown	Unknown	Unknown	Silicon	Unknown	Unknown	Solar cells, optical devices
Kim, 2014	Hydrophilic non-wetting, hydrophobic self- cleaning	Egg-crate structure, broadband, omnidirec-tional, antireflection	Unknown	Unknown	Mechanical robustness	Glass, silicon, optical plastics	Low	Unknown	Solar cells, wind shields, displays
Zhu, 2014	Superhydro-philic self-cleaning, graphene-TiO2	Transparent, broadband photo-response, graphene-TiO2	Unknown	Unknown	Anti-static	Silicon, glass	Unknown	Unknown	Optoelectro-nic devices
Noh, 2014	Photo-induced superhydro-philicity	Nanoporous broadband antireflection	Unknown	Unknown	Mechanical robustness	Silicon	Low	Unknown	Solar cells
Leem, 2014	Superhydro-philic self-cleaning	Omnidirection al, broadband antireflection	Unknown	Unknown	Unknown	Glass	Low	Unknown	Solar cells

Name	Anti-adhesive	Transparency	Thermal stability	Bio-compatibility	Other stability	Substrate material	Costs	Fabrication	Suggested application
Askar, 2013 Does not describe fabrication	Superhydro-phobic self-cleaning	Moth-eye broadband antireflection	200◦ max	Unknown	Mechanical robustness	Glass, silicon	Low	Unknown	Solar cells, optoelectronic devices
Li, 2013 High costs	Water-repellent, hydrophobic self-cleaning	LbL assembly, broadband antireflection	Unknown	Unknown	Unknown	Glass	High	Unknown	Solar cells
Ye, 2013	Hydrophobic self-cleaning	TiO2/SiO2/ TiO2-SiO2 Broadband antireflection	Unknown	Unknown	Unknown	Glass	Unknown	Unknown	Solar cells
Chang, 2013 (no coating)	-	Antireflection	-	-	-	-	-	-	-

Philips, 2013 (book chapter)	-	Antireflection	-	-	-	Glass, silicon	-	-	-

Name	Anti-adhesive	Transparency	Thermal stability	Bio-compatibility	Other stability	Substrate material	Costs	Fabrication	Suggested application
Ji, 2012 (Informational)	-	Moth-eye broadband antireflection, color tuning	-	-	-	Glass	-	-	-
Helsch, 2012 Not (super) hydrophobic	Self-cleaning	Antireflection	Unknown	Unknown	Unknown	Glass	Unknown	Unknown	Solar cells
Cai, 2012 Wrong substrate	Superhydro-phobic self-cleaning	TiO2 quasi-omnidirec-tional, broadband antireflection	Good	Unknown	Chemical	Titanium	Unknown	Unknown	Solar cells, displays, chemical sensors
Joo, 2011 Wrong application	Hydrophobic	Antireflection	Unknown	Unknown	Unknown	Silicon	Unknown	Unknown	Optoelectro-nic devices
Liu, 2011	Superhydro-phobic	Hierarchical structured antireflection	Unknown	Unknown	Unknown	Silicon	Unknown	Unknown	Solar cells

Name	Anti-adhesive	Transparency	Thermal stability	Bio-compatibility	Other stability	Substrate material	Costs	Fabrication	Suggested application
Lin, 2010	Hydrophobic self-cleaning	Omnidirectio-nal anti-reflection	Unknown	Unknown	Unknown	Silicon	Unknown	Unknown	Optical media
Lin, 2009	Self-cleaning	Omnidirectio-nal, broadband anti-reflection	Unknown	Unknown	Unknown	Silicon	Unknown	Unknown	Solar cells
Min, 2008	Superhydro-phobic self-cleaning	Moth-eye broadband antirefelction	Unknown	Unknown	Unknown	Silicon	Unknown	Unknown	Solar cells, optoelectro-nics, biological sensing
Min, 2008 (2)	Superhydro-phobic self-cleaning	Broadband antireflection	Unknown	Unknown	Unknown	Silicon, glass	Unknown	Unknown	Solar cells, optoelectronic s, displays
Wissen, 2008 (unsuitable)	-	-	-	-	-	-	-	-	-

Name	Anti-adhesive	Transparency	Thermal stability	Bio-compatibility	Other stability	Substrate material	Costs	Fabrication	Suggested application
Huang, 2007	-	Quasi-omnidirec-tional, broadband antireflection	-	-	-	Silicon	-	-	Solar cells, optoelectrical devices
Niggemann, 2001 (informational)	-	-	-	-	-	-	-	-	-
Ye, 2015	Superhydro-philic	Broadband antireflection	Unknown	Unknown	Unknown	Fused silica	Low	Easy, 1 step 90◦C – 2hrs	Goggles, windshields, solar cells, optical devices
Teflon	Non-stick, hydrophobic	Transparent	Up to 287◦C	Unaffected by chemical environments	-	Glass	Unknown	Unknown	Cooking

Appendix J: Specifications - Aluminum coated fiber

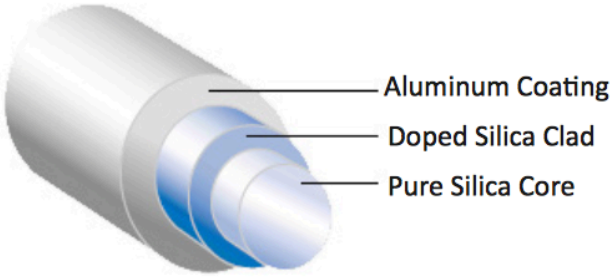

Aluminum Coated Fiber

Fiberguide's Aluminum Coated Fibers are designed for a wide temperature range (-269°C to +400°C) and superior strength (> 100kpsi). This allows for long life at extended stress levels in applications that require tight bends. Also, the strong chemical bond between the silica cladding and the aluminum enables direct termination without pistoning. This bond also makes Aluminum coating the ideal choice to preserve deep UV performance in Fiberguide's Solarguide product family.

FIBER SPECIFICATIONS

STEP INDEX MULTIMODE

- oPure Fused Silica Core / Fluorine Doped Silica Cladding
- o Core / Cladding Sizes: 50/125µm to 400/440µm
- o Numerical Aperture (NA): 0.12, 0.22, 0.26
- o Standard Core/Clad Ratio: 1.1
- o Available Core/Clad Ratios: 1.2, 1.4 and 2.5

GRADED INDEX MULTIMODE

- o Germanium Doped Fused Silica Core / Pure Fused Silica Cladding
- o Core / Cladding Sizes: 50/125µm, 62.5/125µm
- o Numerical Aperture (NA): 50µm: 0.200 / 62.5µm: 0.275

COMMON SPECIFICATIONS

- Recommended Bend Radius:
  - o Short Term: 100 X Clad Diameter
  - o Long Term: 200 X Clad Diameter

Please note that these figures represent best practice recommendations. In applications where tighter bends are required, Fiberguide can assist you in estimating what impact they may have on fiber reliability.

- 100% Proof Test Using 4-Axis Bend Method

SINGLE MODE

- o Germanium Doped Fused Silica Core / Pure Fused Silica Cladding
- o Mode Field Diameter / Cladding Sizes: 4.3/125µm, 9.0/125µm
- o Numerical Aperture (NA): 0.12

Applications:

- •High temperature and cryogenic temperature sensing
- •Semi Conductor Manufacturing
- •Corrosive and caustic environments
- •Ultra high vacuum devices
- •Radiation resistant sensors
- •Rocket, turbine and jet engine monitoring

Aluminum Coating

Temperature: -269˚C to +400˚C / -452˚F to + 752˚F

Fiber Type: Anhydroguide™ Pure Fused Silica Core/ Fluorine Doped Silica Cladding - Step Index Multimode

Wavelength: VIS-IR (Low OH): 300 nm - 2400 nm

Numerical Aperture (NA):

Standard: 0.22 ± 0.02 (Full acceptance Angle 25˚) - Prefix AFS or SFS

Low: 0.12 ± 0.02 (Full Acceptance Angle 14˚) - Prefix AFM or SFM

Hi: 0.26 ± 0.02 (Full Acceptance Angle 30˚) - Prefix AFH or SFH

Proof Test: 100 KPSI 4-Axis Bend Test

Product Code	Core Diameter (µm)	Cladding Diameter (µm)	Coating Diameter (µm)	Bend Radius Short Term/ Long Term (mm)
AFS50/125/175A	50 ± 2	125 + 1/-3	175 ± 18	≥ 13/25
AFS100/140/200A	100 ± 2	140 + 1/-3	200 ± 20	≥ 14/28
AFS105/125/175A	105 ± 2	125 + 1/-3	175 ± 18	≥ 13/25
AFS200/220/280A	200 ± 4	220 ± 4.4	280 ± 28	≥ 22/44
AFS300/330/430A	300 ± 6	330 ± 6.6	430 ± 43	≥ 33/66
AFS400/440/530A	400 ± 8	440 ± 9	530 ± 53	≥ 44/88

Aluminum Coating

Temperature: -269˚C to +400˚C / -452˚F to + 752˚F

Fiber Type: Superguide™ Pure Fused Silica Core/ Fluorine Doped Silica Cladding - Step Index Multimode

Wavelength: UV-VIS (High OH): 190 nm - 1250 nm

Numerical Aperture (NA):

Standard: 0.22 ± 0.02 (Full acceptance Angle 25˚) - Prefix AFS or SFS

Low: 0.12 ± 0.02 (Full Acceptance Angle 14˚) - Prefix AFM or SFM

Hi: 0.26 ± 0.02 (Full Acceptance Angle 30˚) - Prefix AFH or SFH

Proof Test: 100 KPSI 4-Axis Bend Test

Product Code	Core Diameter (µm)	Cladding Diameter (µm)	Coating Diameter (µm)	Bend Radius Short Term/ Long Term (mm)
SFS50/125/175A	50 ± 2	125 + 1/-3	175 ± 18	≥ 13/25
SFS100/140/200A	100 ± 2	140 + 1/-3	200 ± 20	≥ 14/28
SFS105/125/175A	105 ± 2	125 + 1/-3	175 ± 18	≥ 13/25
SFS200/220/280A	200 ± 4	220 ± 4.4	280 ± 28	≥ 22/44
SFS300/330/430A	300 ± 6	330 ± 6.6	430 ± 43	≥ 33/66
SFS400/440/530A	400 ± 8	440 ± 9	530 ± 53	≥ 44/88

Aluminum Coating
Temperature: -269˚C to +400˚C / -452˚F to + 752˚F

Fiber Type: Anhydrous Graded Index (AGI™) Multimode
Wavelength: Optimized for 850nm & 1300nm

Numerical Aperture (NA):
50µm: 0.200 ± 0.02 (Full acceptance Angle 23.6˚)
62.5µm: 0.275 ± 0.02 (Full acceptance Angle 33.4˚)

Proof Test: 100 KPSI 4-Axis Bend Test

Product Code	Core Diameter (µm)	Cladding Diameter (µm)	Coating Diameter (µm)	Bend Radius Short Term/ Long Term (mm)
AGI50/125/175A	50 ± 2	125 + 1/-3	175 ± 18	≥ 13/25
AGI62.5/125/175A	62.5 ± 1	125 + 1/-3	175 ± 18	≥ 13/25

Aluminum Coating
Temperature: -269˚C to +400˚C / -452˚F to + 752˚F

Fiber Type: Anhydrous Silica (ASI™) Single Mode
Wavelength:
ASI 633 (4.3/125µm): 633nm - 680nm
ASI 1500 (9.0/125µm): 1310nm

Numerical Aperture (NA):
0.12 ± 0.02 (Full Acceptance Angle 14˚)

Proof Test: 100 KPSI 4-Axis Bend Test

Product Code	Core Diameter (µm)	Cladding Diameter (µm)	Coating Diameter (µm)	Bend Radius Short Term/ Long Term (mm)
ASI4.3/125/175A	4.3 ± 0.3	125 + 1/-3	175 ± 18	≥ 13/25
ASI9.0/125/175A	9.0 - 0.5	125 + 1/-3	175 ± 18	≥ 13/25

Appendix K: Test results - Light intensity test

The table provided below shows all measurements taken during the light intensity test. Calculations of the mean, standard deviations and signal losses are included as well.

Table 20: Results of the light intensity test performed on both unused and used fibers and on both unmodified and modified fibers.

Fiber condition	Control	Sample 1	Sample 2	Sample 3	N	Mean	SD	Signal loss	% Signal loss
A.	12 µW	7 µW	6 µW	-	2	6.5 µW	0.7	5.5 µW	45.8%
B.	11 µW	6 µW	9 µW	6 µW	3	5.7 µW	0.6	5.3 µW	48.5%
C.	11 µW	5 µW	6 µW	6 µW	3	7.0 µW	1.7	4.0 µW	36.4%
D.	10 µW	6 µW	6 µW	-	2	6.0 µW	0.0	4.0 µW	40%

Appendix L: Test results - Optical microscope

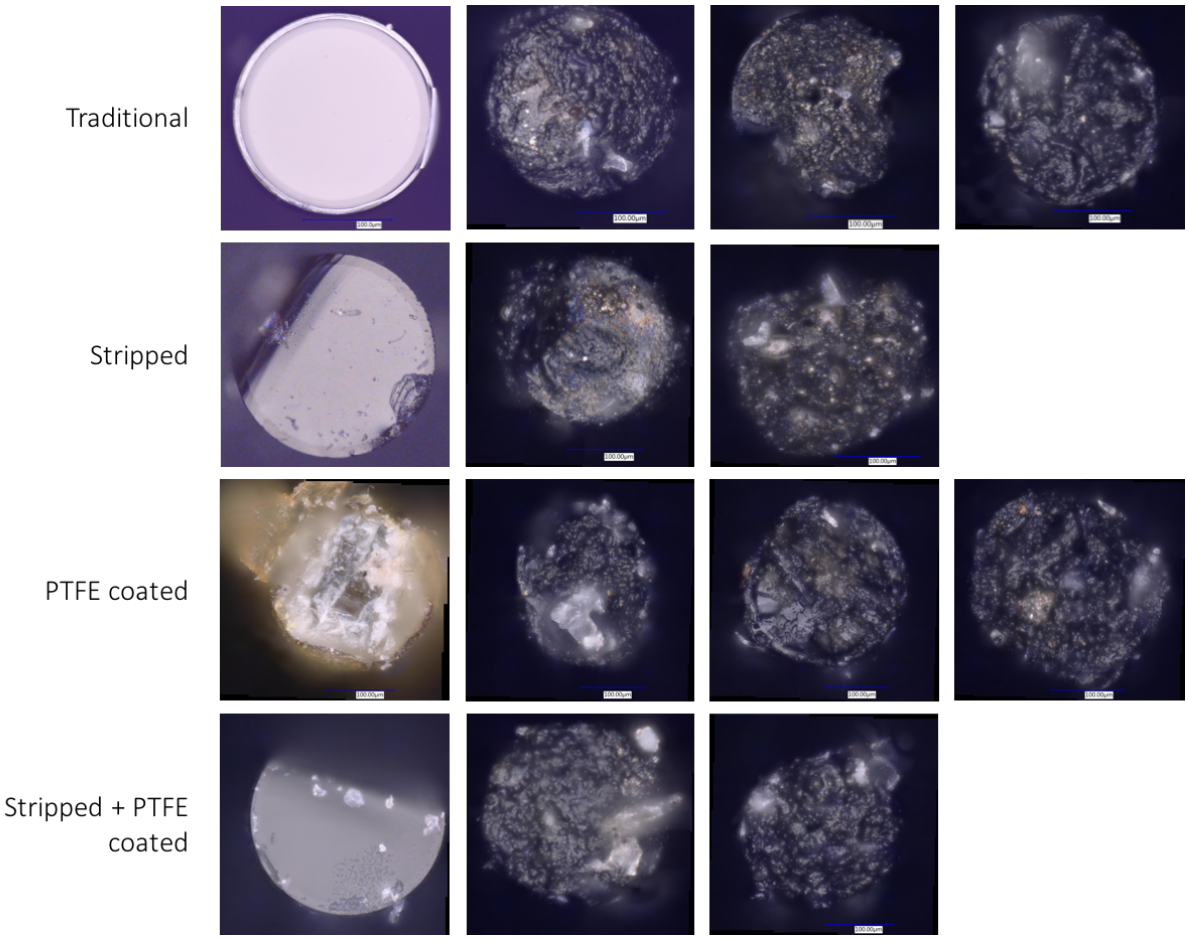

Figure 85: Optical microscope images showing the different fiber tips in top view.

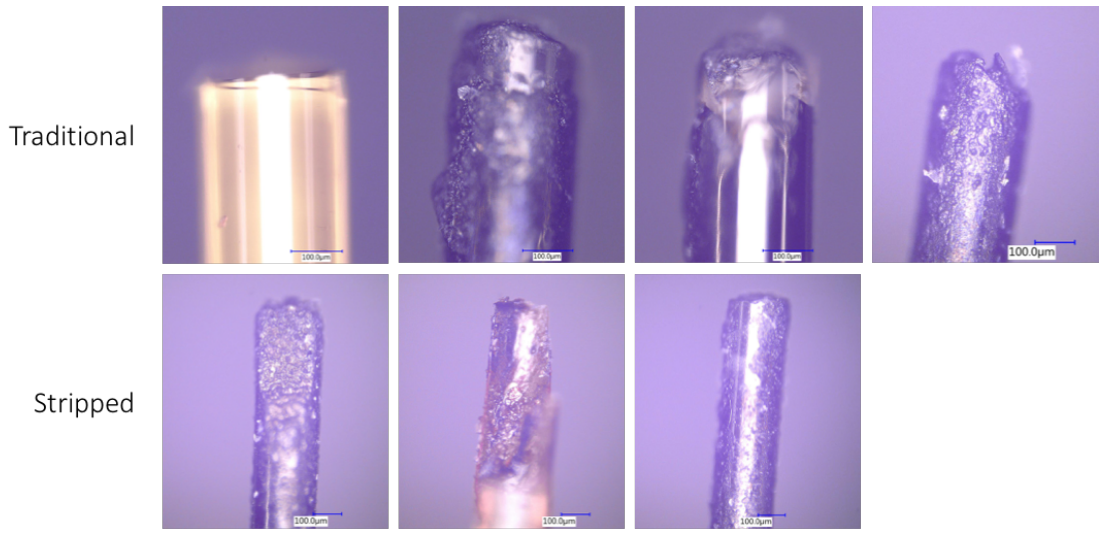

Figure 86: Optical microscope images showing two different kinds of fiber tips in side view.

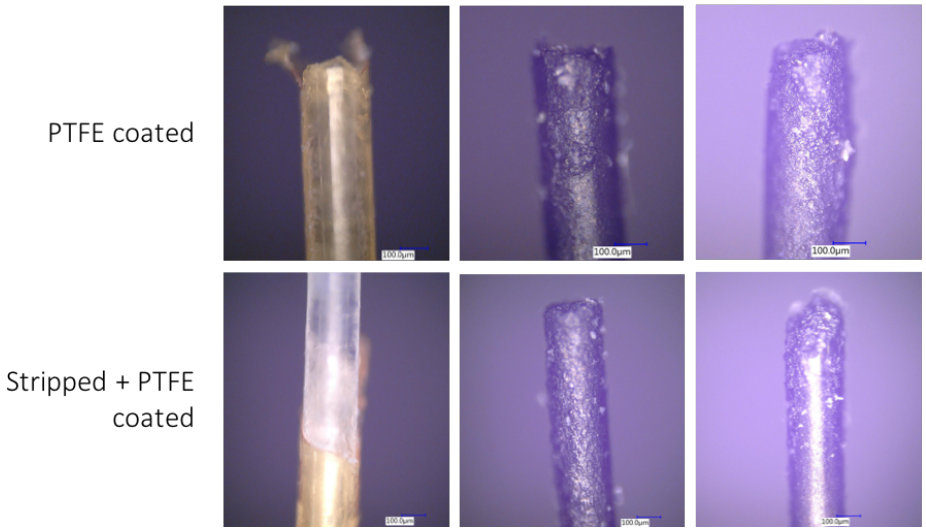

Figure 87: Optical microscope images showing two different kinds of fiber tips in side view.

Appendix M: Test results - Energy-dispersive spectroscopy

1. EDS images

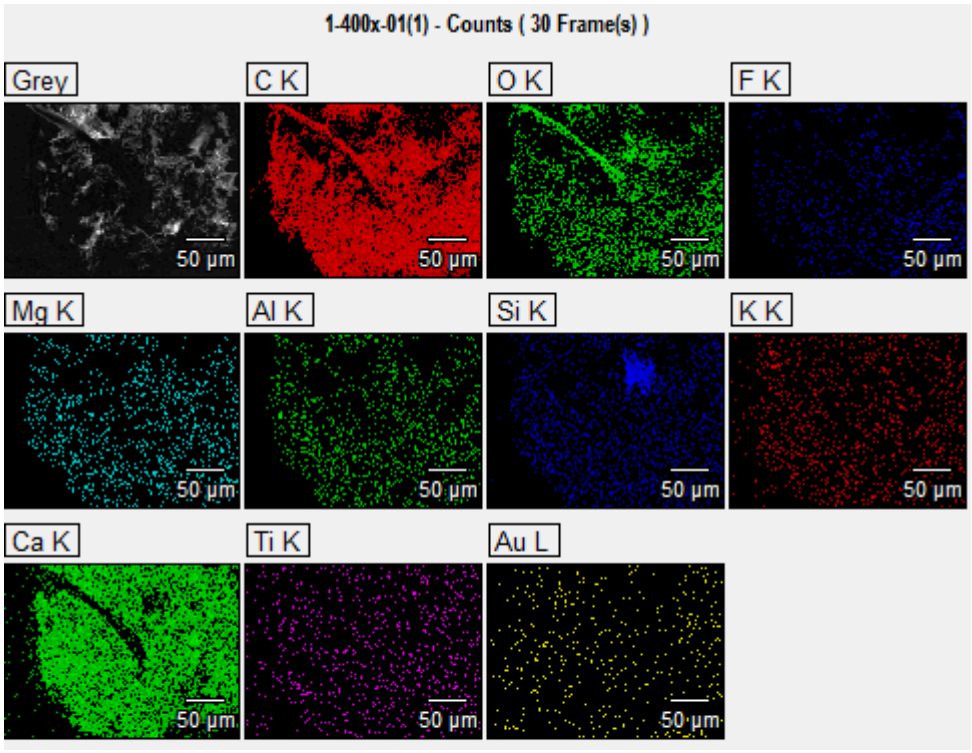

Figure 88: EDS images showing the different elements present on an unused, PTFE coated fiber tip.

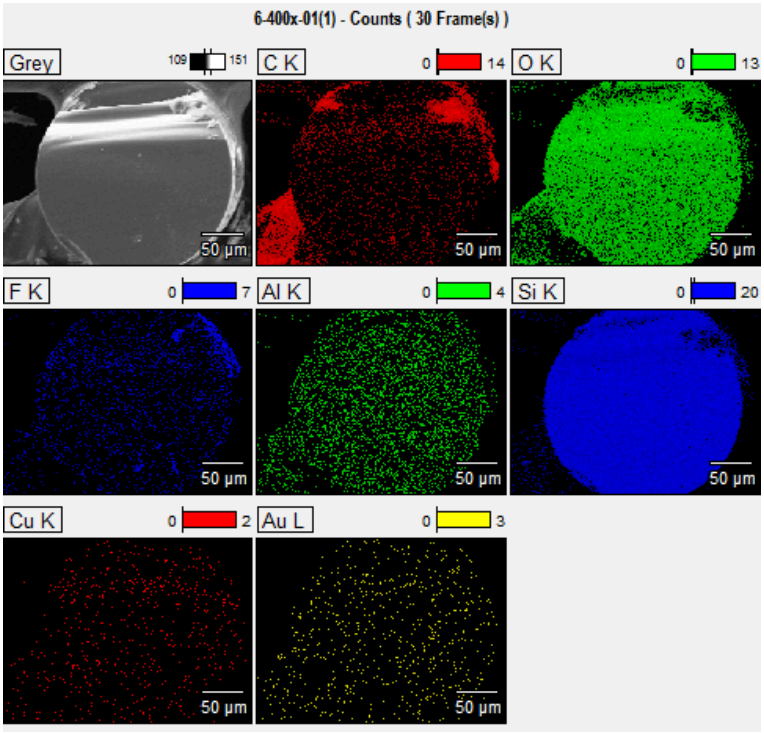

Figure 89: EDS images showing the different elements present on an unused, stripped + PTFE coated fiber tip.

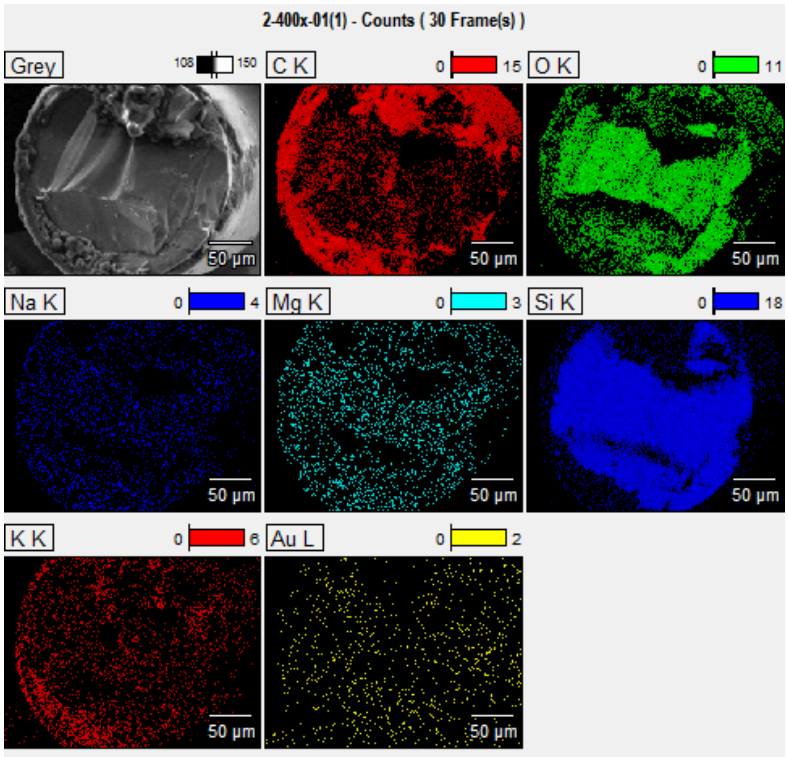

Figure 90: EDS images showing the different elements present on a used, traditional fiber tip.

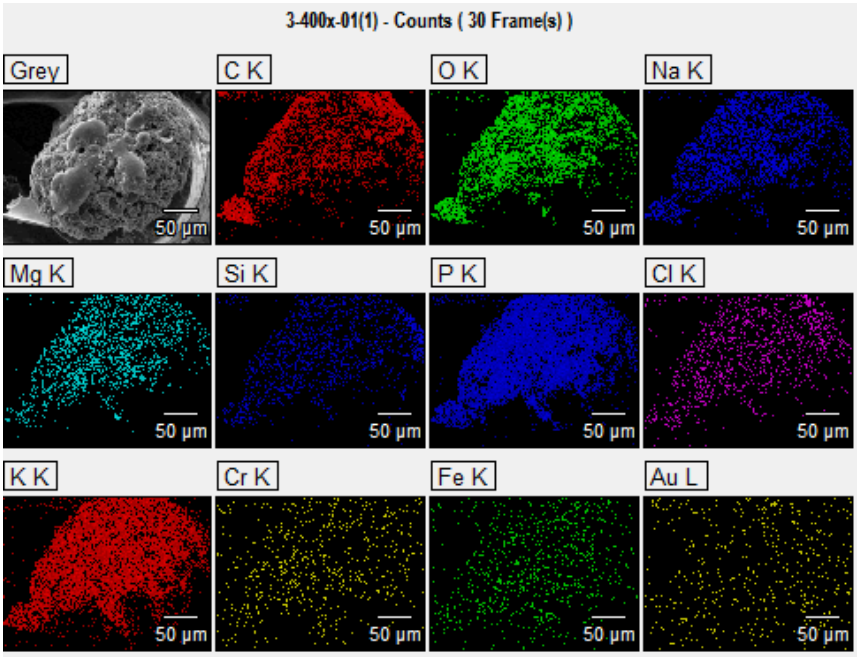

Figure 91: EDS images showing the different elements present on a used, stripped fiber tip.

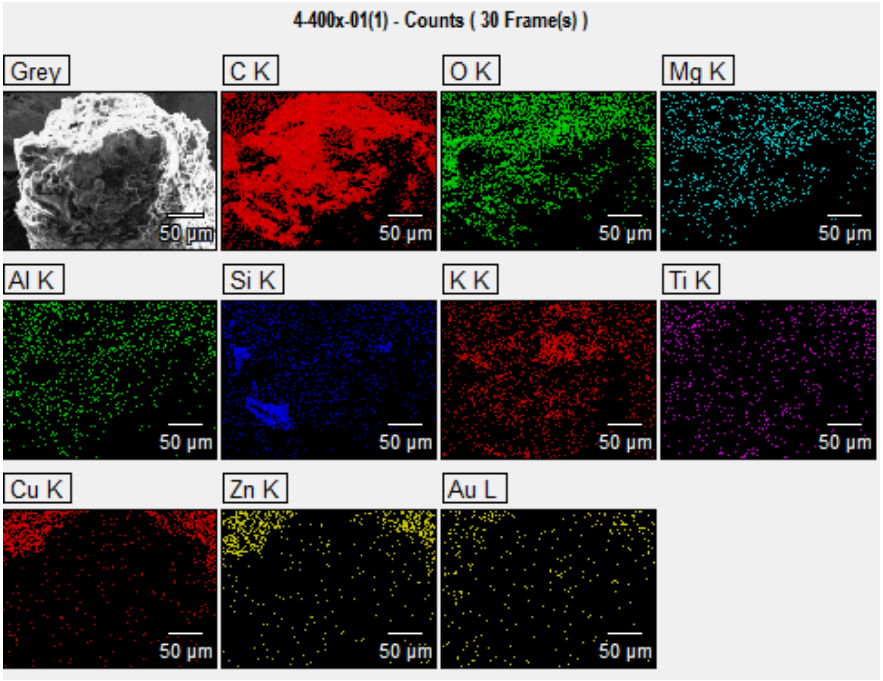

Figure 92: EDS images showing the different elements present on a used, PTFE coated fiber tip.

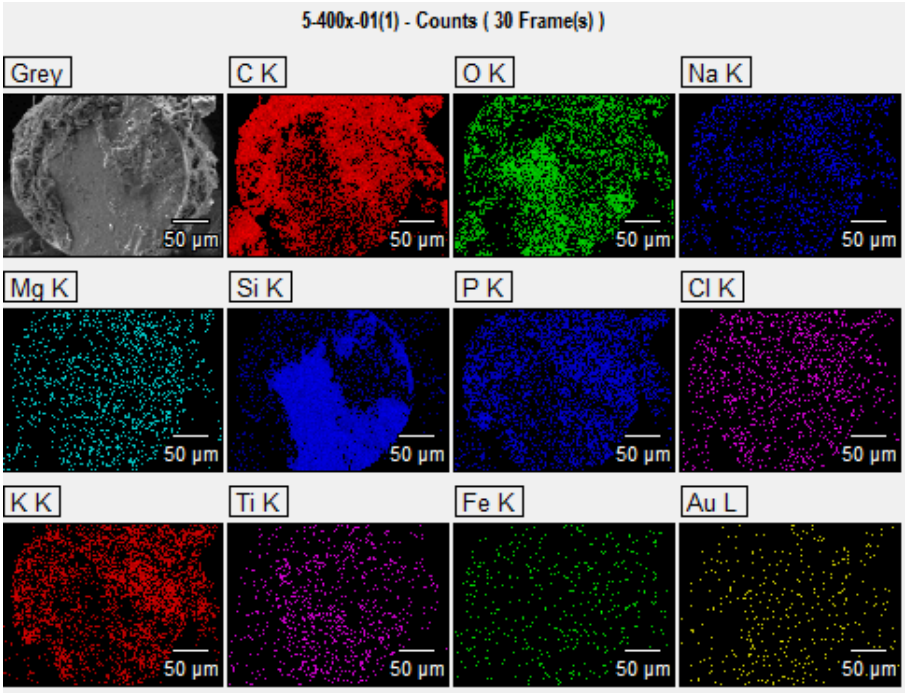

Figure 93: EDS images showing the different elements present on a used, stripped + PTFE coated fiber tip.

2. EDS elements

Table 21: Elements detected with EDS on the unused, PTFE coated fiber tip.

#	Element Line	Weight %	Weight % Error	Atom %	Atom % Error
1	C	71.03	± 0.33	82.47	± 0.38
2	O	13.44	± 0.29	11.71	± 0.25
3	F	0.76	± 0.09	0.56	± 0.07

4	Mg	0.04	± 0.01	0.02	± 0.01
5	Al	0.07	± 0.01	0.04	± 0.01
6	Si	0.79	± 0.02	0.39	± 0.01
7	K	0.14	± 0.02	0.05	± 0.01
8	Ca	13.41	± 0.10	4.66	± 0.03
9	Ti	0.31	± 0.03	0.09	± 0.01
	Total	100.00		100.00	

Table 22: Elements detected with EDS on the unused, stripped + PTFE coated fiber tip.

#	Element Line	Weight %	Weight % Error	Atom %	Atom % Error
1	C	38.62	± 0.41	49.73	± 0.52
2	O	38.25	± 0.22	36.98	± 0.22
3	F	2.06	± 0.18	1.68	± 0.14
4	Al	0.03	± 0.01	0.02	± 0.01
5	Si	21.04	± 0.07	11.59	± 0.04
	Total	100.00		100.00	

Table 23: Elements detected with EDS on the used, traditional fiber tip.

#	Element Line	Weight %	Weight % Error	Atom %	Atom % Error
1	C	63.24	± 0.34	72.99	± 0.40
2	O	23.99	± 0.18	20.79	± 0.16
3	Na	0.26	± 0.03	0.15	± 0.02
4	Mg	0.06	± 0.01	0.03	± 0.01
5	Si	11.62	± 0.04	5.74	± 0.02
6	K	0.83	± 0.02	0.29	± 0.01
	Total	100.00		100.00	

Table 24: Elements detected with EDS on the used, stripped fiber tip.

#	Element Line	Weight %	Weight % Error	Atom %	Atom % Error
1	C	51.12	± 0.42	65.75	± 0.54
2	O	22.95	± 0.34	22.16	± 0.33
3	Na	3.78	± 0.07	2.54	± 0.05
4	Mg	0.70	± 0.04	0.44	± 0.02
5	Si	0.28	± 0.02	0.15	± 0.01
6	P	7.77	± 0.08	3.88	± 0.04
7	Cl	0.44	± 0.04	0.19	± 0.02
8	K	10.80	± 0.10	4.27	± 0.04
9	Cr	0.51	± 0.09	0.15	± 0.03
10	Fe	1.66	± 0.17	0.46	± 0.05
	Total	100.00		100.00	

Table 25: Elements detected with EDS on the used, PTFE coated fiber tip.

#	Element Line	Weight %	Weight % Error	Atom %	Atom % Error
1	C	83.49	± 0.34	88.00	± 0.35
2	O	13.94	± 0.22	11.03	± 0.18

3	M	0.22	± 0.01	0.11	± 0.01
4	Al	0.10	± 0.02	0.05	± 0.01
5	Si	0.73	± 0.02	0.33	± 0.01
6	K	1.37	± 0.02	0.44	± 0.01
7	Ti	0.16	± 0.03	0.04	± 0.01
	Total	100.00		100.00	

Table 26: Elements detected with EDS on the used, stripped + PTFE coated fiber tip.

#	Element Line	Weight %	Weight % Error	Atom %	Atom % Error
1	C	76.16	± 0.37	84.30	± 0.40
2	O	13.43	± 0.21	11.16	± 0.18
3	Na	0.66	± 0.02	0.38	± 0.01
4	Mg	0.12	± 0.02	0.06	± 0.01
5	Si	6.17	± 0.04	2.92	± 0.02
6	P	0.39	± 0.05	0.17	± 0.02
7	Cl	0.15	± 0.02	0.05	± 0.01
8	K	2.21	± 0.04	0.75	± 0.01
9	Ti	0.57	± 0.02	0.16	± 0.01
10	Fe	0.15	± 0.04	0.04	± 0.01
	Total	100.00		100.00	